Geothermal Power from co-produced fluids and hydrocarbon reservoirs throughout the Western Canadian Sedimentary Basin (WCSB)

Compiled and edited by:

Dr. Jonathan Banks

Research Associate

Dept. of Earth and Atmospheric Sciences

University of Alberta

With contributions from (alphabetically):

Dr. Victor Adamowicz; Dr. Nicholas B. Harris; Dr. Xincheng Hu; Garret Key; Dr. Lianne Lefsrud; Dr. Wei Victor Liu; Kabir Nadkarni; Chris Noyahr; Spencer Poulette; Dr. Arif Rabbani; Daniel Schiffner; Evan Renaud; and Dr. John Weissenberger

Alberta Innovates Project # G2018000632
Prepared for: Vanessa White, Director, Renewable and Alternative Energy
February 7, 2022

Disclaimer
Alberta Innovates (Al) and Her Majesty the Queen in right of Alberta make no warranty, express or implied, nor assume any legal liability or responsibility for the accuracy, completeness, or usefulness of any information contained in this publication, nor that use thereof infringe on privately owned rights. The views and opinions of the author expressed herein do not necessarily reflect those of Al or Her Majesty the Queen in right of Alberta. The directors, officers, employees, agents and consultants of AI and the Government of Alberta are exempted, excluded and absolved from all liability for damage or injury, howsoever caused, to any person in connection with or arising out of the use by that person for any purpose of this publication or its contents.

Acknowledgments

The primary partners on this research project were Alberta Innovates and the Department of Earth and Atmospheric Sciences at the University of Alberta. The Alberta Geological Survey's hydrogeology group, headed by Dan Palombi, also gave significant in-kind contributions in terms of data, labour, and expertise. Razor Energy, through Lisa Mueller, their VP for New Ventures, also played an important role in providing early-stage capital for the research program. We are deeply appreciative of their contributions.

We would like thank Dr. Maureen Kolla and Vanessa White at Alberta Innovates for their patient and expert guidance throughout the program. We would also like to thank Dr. M. Anne Naeth for providing significant material support for the project via the University of Alberta's Future Energy System's Program, part of the federal Canada First Research Excellence Fund (CFREF). An additional thank you goes to Drs. Stephen Johnston and Thomas Chacko, chair and acting chair, respectively, in the Department of Earth and Atmospheric Science, for giving a stable and supportive home base for this project.

As is the case with any academic pursuit, this work is the fruit of many researchers. Special recognition goes to Dr. Nick Harris, Dr. John Weissenberger, Chris Noyahr, and Evan Renaud for the work they did on the Devonian carbonate reefs throughout the Western Canadian Sedimentary Basin. Drs. Wei Victor Liu and Xincheng Hu were the lead researchers in developing the concepts and models surrounding deep well bore heat exchanger retrofits. Drs. Lianne Lefsrud and Victor Adamowicz, along with their students Daniel Schiffner and Kabir Nadkarni where responsible for the economic and socio-political components of the research. Dr. Arif Rabbani and Spencer Poulette both provided extensive research into the geochemistry of formation fluids in the Western Canadian Sedimentary Basin. Garrett Key was responsible for developing the beta-version of the Geothermal Atlas of the Western Canadian Sedimentary Basin, as well as a host of other behind the scenes activities. Finally, this project would not have been possible without the administrative and technical support of Shyra Craig and Randy Kofmann, respectively.

Executive Summary

This report details the results of a 3-year, $2.85 million dollar research program that investigated the potential for repurposing Alberta's world-class hydrocarbon production infrastructure for geothermal energy exploitation. The project was primarily a partnership between the Climate Change Innovation Technology Fund (CCITF) set up by the Alberta's NDP government in 2015 and the University of Alberta's Future Energy Systems program, part of the federal government's Canada First Research Excellence Fund (CFREF). The CCITF program funded a variety of projects at varying stages of technology readiness. Because this project was headed by researchers at the University of Alberta, it was by definition at the lower end of the technology readiness level (TRL) scale. Rather than focusing predominantly on commercializing innovative technology, this project, in addition to the research outcomes delineated here, was aimed at developing research capacity and methodology in Western Canada. In this regard, funding for this project trained over 30 highly qualified personnel (HQP; students, post-doctoral fellows, and research associates) over the three-year duration of the project. These HQP combined to publish 16 peer-reviewed papers, seven technical reports, four Master's Theses, four Bachelor's theses, and a doctoral dissertation. Researchers involved in this project produced 37 conference proceedings, including 12 keynote speaking engagements. Funding from this project helped set up a $500,000+, state-of-the-art fluid/rock interaction laboratory in the University of Alberta's Department of Earth and Atmospheric Sciences and solidified an international partnership with Karlsruher Institute of Technology in Karlsruhe, Germany.

Geothermal energy development has long been a topic of discussion in western Canada, especially in Alberta, where hundreds of billions of dollars of hydrocarbon production infrastructure has provided a unique window into the geothermal setting of the Western Canadian Sedimentary Basin. Heretofore, much of the research involving geothermics in the basin has focused on greenfield development using conventional geothermal technology with an aim primarily towards producing electricity. As the world clamours for carbon-free energy, however, and as the volatility of the hydrocarbon market continues to strain local economies, researchers, industry players, entrepreneurs, and government agencies have all been searching for ways to use western Canada's stranded hydrocarbon assets as transformational green-energy technology. This is the first large-scale study that looks exclusively at the geothermal power potential of brownfield hydrocarbon resources in the Western Canadian Sedimentary Basin.

Over 10 chapters, we provide an overview of the technology, challenges, opportunities, and obstacles involved with repurposing hydrocarbon production infrastructure for harvesting Alberta's deep subsurface geothermal energy. In the first chapter, we provide a brief overview geothermal research done in Alberta leading up to the present study. In the second chapter, we summarize the state of hydrocarbon production in Alberta, in terms of the number of active fields, their average depths, and their average temperatures. There are currently 480 active field in the province, with average field temperatures ranging from 25 ˚C – 126 ˚C. Only 20 of these fields, however, have temperature in excess of 95 ˚C, which is a minimum temperature required to produce electricity in a cold weather climate.

In the third chapter, we detail three separate methods of quantifying the geothermal potential of a hydrocarbon field. The first method uses a volumetric, heat-in-place calculation that considers the field as bulk reservoir of geothermal energy. The second method considers the sum of individual wellhead generation potential. Both methods employ a Monte Carlo simulation to account for probabilistic distributions of input variables. The third method is a semi-quantitative visual method that overlays reservoir temperature and wellhead flow rate data to create colour-coded favourability maps.

The methods presented in Chapter 3 are applied to the Swan Hills region of Alberta in Chapter 4. We present results from the Virginia Hills field, the largest of the several Devonian carbonate reefs that comprise the Swan Hills carbonate platform in central Alberta. The results show that the heat-in-place method estimates over seven times more geothermal power potential than the wellhead method. This is due to the high variability in flow rates from well to well in any given hydrocarbon field. The favourability map is able to pinpoint exactly where the best areas of a field for new well drilling can be found.

In Chapter 5, we look at some of the geochemical risks associated with circulating the vast quantities of formation fluids required to produce commercial scale geothermal power from a repurposed hydrocarbon field. We employed a principle component analysis combined with a clustering algorithm to identify the main contributors to aqueous geochemical variability in four of the most promising geothermal reservoirs throughout the basin. After analyzing nearly 2000 individual brine samples, we identified the most prevalent geochemical risk is calcite scaling. Calcite scaling is a well-known phenomenon in the geothermal industry, and there are numerous reliable and cost-effective means for its mitigation. Therefore, our study concludes that geochemical risks are not a significant concern for geothermal developers in the Western Canadian Sedimentary Basin.

In Chapters 6-8, we investigate alternative methods for refurbishing hydrocarbon fields for geothermal power production. Conventional geothermal systems rely on circulation of brines through production and injection wells. This process can lead to significant costs and risks, such as expensive pumps, high parasitic loads, and the potential for induced seismicity. In this these chapters, we explore the use of single sealed wells as deep borehole heat exchangers. Such designs do not require the circulation of brine from the reservoir to the surface and back, thereby alleviating many of the risks associated with conventional geothermal energy production. In Chapter 6, we present the basic design of a deep borehole heat exchanger and model its performance based on data inputs for wells in the Hinton, AB area. Deep borehole heat exchangers cannot produce geothermal energy at the temperatures required for making electrical power, but can provide a stable heat source for direct use over many decades.

In Chapter 7, we present a cost model for retrofitting existing wellbores as deep borehole heat exchangers. We use data from the 2019 PSAC report to estimate fixed and variable costs for both suspended and abandoned wells. Retrofit costs range from ~$50,000 per well to over $110,000 per well, depending on well vintage, depth, status, and conditions. Retrofitting wells for geothermal use, in many cases, is less expensive that the cost of remediating and reclaiming an abandoned well.

Because deep borehole heat exchangers can only produce low-enthalpy geothermal power, novel end-uses are required to make this technology feasible. In Chapter 8, we investigate one such novel end-use: heating cattle feed water in the winter. We used the Tomahawk Ranch near Wabamun, AB as a case study for applying the thermodynamic and economic models delineated in Chapters 6 and 7. While the outcomes of this case study did not show this end-use to be cost-effective in today's market, the concept is illustrative of the type of out-of-the-box thinking that will be required to make hydrocarbon-to-geothermal conversions a reality in western Canada.

A major deliverable of this study is the beta-version of the Geothermal Atlas of the Western Canadian Sedimentary Basin, as discussed in Chapter 9. This atlas is an interactive, map-centric, web application that developed and partnership between the University of Alberta and the Alberta Geological Society (AGS). The atlas incorporates data from throughout the basin with the thermodynamic, economic, and resource assessment tools developed in this study to provide essential services to the energy sector along with the academic community, as well as the general public and municipal, provincial, and federal governments. Potential end-users of the atlas span many industries and include entrepreneurial start-ups,

oil and gas producers, oil and gas service providers, drillers, regulatory and legislative bodies, municipalities, academics, data management firms, and the general public.

Finally, in Chapter 10, we perform a comparative jurisdictional review of hydrocarbon-to-geothermal transitions in France's Paris Basin and the Western Canadian Sedimentary Basin. Whereas this transition has been sluggish in Canada, France has seen tangible success in this transition in recent years, especially in regards to thermal power production. We explored a multivariate framework of innovation adoption that includes technical know-how, public discourse, and stakeholder networking to integrate efforts towards a successful transition. We conclude that while western Canada has both significant geothermal resources and world-class geotechnical expertise, much work remains to be done to bring all potential stakeholders on to the same page regarding motivation and outcomes in order to success affect widespread conversion of hydrocarbon infrastructure to geothermal power production.

A concluding chapter (11) summarizes the major findings and provides recommendations for further research.

Table of Contents

1 Brief overview of geothermal research in WCSB

1.1 Early Research

Geothermal research in the Western Canadian Sedimentary Basin has been going on for more than half a century. Early research focused on heat flow throughout the western provinces and territories (Garland and Lennox, 1962). Research into regional heat flow (Majorowicz and Jessop, 1981), thermal conductivity (Lam et al., 1985), geothermal gradient maps (Lam et al., 1982; Lam and Jones, 1984), radiogenic heat production and flow from the Precambrian basement other deep Paleozoic surfaces underlying the WCSB were conducted mainly for the purposes of oil and gas exploration (Jones et al., 1985, Jones and Majorowicz, 1987; Bachu, 1993). Lam and Jones (1985) outlined subsurface temperatures, subsurface geology, water chemistry, water flow rates, potentiometric surfaces and regional variations of TDS to assess specific formations for geothermal energy production potential. Additional research by Lam and Jones (1986) considered potential geothermal reservoirs in Southern Alberta to accommodate the power needs of the Calgary area. Due to inconsistent and limited temperature data, extensive work had to be done to correct temperatures for hydrodynamic influences (Majorowicz et al., 1984, 1985, 1999) and paleoclimatic effects (Majorowicz et al., 2012[a]). Research regarding improving the quality of temperature data available from the WCSB reach a zenith when Niewenhuis et al. (2015) released a database at the World Geothermal Congress 2015 which utilized a culling method to remove inconsistent temperature data and correct those affected by the drilling process.

1.2 Research in the 21st Century

The wealth of geophysical, geochemical, and hydrodynamic data collected from the oil and gas industry is an indispensable resource for geothermal energy research and development in the WCSB. This data, combined with the engineering and drilling expertise that is present in the oil and gas industry makes Alberta an ideal candidate for a boom in geothermal energy development. Thus, there has been considerable research conducted in the WCSB that focuses on the exploitation of geothermal energy for heating and electricity in more recent years. Grasby et al. (2012), in conjunction with the Geological Survey of Canada produced a nation-wide geothermal resource base estimate, including an assessment of the enhanced geothermal potential in Canada. Majorowicz et al. (2012b) investigated the potential to utilize geothermal energy as a heat source for oil-sands production and upgrading. Weides et al. (2013) looked for potential geothermal resources in the Edmonton, AB area which led to further research by Weides et al. (2014a) into using basal Cambrian sandstones and the siliciclastic Granite Wash unit in the Peace River area of Alberta (2014b) as a potential resource for producing electricity. Lack of sufficiently high temperatures restrict the production of electricity from these formations; however, they provide enough energy for direct heat use.

Weides and Majorowicz (2014) also investigated spatial variability in heat flow throughout the WCSB by overlaying the aerial extent of known deep basin aquifers with temperature profiles from geological surfaces throughout the Paleozoic and Mesozoic periods.

The idea of using an enhanced geothermal system (EGS) for oil sands production was introduced by an industry consortium (Geopowering the Oilsands [GeoPos]) in 2006-2008. This idea was investigated in more detail by Majorowicz et al. (2012b) under the auspices of the Helmholtz-Alberta Initiative (HAI), a robust partnership between the German network of Helmholtz research institutes and the University of Alberta. The extraction of deep oil sands requires the use of steam assisted gravity drainage (SAGD), which also requires a significant amount of hot water. This water is currently heated by burning natural gas, thereby creating a significant source of greenhouse gas emissions, as well as significant economic costs to oil sands producers (Majorowicz et al., 2012a; 2012b). An alternative to burning natural gas could be geothermal heat extracted from the basement granitic rocks. This geothermal energy resource could also then be used to provide heat to the nearby communities, further offsetting the CO_2 emissions. Majorowicz et al. (2012b) suggest that EGS in the deep basement of the WCSB is economical, especially when considering both increases to natural gas prices and explicit carbon mitigation costs. They suggest that where electricity generation may not be economic, direct heat extraction may be economic.

The Helmholtz-Alberta-Initiative also produced significant research regarding potential greenfield geothermal power development in the deeper parts of the WCSB. Weides et al. (2013) considered geothermal resources in specific formations in the WCSB and made semi-quantitative evaluations using a number of assumptions and empiric data. They utilized a 3D geological model that was based on ~7000 stratigraphic tops from the Alberta Geologic Survey's (AGS) database, along with geothermal gradients to map temperature distributions of Paleozoic formations. Hot dry rock (HDR) systems are considered for the granitic basement rock of the study area. Specific Devonian carbonate formations that were investigated in their study were the Cooking Lake, Leduc, and Nisku Formations, as well as the Wabamun Group. Utilizing this new data, potential geothermal reservoirs in the Alberta Basin near Edmonton were delineated, allowing for further research and development. Weides et al. (2013) found the Cambrian Basal Sandstone Unit as the most suitable horizon for geothermal applications due to its depth and relatively widespread distribution throughout the study area. No core analysis data exists for this formation, therefore more detailed investigations are necessary. District heating requires 70-80°C (Lindal, 1973) and the Cambrian Basal Sandstone Unit has temperatures that exceed 70°C in most of the study area, including temperatures

81-89°C in the Edmonton area, making it a candidate for direct heating applications. Of the Devonian strata, only the Nisku formation in the southwestern corner of the study area exceeds 70°C. Greenhouses and domestic water provisions require temperatures >40°C (Lindal, 1973; Laplaige et al., 2000). Fluids in all Devonian strata in the western half of the study area are estimated to be >40°C.

In addition to investigations into specific reservoirs, Majorowicz and Moore (2014) looked at geothermal resources as a diffuse, province wide commodity. They assessed the geothermal energy output from resources with temperatures ranging 120 to 150°C at 4-5km deep wells to be as economically competitive as burning natural gas. They also evaluated the potential for direct heating using geothermal resources as low as 60°C as a substitute for burning coal, natural gas, or diesel, but they concluded that there are no significant offset gains from pre-heating in the oil sands region. Heating systems in the deep basin outside the immediate oil sands region, however, may provide a higher direct heat displacement, as well as a higher CO_2 offset equivalence, than fossil fuels.

1.3 The Deep Dive Study

From 2016-2018, in conjunction with Alberta Innovates, the Department of Earth and Atmospheric Sciences at the University of Alberta conducted a Deep-Dive Analysis of the Best Geothermal Reservoirs for Commercial Development in Alberta (Banks and Harris, 2018). The purpose of this undertaking was to catalyze commercial geothermal energy development in Alberta, Canada. Building on previous work from Weides and Majorowicz (2014), they used data from the oil and gas industry to assess the geothermal power potential of hot sedimentary aquifers within the Leduc, Swan Hills, Granite Wash, and the Gilwood formations underlying participating regional municipalities in Western and Central Alberta.

The Deep-Dive provided these municipalities with the precise location of geothermal reservoirs at depth, the gross thermal and electrical power production capacity of the reservoirs, and local options for geothermal power utilization, including cost estimates. Their power potential calculations found nearly 6200 MWt of potential thermal power for a 30-year production period within the search areas. The majority of which was found in the Leduc and Swan Hills formations. Electrical power production potential was calculated to be approximately 1150 MWe for a 30-year production period. Over 50% of this electrical power production potential was found in the Hinton area.

The Deep-Dive also compiled cost estimates for major geothermal power plant components, geothermal energy end-use options, and royalty structures in successful geothermal energy producing nations to present pathways to commercialization within Alberta. The study found that among the major components of geothermal power plant infrastructure – wells, pumps, heat exchangers and piping, turbines, and electrical transmission equipment – wells are the riskiest investment. Based on costs taken from the PSAC 2017 Well Cost Study (PSAC, 2016), they estimated the fixed costs of retrofitting a gas well for use as a geothermal slim hole to be ~$75,000 per well. Retrofitting a 4500m gas well, however, is nearly an order of magnitude cheaper than drilling a new one. A direct use geothermal plant estimated at ~$3,300,000 would be significantly cheaper than an electrical power plant which is estimated at ~$8,700,000. Potential uses of direct use are domestic and commercial space heating, industrial process heat, greenhouse and nursery heating, timber and grain drying, snow melting, and balneology (spas and public baths) – most of which are currently heated by natural gas.

1.4 Current Study

Western Canada's economy is strongly tied to its oil and gas industry. Through the years, over 600,000 oil and gas wells have been drilled in Alberta alone. (Dachis, Shaffer & Thivierge, 2017). The Alberta Energy Regulator (AER) estimates current provincial hydrocarbon reserves at 164 billion barrels of crude bitumen (often referred to as oil sands), 1.7 billion barrels of conventional crude oil, 816 billion cubic metres of natural gas, and 33.1 billion tonnes of coal (AER, May 2019). Due to its economic dependence on hydrocarbon production, Alberta is among Canada's leading emitter of greenhouse gases. In 2017, Alberta was responsible for ~38% of the national total greenhouse gas emissions, despite having just over 10% of Canada's population (Environment and Climate Change Canada, 2018). While oil and gas production is responsible for 48% of those emissions, Alberta's electricity sector also produces more gross greenhouse gas emissions than any other province in Canada due to its reliance on coal-fired generation (Environment Canada, 2019).

Both the provincial and federal governments have acknowledged the importance of climate change and indicated that reducing GHG emissions is a priority. Indeed, Alberta was the first jurisdiction in North America to put a price on carbon emissions in 2007 through the euphemistically named *Specified Emitter Regulations* (ERA Ecosystem Services, 2014). Although this price has been retained and even increased, under a newly elected conservative government in 2019, carbon emissions have continued to increase while other province's emissions have remained relatively static or decreased (Environment and Climate Change

Canada, 2020). New tactics are needed and increasing Alberta's energy generation from renewable sources is one way to achieve reduced greenhouse gas emissions.

Despite the ubiquitous use of data from the oil and gas sector in geothermal research throughout the WCSB, there is a marked lack of research concerning the repurposing of oil and gas infrastructure for geothermal production in Western Canada. The purpose of the research presented in this report is to fill this gap with a comprehensive investigation of geothermal development opportunities in brownfield hydrocarbon settings. Re-purposing existing oil and gas infrastructure for geothermal energy exploitation addresses issues such as high carbon emissions, inactive well liability, stranded asset devaluation, and other challenges faced by an evolving energy market in the 21st century.

In this study, we investigate several salient aspects of large-scale repurposing hydrocarbon production infrastructure for geothermal energy exploitation. First in Chapter 2, we present a basin-wide audit of existing hydrocarbon infrastructure in terms of number of fields, as well as their average depths and temperatures, that could potentially be repurposed. Then, in Chapter 3, we present three separate methods of assessing the geothermal potential of these fields. The methods presented include (1) a Monte Carlo simulation based on heat-in-place methodology, (2) well-head sum total generation, and (3) favourability mapping. These methods are then applied to several hydrocarbon fields in Alberta's Swan Hills region as a case study, as shown in Chapter 4.

Geothermal power production from hydrocarbon reservoirs in the WCSB would involve the circulation of millions of cubic meters of formation fluids per year. Such fluid circulation is accompanied by significant geochemical risk. Therefore, we also conducted a basin-wide survey of the types of formations that may be produced during geothermal power production and, using equilibrium thermodynamics, identified the scale-forming minerals most likely to form as a result of non-isothermal brine circulation. This research is presented in Chapter 5.

After investigation the thermodynamic potential and associated geochemical risks of retrofitting full hydrocarbon fields, we looked at the technology, economics, and applications of repurposing single well bores for geothermal power productions. In Chapter 6, we developed a tube-in-annulus design and thermodynamic models for single sealed well deep borehole heat exchangers. In Chapter 7, we present a cost model for such a design. Deep bore hole heat exchangers may not produce enough heat to generate

electricity, but low-enthalpy applications of geothermal power in a cold climate such as Western Canada are numerous. As an example of a forward-thinking, innovative use of low-enthalpy heat in a local Albertan context, we performed a case study on applying this technology to heat cattle feed water in the winter for large herd maintenance. This case study is presented in Chapter 8.

All of the geotechnical research that went into this project is being summarized and hosted in a product called the Geothermal Atlas of the Western Canadian Sedimentary Basin. In the course of this study, we developed a beta-version of this atlas with full functionality centered around the Swan Hills region. The beta-version of the atlas was developed in partnership with the Alberta Geological Survey, who is also currently hosting the product. An overview of the atlas' development, design, and functionality is presented in Chapter 9.

Finally, in chapter 10, we use a comparative jurisdictional review to delineate some of the social and political structures that could facilitate a successful transition from hydrocarbon to geothermal production. Despite technical capabilities, studies show that public perception and policy can be significant limiting factors in geothermal development. We examine how stakeholders' discourse, networks, and resources interact over time to impact the success or failure of geothermal development within oil producing economies. Convergence of these three elements of agency (discourse, resources, and networks) are keys to the successful repurposing of Western Canada's oil and gas infrastructure for geothermal power production in a new, emergent energy economy.

A summary of major results and recommendations for future research are found in the conclusion.

2 Overview of oil and gas infrastructure in Alberta

2.1 Overview

This section provides a summary of all oil and gas fields in Alberta with potential for being repurposed geothermal power production. Data for all hydrocarbon wells in Alberta deeper than 1500 m were gathered from geoSCOUT's data. This depth was selected to eliminate wells that are too shallow under normal geothermal gradients (i.e. 25 – 35 ˚C/km) for geothermal power production. The data was then organized by individual field name. Individual fields contain data from different depths and different formations. The data fields included for each well entry are listed below in Figure 1

Table 1: Data fields for each geoSCOUT well entry

CPA Pretty Well ID	Well Status Text
Cur Operator Name	Org Operator Name
Date Well Licensed	Surface Abandonment Date
Surface Abandonment Type	Reference (KB) Elev. (m)
Logger (KB) Elev. (m)	MD (All Wells) (m)
TVD (m)	Surf-Hole Latitude (NAD83)
Surf-Hole Longitude (NAD83)	Bot-Hole Latitude (NAD83)
Bot-Hole Longitude (NAD83)	BH Temp. (degC)
Prod./Inject. Frmtn	Prod Status Text
Producing Field/Area Name	Producing Pool Name
Producing Unit Name	Production-Casing Depth (m)
Surf-Hole Easting (NAD83)	Surf-Hole Northing (NAD83)
Surf-Hole Zone (NAD83)	

Data for each field was organized in Excel workbooks. Average Temperatures (°C), average depths (m), number of wells, and land area (km^2) for each field were calculated and displayed in a summary sheet at the beginning of each the workbooks, as well as in a separate master workbook. The temperatures from the well data and the average temperatures calculated for each field are not corrected. For accurate temperatures and geothermal gradients to be expressed, a temperature correction for each well with a BHT must be applied. Correcting temperatures for every well identified in this study was beyond the scope of this project.

All Fields were separated and organized in Excel using the macro shown in Table 1

Table 2: Macro steps to separate and organize oil and gas fields

```
Sub SplitandFilterSheet()
'Step 1 - Name your ranges and Copy sheet
'Step 2 - Filter by Department and delete rows not applicable
'Step 3 - Loop until the end of the list
Dim Fields As Range
Sheets("Master").Select
Set Fields = Range("Fields")

For Each cell In Fields
Sheets("Master").Copy After:=Worksheets(Sheets.Count)
ActiveSheet.Name = cell.Value

With ActiveWorkbook.Sheets(cell.Value).Range("MasterData")
.AutoFilter Field:=19, Criteria1:="<>" & cell.Value, Operator:=xlFilterValues
.Offset(1, 0).SpecialCells(xlCellTypeVisible).EntireRow.Delete
End With

ActiveSheet.AutoFilter.ShowAllData
Next cell
End Sub
```

Porosity and permeability data were gathered from GeoSCOUT's core analysis tab. An example of the data is summarized below in Table 3. Porosity is reported as a volume fraction decimal. Permeability is reported in milliDarcys.

Table 3: Porosity and permeability data example for the Ireton, Leduc, and Ellerslie formations

Formations	Porosity (frac)	Kmax (mD) Avg	Kvert (mD) Avg	K90 (mD) Avg	Depth (m) Avg
Direton	0.08	2.60	5.90	N/A	1542.20
Dleduc	0.06	761.36	291.83	447.07	1558.44
Kellrslie	0.15	84.85	17.44	37.63	1232.09

Each Field contains core data from multiple formations, resulting in the need to separate each of the fields into formations for the porosity and permeability data. The formation data were separated into different sections for wells producing from multiple formations and wells producing from a single formation. Porosities and permeabilities were not averaged for formations due to the numeric and spatial variability of the data. The calculated results would be over generalized and provide little benefit to further research.

The third subcategory are the oil and gas *units*, which are organized using the same Excel macro as the fields category. Many of the wells do not have a unit listed. These wells are separated into a separate workbook. Due to long unit names, each unit has an abbreviated name.

2.2 Results

Most oil and gas wells in Alberta are deeper than 2000 m and are concentrated towards the western parts of Alberta. There are 480 oil and gas fields mapped in Alberta. Average field temperatures range from 25 – 126 ˚C. Average depths range from 1520 – 4578 m. Average geothermal gradients range from 8 – 44 ˚C/km. Fields with highest geothermal potential are in Western and Northern Alberta. The fields with the highest temperatures and depths are located on the south west part of Alberta near the Rocky Mountains.

Table 4 shows the total depth distribution by TVD of the wells gathered from geoSCOUT. This data shows that most of the wells are shallow (<2000m). The deepest wells are over 5000m, but only account for 0.1% of total wells.

Table 4: Depth distribution by TVD (m) of wells gathered from geoSCOUT

Vertical Depth (m)	# of Wells	% of Wells
1000 – 2000	118966	66.3%
2000 – 3000	48958	27.3%
3000 – 4000	10458	5.8%
4000 – 5000	967	0.5%
5000+	97	0.1%

Figure 1 shows a histogram of the oil and gas fields' temperature distributions. These temperature data are averaged from all wells that were drilled in a given field, resulting in data coming from potentially multiple formations in the subsurface.

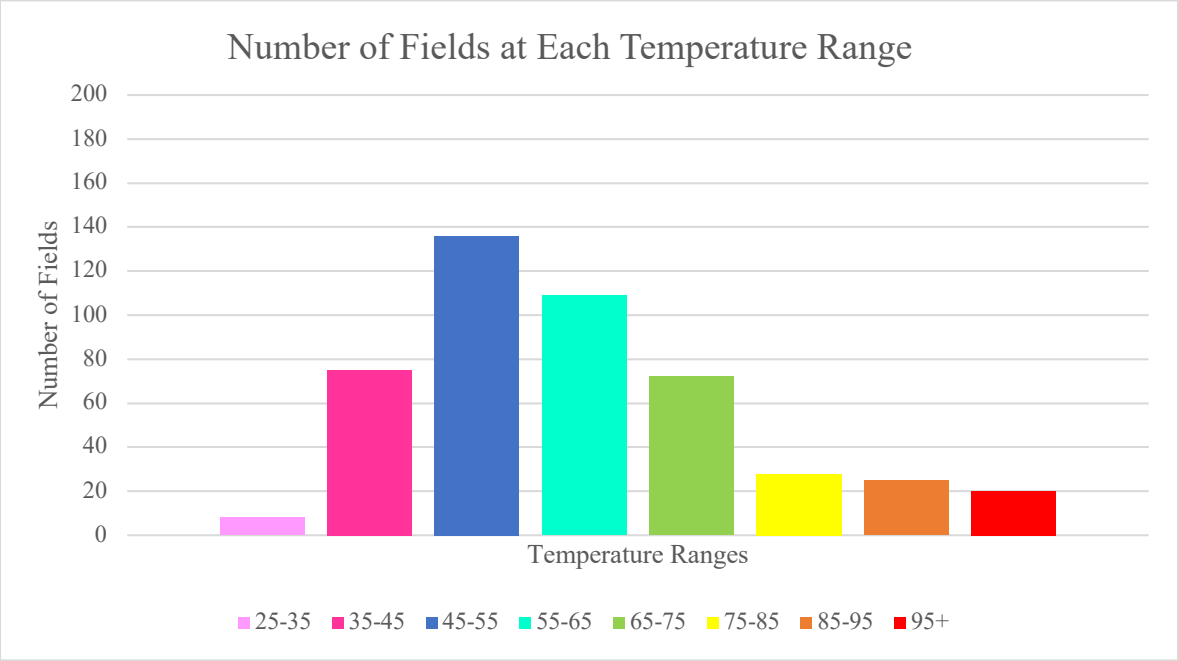

Figure 1: Distribution of temperatures across oil and gas Fields in Alberta. Most of the fields have average temperatures between 45 and 75 ˚C.

Nearly 140 fields have temperatures between 45 and 55 ˚C, and over 100 fields have temperatures between 55 and 65 ˚C. About 20 fields have average temperatures over 95 ˚C, which the required temperature for producing geothermal electrical power in a cold climate. An additional ~20 fields have temperatures between 85 – 95 ˚C. These fields could also produce geothermal electrical power with moderate advancement in low – enthalpy power production technology.

Figure 2 is a map made created using ArcMap that shows the geographic distribution of average oil and gas field temperatures throughout Alberta. The overall trend shows temperatures increasing from the Northeast to the West-Southwest. The hottest temperatures are found in the Jasper – Banff area of the Rockies. The temperatures decrease as one traverse East into the foothills, where medium to high temperatures of 55+ (°C) are located. This temperature trend matches the WCSB's deepening from NE Alberta to SW. Another

trend present is a general increase in temperature from southern Alberta to Northern Alberta; the majority of the lowest temperature fields are present in southern Alberta.

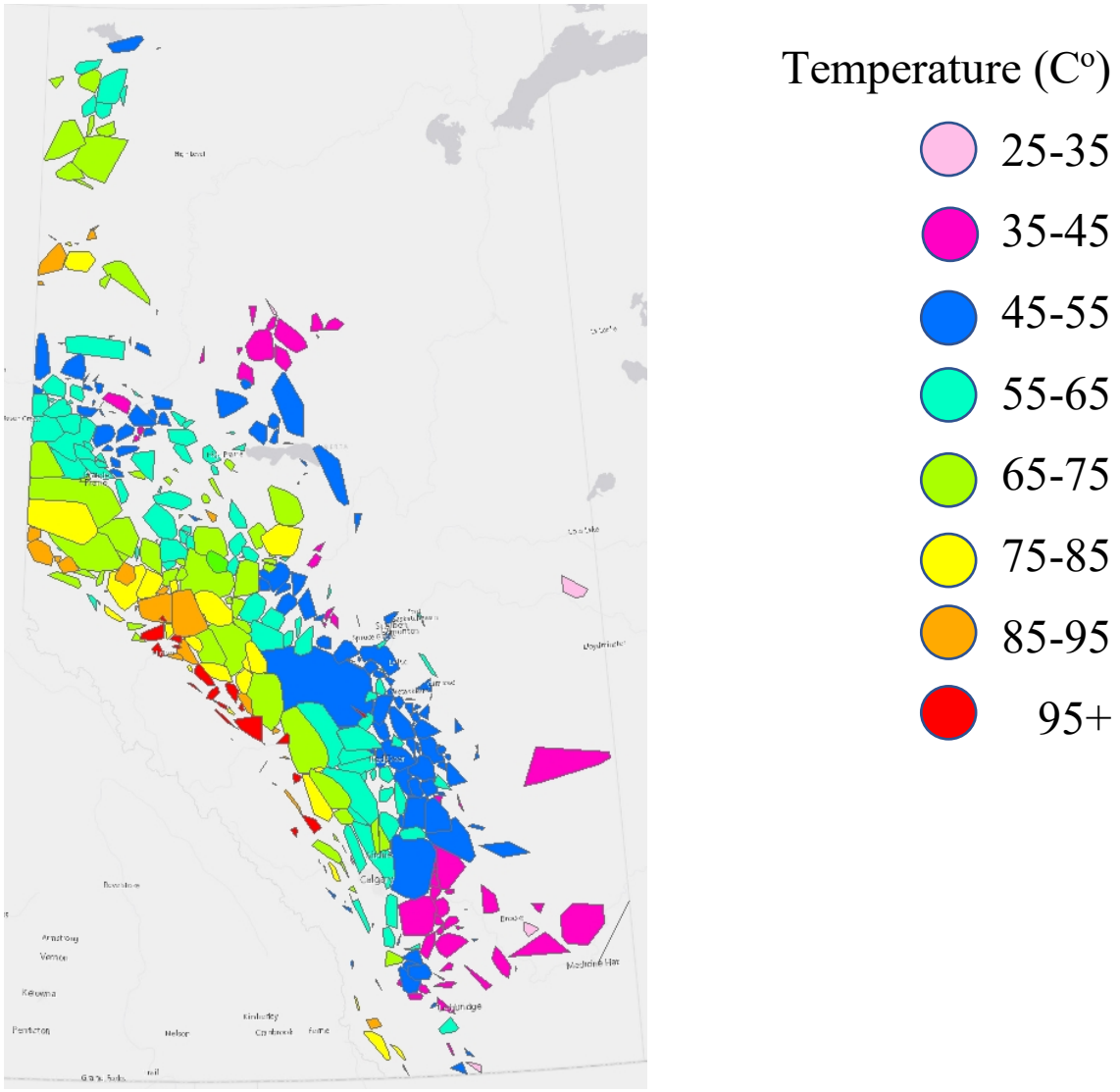

Figure 2 Average temperatures of oil and gas fields across the Western Canadian Sedimentary Basin

The general trend of temperature distribution throughout the basin closely follows the trend in basin depth. Average field depths are shown in Figure 3The depths range between 1500 m to over 3500 m. The deepest fields are in SW Alberta, following the deepening trend of the WCSB. The shallowest fields are present from southern Alberta all the way to Northern Alberta. The shallow wells are present on the eastern side of

the province and are the furthest from the Canadian Rockies. The deepest fields are present near the Rocky Mountains and have the smallest land area coverage.

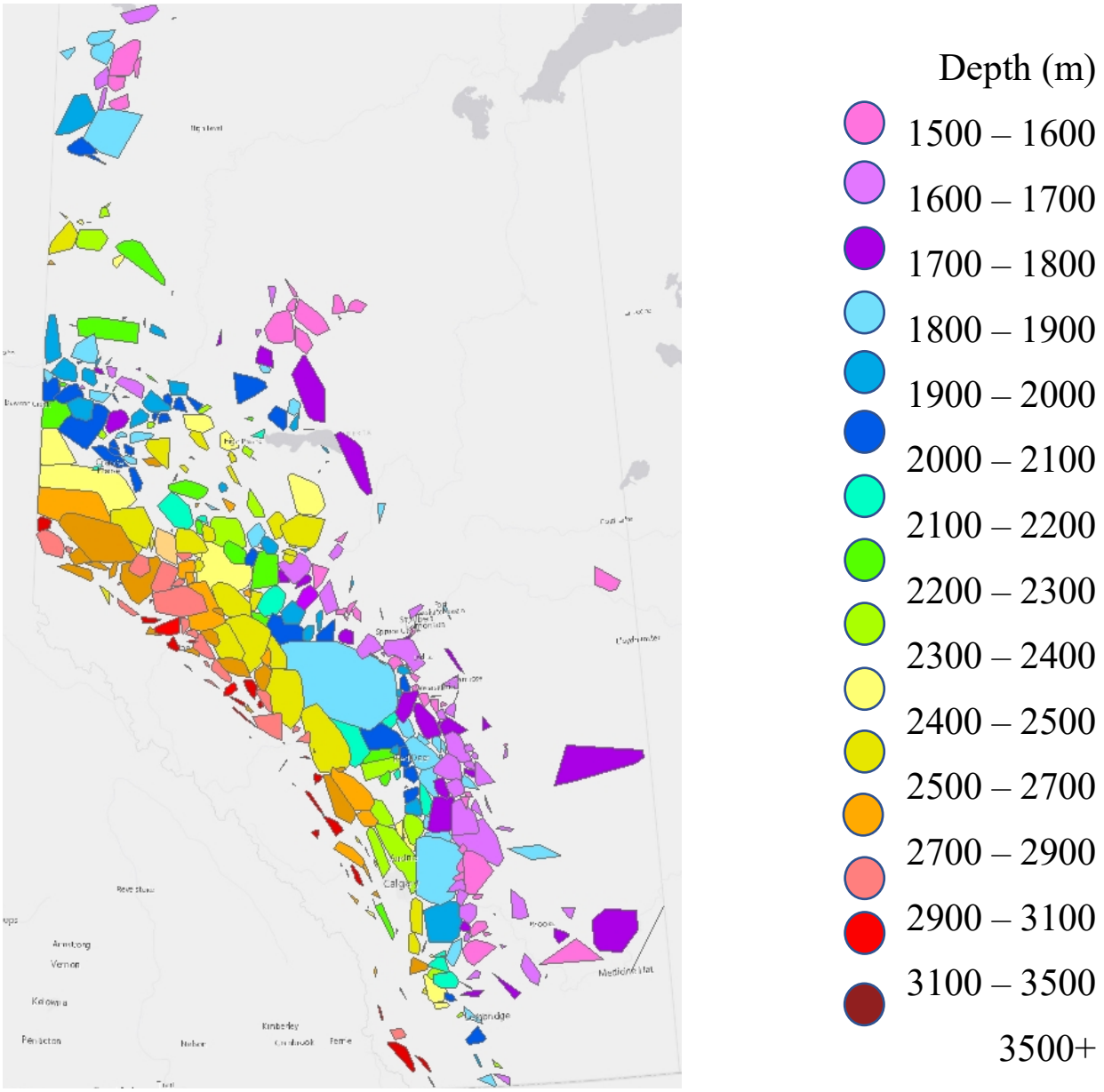

Figure 3 Average depth of oil and gas fields across the Western Canadian Sedimentary Basin

Figure 4 is adapted from Figure 3.4 of the Alberta Geological Survey's Atlas of the Western Canadian Sedimentary Basin. The cross section of the WCSB shows the trend of the sedimentary wedge thickening

towards the Rockies and thinning towards the Canadian Shield which was mentioned previously in the descriptions of Figures 2 and 3. Both the temperature and depth distribution of oil and gas fields throughout Alberta closely follow the thickening trend of the basin from East to West.

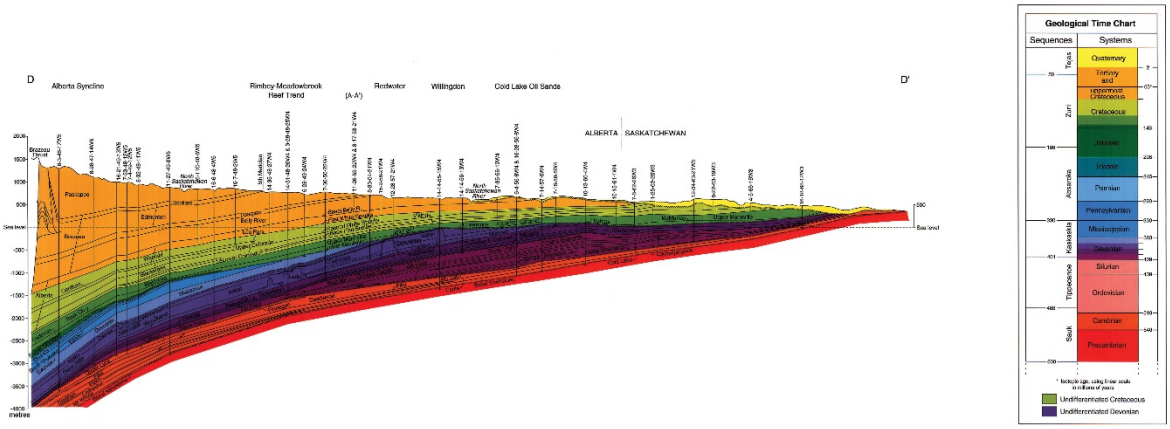

Figure 4: Cross-section of the WCSB (Adapted from Fig 3.4, Chapter 3 of the AGS Atlas of the WCSB)

This overview reveals the potential for the development of geothermal energy for both direct use and as electrical power production. Electrical power production is only possible in areas with the highest temperatures, but is possible with the proper infrastructure and nearby consumers. Direct use can be implemented using lower temperatures and can be accessed in a wide range of fields throughout Alberta. Areas that can potentially exploit geothermal electrical power are communities within the Rockies and Foothills sections of Alberta. Fields near communities with average temperatures above 60 (ºC) have high potential to be exploited. These Fields are located in Northwestern Alberta, specifically the Fields around and north of Grand Prairie. The coldest temperatures with little to no geothermal potential for electrical or direct use are in Southern Alberta. One possible immediate application of geothermal resources is assisting with oil extraction from the oil sands in Alberta and heating homes during the winter. A possibility for further research and another possible exploitation of geothermal resources is in the storing of heat during the summer to then use in the winter, but this would require a very particular set of variables to align, and a more complex economic model to see if it is viable.

3 Methods for the determining the geothermal power potential of an oil and gas field

3.1 Overview

This section details three separate methods for determining the geothermal power potential of a repurposed oil and gas field. The first method combines a Monte Carlo simulation with a volumetric heat-in-place method to determine the power potential of an oil and gas field as a bulk reservoir as geothermal energy. The second method calculates the power potential of the field based on the sum of the production potentials at each individual well head. The third method overlays field temperatures and well bore water flow rates to create semi-quantitative favourability maps of the most promising regions within field for geothermal power production.

3.2 Volumetric Method

The gross thermal and electrical power potential for a hydrocarbon field taken as a single geothermal reservoir was estimated according to a method described first by Banks and Harris (2018) and then updated using a Monte Carlo simulation with 10,000 iterations (Banks et al 2020). This method was developed within the context of this study and was subsequently (in the next section) applied to the reefs of the Swan Hills regions.

A table (Table 5) of variables associated with this method and used in the following equations is found later in this section. First, a uniform distribution of a reservoir's estimated volume is calculated. Then the method calculates the bulk energy of content of the reservoir with respect to the ambient environmental conditions at the surface:

(eq. 1) $$(Q_r) = (V_{rock}Cp_{rock)} + (V_{brine}Cp_{brine})]*(T_r - T_0)$$

Where Q_r is the thermal energy content of the reservoir in kilojoules (kJ), $V_{rock,brine}$ is the volume of the subscripted material in cubic meters (m^3), and $Cp_{rock,brine}$ is the volumetric heat capacity of the subscripted material in kilojoules per cubic meter Kelvin (kJ/m^3K). T_r and T_0 are the reservoir and ambient environmental temperatures, respectively, in K. Reservoir temperatures are custom inputs from the well data. Ambient conditions are a Gaussian distribution of monthly air temperatures taken from nearby weather stations.

The rock and brine volumes are functions of the reservoir's porosity (θ) and bulk volume (V_{bulk}):

(eq. 2) $V_{rock} = (1-\theta V_{bulk})$

(eq. 3) $V_{brine} = \theta V_{bulk}$

Porosity values must be derived from field-specific data.

The amount of the reservoir's heat (Q_r; kJ) that can be brought to the surface (Q_{surf}; kJ) is estimated by applying a recovery factor (γ):

(eq. 4) $Q_{surf} = \gamma Q_r$

An even distribution of recovery fractions between 5% and 15% is assigned as the simulation input. This is a conservative estimate based on the work of Williams (2007). The amount of fluid in kilograms required to transport this heat to the surface (M_{surf}) is defined by the quotient of the Q_{surf} and the difference in the transport fluid's enthalpy (ΔH) between the reservoir and ambient temperatures:

(eq. 5) $M_{surf} = Q_{surf} / \Delta H$

Any of several online steam tables will show the enthalpy of liquid water to be a linear function of temperature (T):

(eq. 6) $H = (4.2477*T) - 1{,}163.5735$

The exergy (W_A; kJ) of the reservoir, or amount of energy available to perform useful work is a product of surface flow rate and the thermodynamic losses associated with the fluid's temperature drop between the reservoir and ambient temperatures:

(eq. 7) $(W_A) = M_{surf}*(\Delta H - T_0\Delta S)$

Here, similar to the enthalpy, the change in entropy (ΔS) is a regressive function available from standard steam tables:

(eq. 8) $\Delta S = 3.521E\text{-}08\ T_{(r,0)}^3 - 2.461E\text{-}05T_{(r,0)}^2 + 1.516E\text{-}02T_{(r,0)} + 2.504E\text{-}03$

The system's gross thermal power potential in megawatts (MW_{th}) is then obtained by dividing the exergy (W_A) by 1000 times the duration of production (t) in seconds. The divisor of 1000 is used to convert from kilowatts to megawatts:

(eq. 9) $MW_{th} = W_A /1000*t$

The gross electrical power is calculated by applying a heat-to-electricity conversion factor (η) to the gross thermal power:

(eq. 10) $MW_e = \eta MW_{th}$

where η is function of $T_{r,}$ according to the work of Augustine et al. 2009:

(eq. 11) $\eta = [(0.3083*T_r)-98.794]/100$

A number of other meaningful output variables can be derived from this heat-in-place analysis, including the bulk flow rate (M_{bulk}; kg/s) required for maximum resource exploitation:

(eq. 12) $M_{bulk} = 1000*MW_{th}/(Cp_{brine}*\Delta T)$

the specific flow rate (M_{sp}) required per unit thermal or electrical power production ($MW_{th,e}$):

(eq. 13) $M_{sp} = M_{bulk}/MW_{th,e}$

and the specific power potential (MW_{sp}) per unit reservoir volume (km^3):

(eq. 14) $MW_{sp} = (MW_{th,e}/V_{bulk})^{*}10^{\wedge 9}$

Table 5: Table of variables, symbols, units, and input types for Monte Carlo simulations

Variable	Symbol	Units	Type	Values
Reservoir bulk energy	Q_r	kJ	Output	= (VrockCprock) + (VbrineCpbrine)]*($T_r - T_0$)
Rock heat capacity	Cp_{rock}	kJ/m^3K	Custom	From user input
Brine heat capacity	Cp_{brine}	kJ/m^3K	Custom	From user input
Reservoir bulk volume	V_{bulk}	m^3	Even	Query result of full reservoir volume
Porosity	Φ	decimal	Custom	Query result from well data
Reservoir rock volume	V_{rock}	m3	Output	= (1-Φ)Vbulk
Reservoir brine volume	V_{brine}	m3	Output	= ΦVbulk
Reservoir temperature	T_r	K	Custom	Query result from well data
Reference temperature	T_0	K	Gaussian	From user input
Recovery factor	γ	decimal	Custom	From user input
Gross surface energy	Q_{surf}	kJ	Output	= γQ_r
Gross mass of fluid	M_{surf}	kg	Output	= Q_{surf} /ΔH
Enthalpy	H	kJ/kg	Output	= (4.2477*T) - 1,163.5735
Entropy	S	kJ/kgK	Output	= ΔS = 3.521E-08 T^3 – 2.461E-05T^2 + 1.516E-02T + 2.504E-03
Exergy	W_A	kJ	Output	= M_{surf}*(ΔH – T_0ΔS)
Time	t	seconds	Custom	From user input
Gross Thermal Power	MW_{th}	MW	Output	= (W_A/t)/1000
Gross Electrical Power	MW_e	MW	Output	= ηMW_{th}
Electricity conversion factor	η	Decimal	Output	= [(0.3083*T_r)-98.794]/100
Gross bulk flow rate	M_{bulk}	kg/s	Output	= 1000*MW_{th}/(Cp_{brine}*ΔT)
Specific flow rate	$M_{sp,th,e}$	(kg/s)/MW	Output	= $M_{bulk}/MW_{th,e}$
Specific power potential	MW_{sp}	MW/km^3	Output	= $MW_{th,e}/V_{bulk}$*$10^{\wedge 9}$
Well head thermal potential	kW_{th}	kW_{th}	Output	= ṁ*Cp_{brine}* ΔT
Well head electrical potential	kW_e	kW_e	Output	= ηkW_{th}

3.3 Well head power generation

The well head power generation method calculates the geothermal power potential of a hydrocarbon field as the sum of the geothermal power potential at each individual well head within the field. Well head power generation is determined based on the standard thermal power equation:

(eq. 15) $$kW_e = \eta\ (\dot{m})(C_{p(brine)})(dT)$$

where kWe is the gross electrical output, $\dot{m}$ is the brine's flow rate, C_p is the brine's specific heat and η the heat to electricity conversation factor defined in equation 11. The temperature and flow rate data are specific to local field conditions. The specific heat of water is a function of temperature that can be found on the United States' National Institute of Standards and Technology (NIST) website.

3.4 Favourability Mapping

3.4.1 Data and Methods

Geothermal favourability maps are designed to locate favourable sites within existing oil and gas fields for the development of geothermal energy resources. They are produced by geospatially overlapping bottom hole temperature and flow rate data taken from drill stem tests (DSTs). Bottom hole temperature and flow rates are site specific and must be obtained from current field operators for most accurate results.

3.4.2 Favourability mapping procedure

Geographic information system software (i.e. ArcMap) overlays sets of geospatial data related to criteria involved in determining favourable areas for geothermal energy developments into a 'geothermal favourability map' of each field. These maps display a visualization of the 'favourability score' at any given location within each field. The favourability score is the weighted sum of the criteria scores based on bottom hole temperatures and flow rates.

The favourability score is generated using a weighted linear combination of two criteria related to geothermal energy production, flow rate of water and temperature. Input data from these criteria cannot be

summed directly because of the different units and scales of each. In order to enable the weighted summation, the flow rates (kg/s) and temperatures (ºC) are converted into a common unit-less scale based on a linear decay. The lowest values are converted to 0 and the highest values are converted to 1. These new values on a scale of 0 to 1 are the favourability scores of each criterion. They identify the degree to which each criteria is satisfied at any given location.

A geostatistical interpolation is used to create a layer based on the newly converted temperatures and flow rates. These layers are converted into rasters that contain georeferenced 100 x 100 m cells containing individual favourability scores of each criterion. The raster layers for each criterion are assigned weights of 0.5 and are summed together using the raster calculator tool in ArcMap. Figure 5 shows a flow chart of the favourability scoring. We assumed the maximum extent of each reservoir to be 800m around the outermost wells of each field. The areal extent of each field was applied to the favourability score layers as the reservoir boundaries. The resulting favourability score outputs of the weighted summation process are plotted on a geospatially referenced map using a colour scale. The final favourability map (Chapter 4; Figure 16) highlights locations where geothermal energy production is most favourable in any given field.

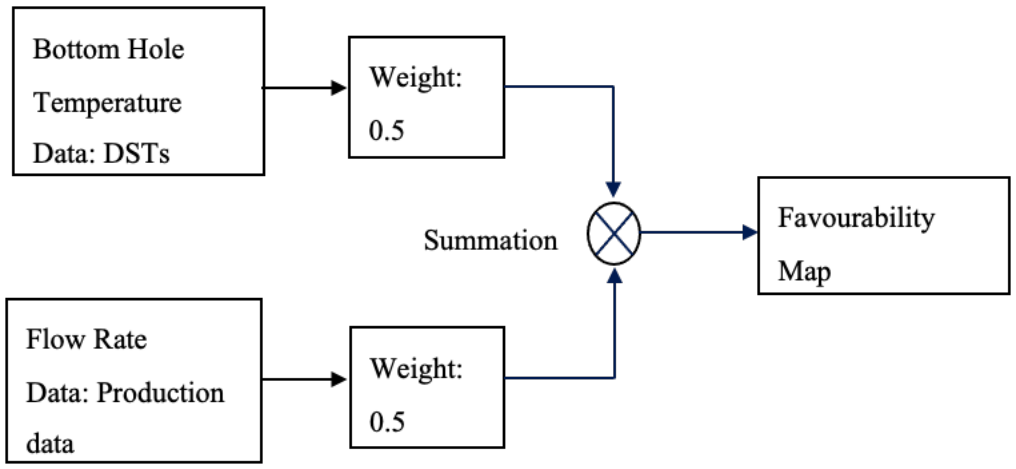

Figure 5: Schematic Representation of Favourability mapping methodology

4 Application the methods to the Swan Hills region

4.1 Geology of the Swan Hills reef complex

The Swan Hills reef complexes are a part of the larger Beaverhill Lake Group which was deposited during the middle to late Devonian in Central Alberta. This formation is composed of large carbonate platforms and reef complexes. The Swan Hills Formation, specifically, is composed of two members – an overlying reef member, and an underlying platform member which are predominantly composed of limestone with spatially heterogeneous lithofacies. These complexes are the target of this investigation into geothermal development potential due to existing infrastructure which would allow for the production of geothermal energy using a co-produced fluid design.

The carbonate reefs and platforms of the Swan Hills Formation, as shown in Figure 6, are members of the larger Beaverhill Lake Group. This package of sediment was deposited between the late Middle Devonian and early Late Devonian over Central Alberta, when northern seas invaded the craton, forming a basin. This basin was situated within 20 degrees of the paleo-equator and was in a northeast-trending trade wind belt (Weissenberger et. al. 2016). These conditions allowed for widespread growth of platform carbonates along landmasses at the eastern margin of the continent and topographic highs west of the margin. The Western topographic highs are known as the Peace River Arch and Alberta Ridge. Carbonate development occurred on both the Western and Eastern sides of these landmasses. The Swan Hills Formation is the shelf complex that formed to the east of the Alberta Ridge. The Eastern Shelf margin carbonates and the Swan Hills Formation are separated by a deeper basin known as the Waterways Basin.

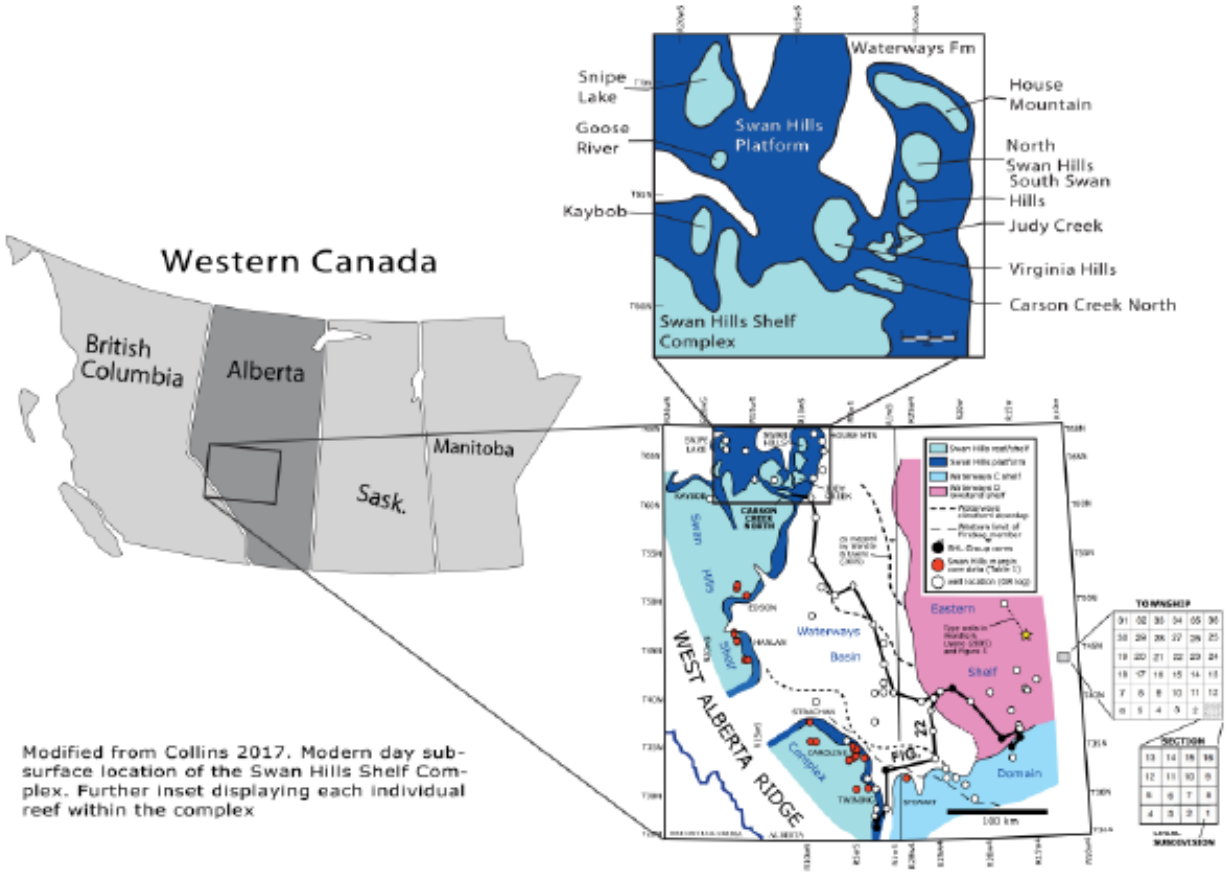

Figure 4: Modern subsurface location of the Beaverhill Lake group shelf distribution, reproduced from Collins (2017).

The Swan Hills Formation is composed of an upper and a lower member. The lower member is a regionally extensive underlying carbonate platform with thicknesses ranging from 40 to 60 metres. The platform is overlain by patchy reef complexes, generally trending in a N-S pattern. The reef complex sizes vary from reef to reef and are typically tens of kilometres wide and from 30 to 70 meters in thickness. The Swan Hills Formation is surrounded by the Waterways Formation, which is composed of tight calcareous shales that deposited contemporaneously and filled the basin around the reef complexes.

The platform and subsequent reefs grew in three distinct cycles, related to sea level changes occurring over 1 to 10 million years. The first transgressive sequence (BHL1) is responsible for the deposition of the Swan Hills platform, followed by significant sea level drop and exposure. The second transgression is responsible for atoll growth over the platforms (BHL2), once again followed by major exposure during sea level fall.

The final transgression (BHL3) is associated with a change in depositional style to ramp-like sediments capping the reef complexes and drowning of the reef.

Individual reef complexes have a stepwise taper towards the interior as they develop vertically. Figure 7 shows a schematic drawing of this geometry. These "backsteps" are a result of finer sea level cycles occurring on the order of ten to one hundred thousand years (4th order cycles). Evidence of these backsteps is present in exposure surfaces correlated across the reefs. Mapping the fourth order cycles is critical to understanding how the vertical geometry of reservoir-associated lithofacies transposed over time.

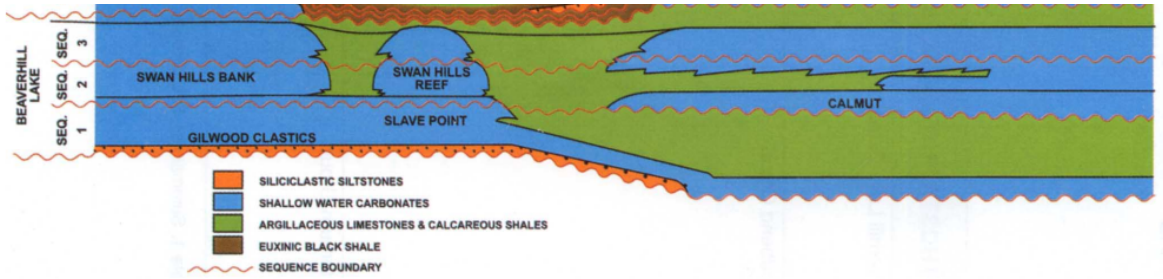

Figure 5: Reproduced from Potma (2001). BHL sequences and sequence boundaries for the Swan Hills Shelf Complex

4.2 Lithology and facies distribution

The reefs in the Eastern shelf complex of the Swan Hills Formation are not significantly dolomitized and retain much of their original limestone composition and original rock fabric. Although the reef complexes and platforms are largely limestone, the depositional style of the reef is heterogeneous and, depending on the lateral position, different lithofacies will be observed. The lithofacies deposited at any given location is dependent on the original environmental setting. By modern and ancient analogue, the depositional styles of the reefs are known, and facies models can be used to describe and link the observed lithofacies to their environmental setting and lateral position on the reef. South Swan Hills has developed with rim-bounded character, as seen in Figure 8. The hydrogeologic properties of the subsurface reservoirs (porosity and permeability) are primarily controlled by the original depositional texture of the rock. By understanding the facies distribution in the subsurface, it is possible to map out the lateral reservoir units.

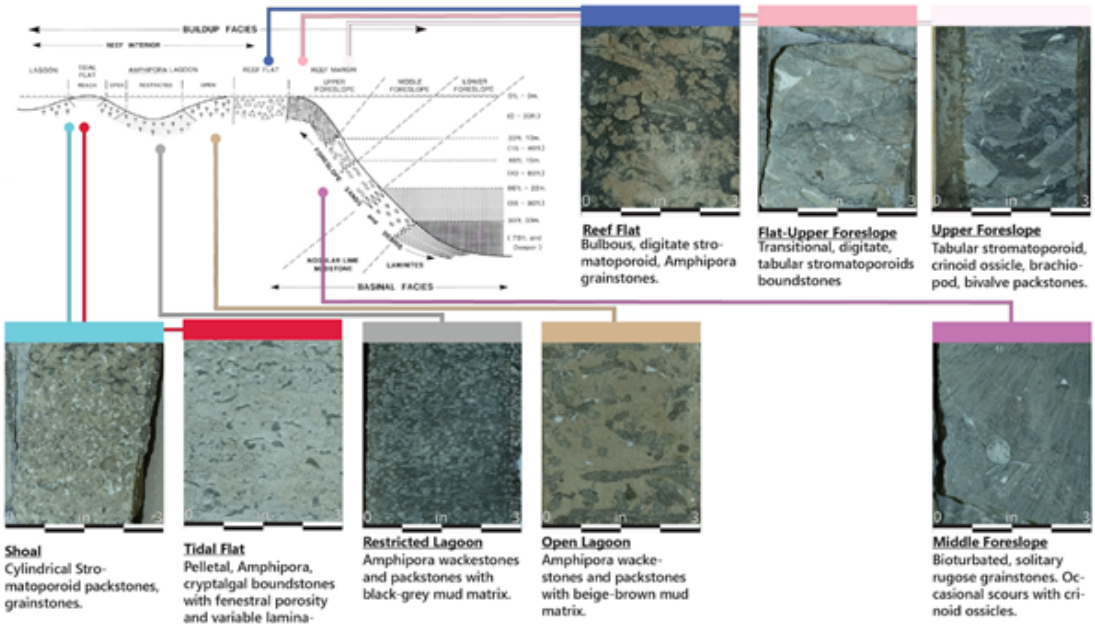

Figure 6: A rim-bounded reef facies model (modified from Wendte 1992), superimposed with core photographs of the different lithofacies of the South Swan Hills reef complex. Higher, turbulent conditions at the reef flat deposited coarser grainstones. These grainstones are considered to be the primary reservoir target with permeability values ranging from 10-100 mD and porosity values from 10-20%

4.3 Hydrocarbon production in the Swan Hills region

Hydrocarbon production in the Swan Hills region began in 1957, with the first well exploiting oil from the Virginia Hills reef complex. By the 1970s, over 1500 wells were drilled into reef complex reservoirs, effectively mapping out the extent of the atolls (Viau, 1987). Currently, there are about 3000 wells in total across all the atolls in the Swan Hills. Current estimates of the reef suggest that the total reserves in the Beaverhill Lake Group are 5.6 billion barrels of oil, of which, 2.9 billion barrels of oil have been extracted. Additionally, 7.62 trillion cubic feet (Tcf) of natural gas has been extracted. By the 1980's, the reservoirs were largely driven by waterflooding. Today, the reservoirs are still prolific oil and gas reservoirs but also produce up to 15000 m^3 of hot water daily making them attractive reservoirs for co-production of geothermal energy.

4.4 Detailed results for the Virginia Hills field

In this course of this study, all 8 of the reefs in the Swan Hills complex were analyzed for Razor Energy with all three of the aforementioned evaluation methods. In this report, we provide detailed results for the

Virginia Hills field as an example of how the results appear. Virginia Hills is the largest of the reefs in the Swan Hills complex. All data used in this evaluation was taken from geoSCOUT. A summary of the results is shown in Table 6. A detailed discussion of the field-specific inputs and results are found below.

Some 320 wells were drilled into the Virginia Hills oil field, of which 30 have cored sections and 150 have depth data on the top and base of the Swan Hill Formation. Fluid properties and historical production data from 190 suspended oil wells in the field were taken from geoSCOUT. These production data included Bottom Hole Temperature and average daily oil and water production rates from the last year of operation. Bottom hole temperature corrections were made using a 'time since circulation' method (Corrigan, 2003). Only data from suspended oil wells were collected. Abandoned wells were neglected due to the difficulty of bringing these wells back into operation.

Table 6: Results of heat-in-place Monte Carlo Simulation for the Virginia Hills oil field in the Swan Hills region of Alberta

Virginia Hills	Range	Mode	Median	25%	75%	Mean	Std. Dev.
Bulk Res. Energy (PJ)	152-522	316	325	296	353	324	43
Energy at Surface (PJ)	9-67	34	32	24	40	32	10
Exergy (PJ)	2-29	8	10	8	14	11	4
Thermal Power (MWth)	3.05-36.33	10	13.30	9.95	17.27	13.91	5.08
Electrical Power (MWe)	0.30-7.03	2	2.05	1.49	2.74	2.17	0.90
Specific thermal Flow rate (kg/s/MWth)	1.53-5.16	2	2.42	2.23	2.66	2.48	0.36
Specific electric Flow rate (kg/s/MWe)	7.91-57.05	14	15.38	13.53	17.89	16.70	5.47
Specific Electrical Power (MW/km^3)	0.22-5.23	1	1.52	1.11	2.04	1.62	0.67
Specific Thermal Power (MW/km^3)	2.27-27.03	8	9.90	7.40	12.85	10.35	3.78
Per Wellhead Electrical Power (MWe)	0-1.20	0	0.0141	0.00164	0.178	0.111	0.175
Per Wellhead Thermal Power (MWth)	0-6.64	0.10	0.0984	0.011	1.25	0.714	1.09

4.5 Detailed data inputs and results

A uniform distribution of the estimated bulk rock volume was assumed. The maximum bulk rock volume in this distribution was the volume of the entire Swan Hills Formation. This volume was derived from the top and base surfaces of the Swan Hills Formation in the Virginia Hills field, which were generated using formation depth data points from the geoSCOUT database. The minimum bulk rock volume was estimated by using core-plug porosity logs to establish a shallower base reservoir surface. These logs indicate that mainly the top layer of the carbonate platform is porous. The base of this porous rim was interpreted on the logs by assuming a porosity cutoff value of 5%. By interpolating the depth of these interpretations between wells, the base of the reservoir for the minimum bulk rock estimate was generated. The minimum bulk rock volume was calculated as the volume between the top of the Swan Hill Formation and this surface, as shown in Figure 9. For simplicity, the angle of the reef margin slope volume was assumed to be vertical. We assumed that the maximum extent of the reservoir was 800 m around the outermost wells of the field. This is the distance between wells in the nine-spot grid. We used this value because we assumed that if the reservoir would extend further, an additional rim of wells would have been drilled.

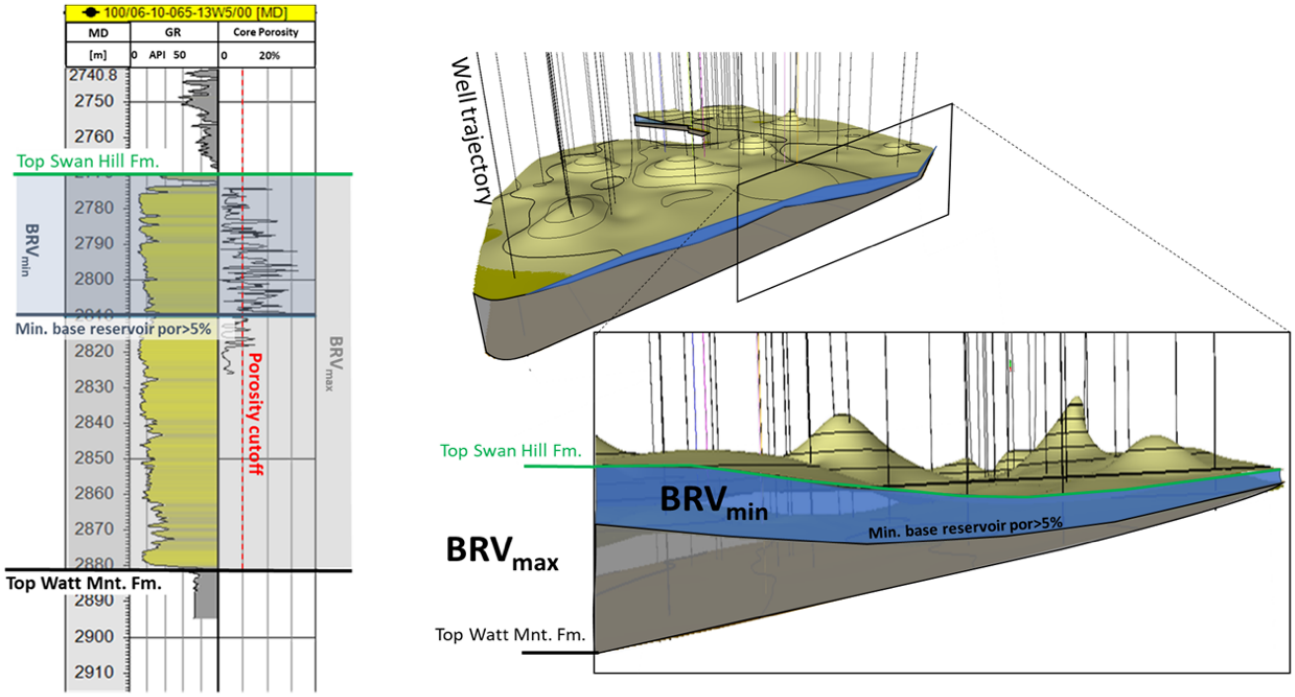

Figure 7: Example of derivation of the minimal and maximal reservoir base surface on a Gamma Ray (GR) log and core-plug porosity log. Interpolation of these surfaces formed the bases for calculating the maximum and minimum value of the bulk rock volume distribution.

4.6 Input Variable Distributions

The top of the Swan Hill Formation in the Virginia Hills field is characterized by mounds of carbonate reef ranging from 40 to 60 m in height (**Error! Reference source not found.**). The base of the Swan Hill F ormation is formed by the southwest dipping shelf of the Watt Mountain Formation, on which the carbonate complex developed. The thickness of the Swan Hills Formation varies from some 20 m in the eastern part of the field to 120 m in the southwest and extends ~180 m below the mounds. The volume of the entire Swan Hills Formation is 2.3e10 m^3, which is the high end of the uniform distribution of the bulk reservoir volume in the Monte Carlo simulation estimate. The low end of the bulk reservoir distribution, which was derived from the 5% porosity cutoff, is 9.6e9 m^3.

With these input parameters, the bulk reservoir volume calculated by the Monte Carlo simulation is 16.3 ± 3.88 km^3. The mean and median of the porosity calculated porosity distribution, based on a custom input

distribution, are 0.08 ± 0.02 (one standard deviation) and 0.08. The mode of the porosity distribution is 0.06. Thus, the simulation calculates the volume of reservoir rock and brine in the Virginia Hills field to be 14.96 ± 3.59 km^3 and 1.35 ± 0.46 km^3, respectively.

The corrected bottom hole temperatures for the wells in the Virginia Hills field range from 63 – 114 °C with an average 95 ± 10 °C. The custom distribution of reservoir temperatures entered into the Monte Carlo simulation results in a calculated distribution of 100.35 ± 47.3 ˚C (mean ± 1 standard deviation), with a median of 99.75 ˚C and a mode of 98.45 ˚C. Monte Carlo simulation inputs for the ambient temperature were given as a Gaussian distribution of the mean and standard deviation of the average air temperature in Swan Hills, AB, i.e. -0.5 ± 10.8 ˚C. The resulting Monte Carlo distribution of ambient temperatures is -0.65 ± 10.7 ˚C. Both the median and mode of the distribution are also -0.65. Monte Carlo distributions for both the reservoir and ambient temperatures are shown in Figure 10.

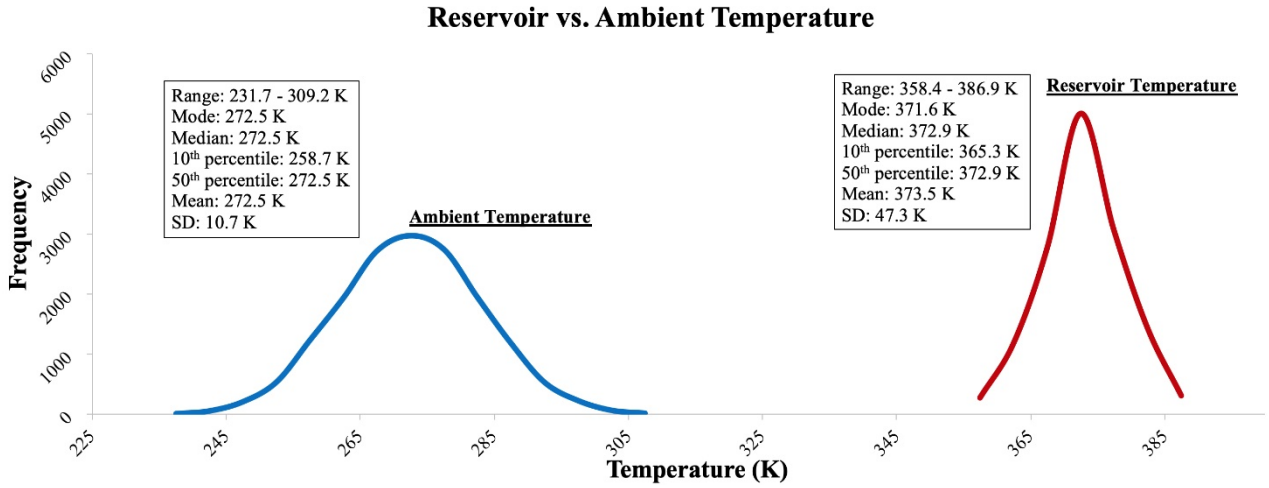

Figure 8: Ambient (blue) and reservoir (red) temperature input distributions

4.6.1 Reservoir energy content

The energy content of the Virginia Hills reef was calculated as a bulk property of the reservoir, a property of the reservoir considered in light of a recovery factor, and in terms of the field's exergy. Results from all three of these calculations are shown in Figure 11. The total energy content of the reservoir, Q_r is calculated to be 4.03 ± 1.08 Petajoules (PJ). An even input distribution of 0.05 – 0.15 recovery factors yields simulated

recovery factor of 0.1 ± 0.03. Applying this recovery factor results in surface energy content (Q_{surf}) of 0.4 ± 0.16 PJ. Delivering this heat to the surface requires moving 9.44e11 ± 3.61e11 kilograms of fluid to the surface. Factoring in the thermodynamic losses associated with producing this fluid yields 0.14 ± 0.06 PJ of exergy, or useable work, at the surface.

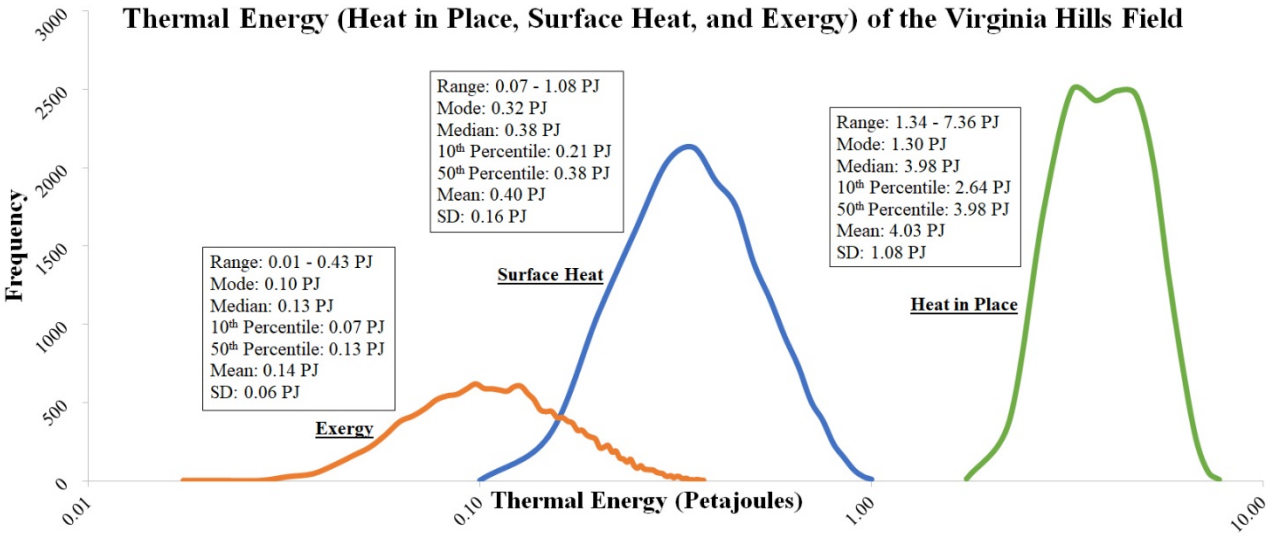

Figure 9: Thermal energy content of the Virginia Hills oil field

4.7 Power Potential Calculation

Results for gross thermal and electrical geothermal power potential from the Virginia Hills oil field are shown in Figure 12. Amortizing the field's thermal exergy over a 25-year production period results in a gross thermal power potential of 172.4 ± 75.7 MW_{th}, with a median and mode of 159.3 MW_{th} and 125.0 MW_{th}, respectively. Based on the range of input temperatures, the average heat-to-electricity conversion factor (γ) is 0.16 ± 0.02. This factor yields a gross electrical power potential of 29.9 ± 13 MW_e, with a median of 25.5 MW_e and a mode of 22.5 MW_e.

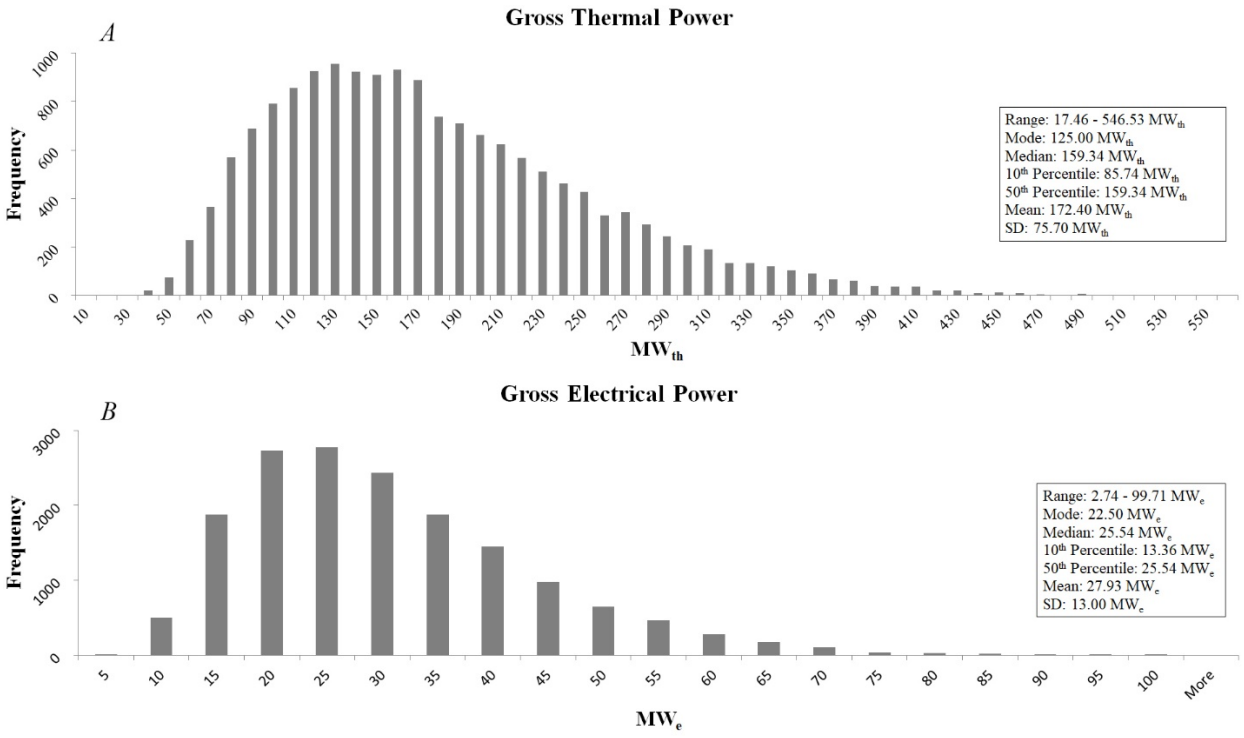

Figure 10: Gross thermal (left) and electrical (right) power production predictions for the Virginia Hills oil field

4.8 Specific Power Metrics

Results from the gross power calculations are used to estimate the power potential on a per-cubic kilometer of reservoir basis, as well as to compute the flow rate (in kg/s) required to produce a megawatt of power. These results are shown in Figure 13. According to our simulation, a cubic kilometer of reservoir has an average geothermal power potential of 10.5 ± 3.8 MW_{th}/km^3. Applying the same heat-to-conversion factor discussed above (eq. 11) results in a specific electrical power potential of 1.71 ± 0.67 MW_e/km^3. The flow rates required to produce 1 megawatt of thermal and electrical power are $2.41 \pm .031$ kg/s per MW_{th} and 15.22 ± 3.12 kg/s MW_e, respectively.

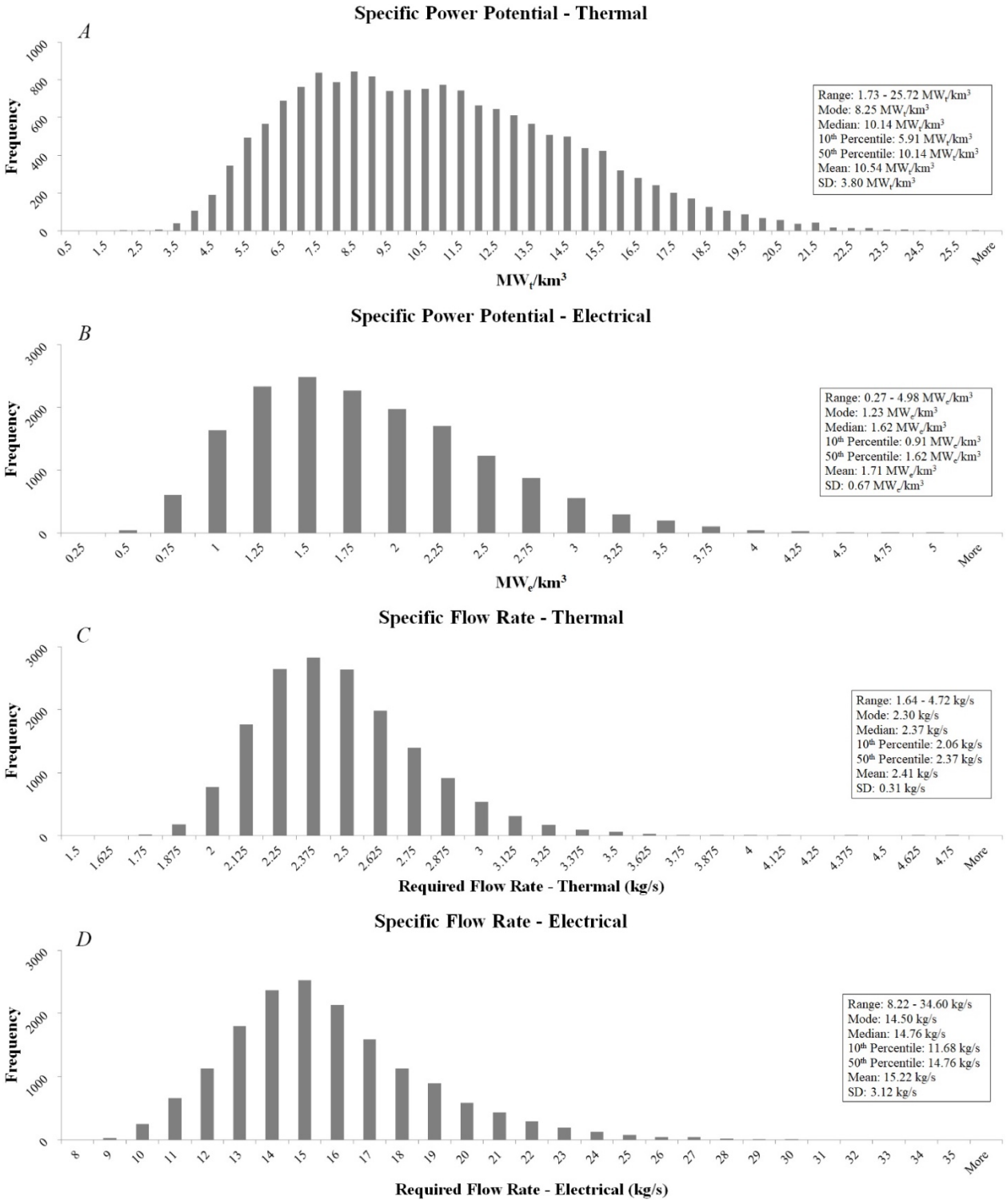

Figure 11: Specific power (MW/km3; above) and specific flow rate (kg/s per MW; below) for thermal (left) and electrical (right) power

4.9 Wellhead Power Potential

4.9.1 Deterministic wellhead calculations

A scatterplot of the well temperatures and flow rates used in the deterministic calculations of wellhead power potential are shown in Figure 14. The temperature inputs are the same custom reservoir temperature distribution used as the Monte Carlo simulation input, i.e. 95 ± 10 ˚C. The average flow rate is 1.56 ± 2.68 kg/s. Wells with the highest water cut also have the highest flow rates, as shown in Figure 7. Eight of the wells have flow rates of at least 10 kg/s, and twenty-wells have flow rates greater than 5 kg/s.

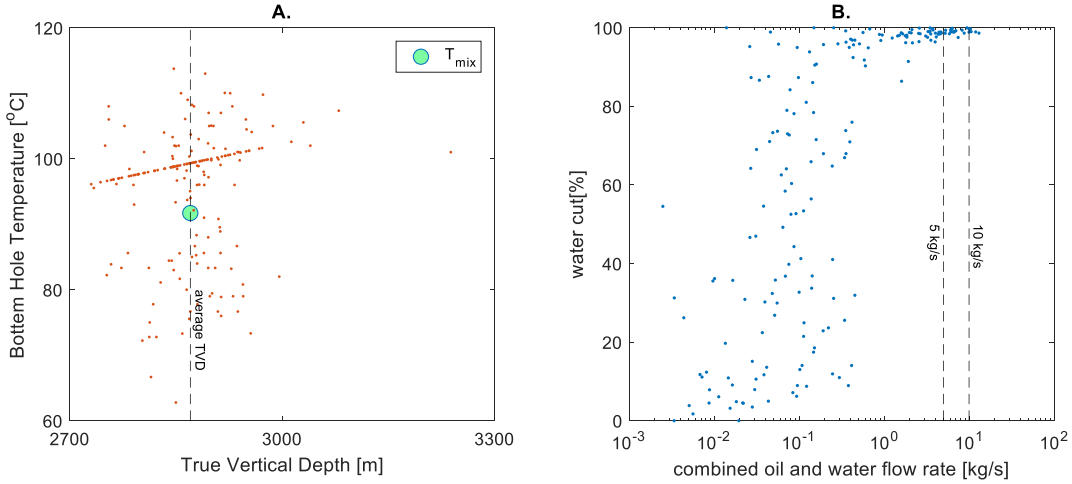

Figure 12: (A) Bottom Hole Temperature and (B) frequency distribution of oil and gas flow rates all 190 suspended oil wells in the Virginia Hills field.

The average thermal and electrical power potential per well is 0.6 ± 1.0 MW_{th} and 0.085 ± 0.15 MW_e respectively. The total power available from all wells is ~115 MW_{th} and 16 MW_e. The large standard deviation is due to the bimodal distribution of flow rates, with several values being greater than 5 kg/s and many values being fractions of kg/s. If only the top 20 producing wells are chosen, the average well head production estimates are 3.05 ±0.84 MW_{th} and 0.436 ± 0.162 MW_e. The total power available from the top 20 performing wells (a somewhat arbitrary cutoff) is ~64 MW_{th} and ~9.2 MW_e. Under the given conditions, 53 wells may produce more than 100 kW_e. The average power potential of these 53 wells is 1.97 ± 1.1 MW_{th} and 0.28 ± 0.17 MW_e. The total power potential for these 53 wells is ~104 MW_{th} and 14.9 MW_e.

4.9.2 Wellhead Monte Carlo Simulation

According to the Monte Carlo simulation, the average thermal and electrical power capable of being produced at individual well flow rates is 0.63 ± 1.09 MW_{th} and 0.102 ± 0.18 MW_e, respectively. The wells range in thermal and electrical power production from 3.88e-5 to 7.37 MW_{th} and 5.57e-6 to 1.32 MW_e respectively. The thermal and electrical power output of wells is skewed towards the lower range of values, with median values being below the mean in both cases, indicating that a small number of high output wells are increasing the average power output. Summary of statistics can be found for individual wellhead thermal and electrical power analyses in Figure 15. If the average per-wellhead power potential from the Monte Carlo simulation is applied to the whole Virginia Hills field (n_{wells} = 316), the total thermal and electrical power potential is 199.08 MW_{th} and 32.36 MW_e, respectively.

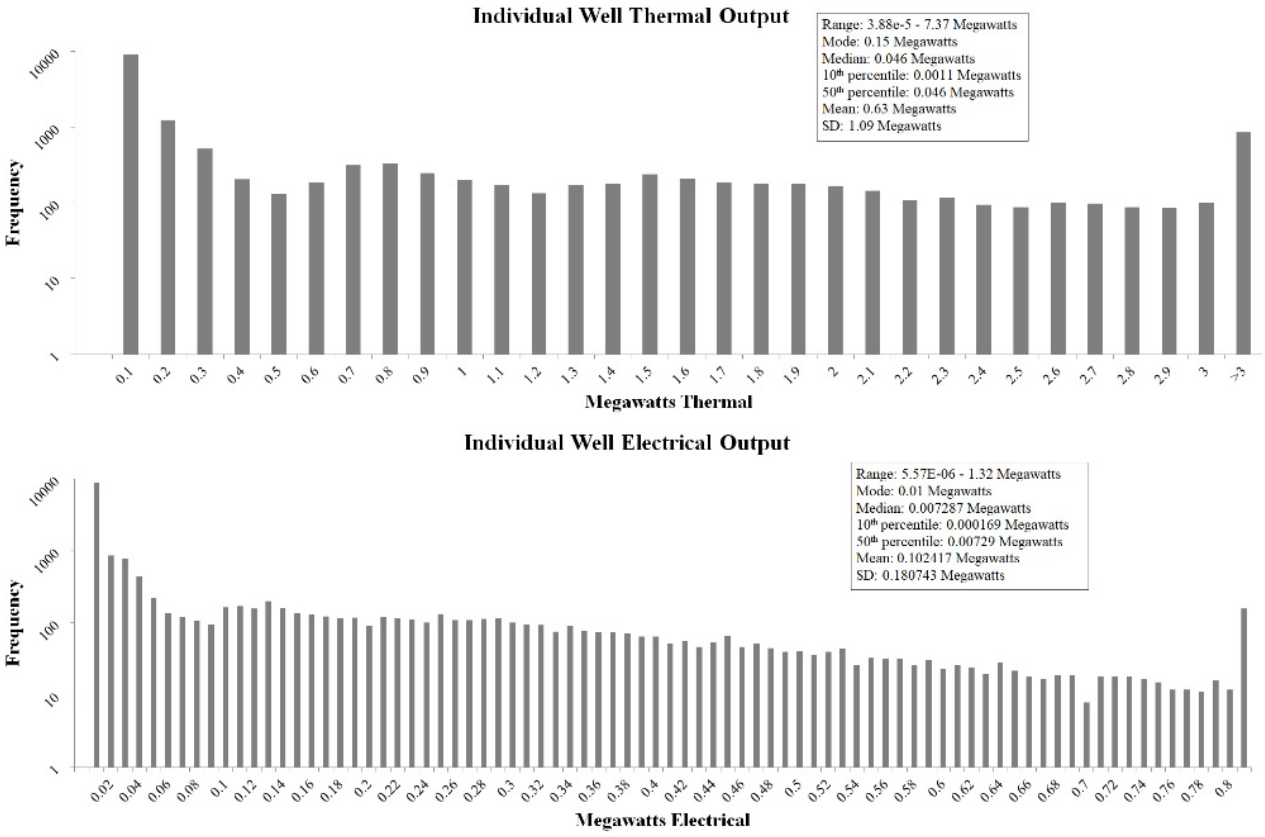

Figure 13: Monte Carlo results for individual well gross thermal (top) and electrical (bottom) power potential

4.10 Favourability Map

Figure 16 show a geothermal power favourability map of the Virginia Hills field. The favourability scores range from ~0.50 to greater than ~0.75. Overall, these results suggest that whole field is suitable for geothermal power production. The most favourable areas are found in the East-central and northern parts of the field. In particular, there are three wells in East-central part of the field that are most favourable for geothermal power production.

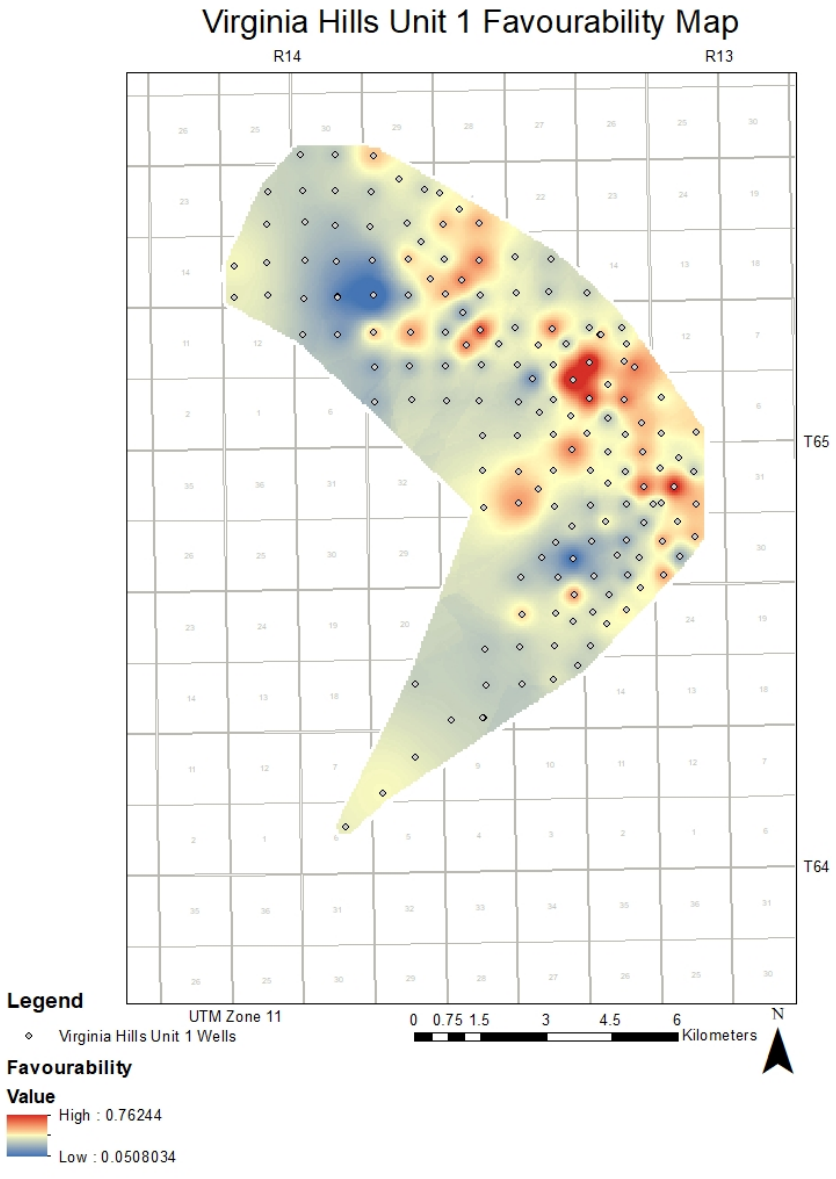

Figure 14 Geothermal favourability map for the Virginia Hills field

5 Geochemistry

5.1 Introduction

Producing geothermal power from repurposed hydrocarbon fields requires circulating millions of cubic of meters of formation fluids from a reservoir, to the surface, and back into the reservoir. This non-isothermal circulation of brine is accompanied by significant geochemical risk. In this section, we present a principle-component analysis and multivariate statistical categorization of the brine chemistry found in four major Devonian formations in the Western Canadian Sedimentary Basin. The goal of this work is to understand how regional brine chemistry variability may affect local geothermal development outcomes. The four formations are the Leduc, the Swan Hills, the Granite Wash, and the Gilwood. These formations host abundant oil and gas resources and have been previously identified as prime targets for geothermal power development (Banks and Harris, 2018).

Over the last 50 years, numerous studies have focused on the geochemical and hydrogeological evolution of formation waters in the Western Canada Sedimentary Basin (Anfort, 1998; Bachu, 1995, 1997; Billings et al., 1969; Connolly et al., 1990; Hitchon et al., 1994; Michael et al., 2003; Rostron et al., 1997). Due to easy access to well test data from hydrocarbon activities, a plethora of basin-scale flow models have been developed for the WCSB. All of these studies cumulatively reveal a dominant gravity-driven flow system through Paleozoic carbonates, from south to north in the Alberta basin (Anfort et al., 2001; Bachu, 1997, 1995; Bachu and Hitchon, 1996; Garven, 1985). Hitchon et al. (1971) performed a volume-weighted mean composition analysis of 78 formation waters from the Western Canada Sedimentary Basin that revealed a composition with 1.3 times the salinity of seawater. In the Alberta portion of the Western Canada Sedimentary Basin, Connolly et al. (1990) studied the isotopic and chemical characteristics of forty-three formation waters sampled from different formations and geographical locations, from the Devonian to the Cretaceous periods. The samples were, for the most part, Na-Cl brines, where sodium comprised >90% of the total cations and chlorine comprised >98% of the total anions. With charge balance errors < ±2%, the formation waters ranged from 4 g/l to 235 g/l (80 ± 47 g/l; mean ± 1 standard deviation) of total dissolved solids. These waters' temperatures ranged from 35 °C to 75 °C (53 ± 10 ºC), with depths from 680 m to 1970 m (mean: 1333±312 m). Connolly et al. (1990) distinguished three groups based on the chemistry of the formation waters: (I) carbonate-hosted with the deepest stratigraphy, (II) clastic reservoirs, and (III) entirely clastic hosted with the shallowest zone of stratigraphy. The end-member brines in groups I and II were formed by seawater evaporation, which was then later diluted (50-80%) by meteoric waters to form sodium-bicarbonate dominant chemistry assigned to group III.

Previous hydrogeochemical studies in the Western Canada Sedimentary Basin often focused on singular aspects of groundwater resources (e.g. groundwater flow) or assessed groundwater hydrochemistry at a local scale and with a reasonably smaller number of water samples (e.g., Connolly et al., 1990). The need to conduct a comprehensive study of regional deep basin brine geochemistry, therefore, is a crucial requirement for geothermal energy development. A multivariate statistical approach, such as principle component analysis and hierarchical cluster analysis, provides a tool to capture regional variability in fluid chemistry and its effects on geothermal energy development. Many researchers have implemented principle component analysis and hierarchical cluster analysis for visualizing and evaluating potential geothermal resource areas and comparing them with proven resources (e.g., Shi et al., 2017; Chatterjee et al., 2019 and 2017; Lindsey et al., 2018). Although Hitchon et al. (1971) carried out factor analysis for 78 formation waters from the Western Canada Sedimentary Basin, a detailed multivariate analysis throughout the basin had yet to be done either for groundwater characterization or for geothermal exploration.

Our study aimed to find the most significant chemical constituents of the brine samples found throughout major geothermal reservoirs in the Western Canadian Sedimentary Basin and their influence on geothermal power production parameters, such as pumping power and scaling risks. We used 1963 brine sample data points, which is two orders of magnitude greater than the number employed in any previous study. After conducting rigorous quality control to select the highest quality and representative brines samples found in four formations in the WCSB, we implemented a principle component analysis to evaluate the chemical variability. We then executed clustering algorithms, i.e. hierarchical and k-means cluster analysis, to assess potential hydrogeological groupings. The influential parameters in each group assisted in establishing representative brine samples to incorporate into geothermal maps and models of the WCSB.

5.2 Geochemistry Methods

Data for fluid analyses, depths, and well locations used in this study were primarily obtained from IHS' AccuMap® and geoLOGICS's geoSCOUT. We employed various data-culling techniques for quality control of the dataset. The final numbers of samples used in this study are 598, 609, 498, and 258 for the Leduc, Swan Hills, Granite Wash, and Gilwood formations, respectively. Once we completed the principle component analysis, clustering algorithms were implemented to evaluate potential hydrogeological groupings. Next, to assess the physicochemical processes of groundwater evolution, the groups were spatially displayed on the map of Alberta. Finally, we analyzed the influence of the transport properties of the fluids concerning parasitic power loads and the geochemical risks in terms of scaling.

Several factors can lead to erroneous incorporation of this data, such as incorrect data entry, poor logging practices, and insufficient quantities of recovered formation fluids. Our chemistry data was subjected to systematic culling. For example, samples were flagged or excluded if (i) sample locations were ambiguous, or test types were inappropriate (ii) the charge balance error was more/less than 10%; (iii) the ratio of sodium and chloride is more than 1.0, but the sodium and calcium ratio is less than 1.2 (indicating acid water completion fluid and presence of significant mud in the samples (iv) pH values were less than 4 or more than 9 (indicating samples dominated by acid water, or corrosion inhibitor completion fluid); (v) densities are less than 1.0 g/cm^3 (indicating alcohol contamination);; (vi) the sample interval is more than 50 m and/or straddles multiple formations; and (vii) fluid was recovered over an interval of less than 100 m along the drill stem during well testing. Figure 17 shows an abridged flowchart of the data processing method.

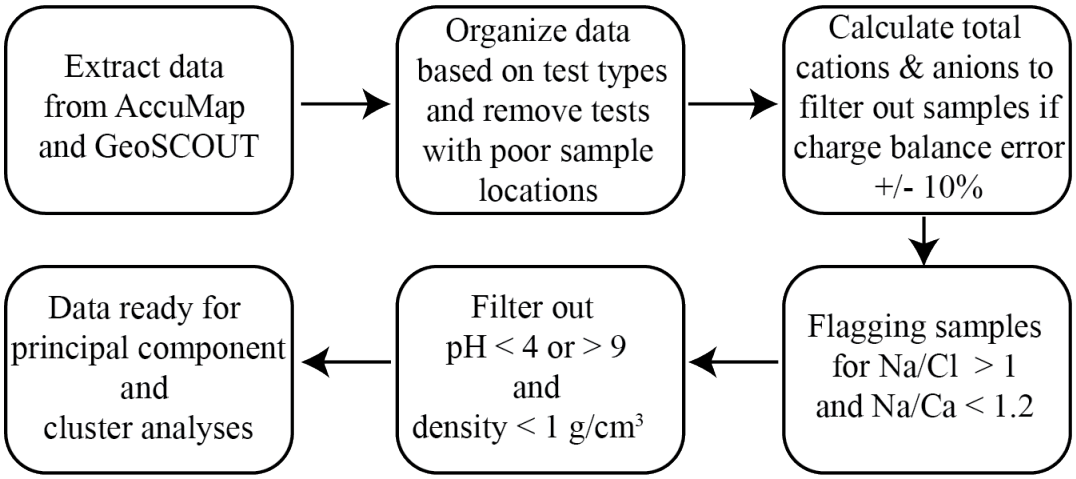

Figure 15: Flowchart describing the culling criteria for the chemistry data in order to identify formation water from contaminated samples to perform the multivariate analyses.

The final dataset for the principle component analysis was compiled with 8 continuous, real number-valued variables. These variables include sodium (Na^+), potassium (K^+), calcium (Ca^{2+}), magnesium (Mg^{2+}), chlorine (Cl^-), bicarbonate (HCO_3^-), sulfate (SO_4^{2-}), and pH. The coordinates of the wells, Easting and Northing, are included to assist in visualizing their locations during the spatial displays of the groups derived from cluster analysis. The most critical components for geothermal development are suitable temperatures. The temperature measurements for these wells, however, are often missing or erroneous. The

much-studied temperature gradients in the WCSB are considered a better representation of the temperature (Nieuwenhuis et al., 2015). Therefore, often the depths are considered more appropriate to estimate the temperature from the geothermal gradient. Around 50% of our samples have reliable temperature data.

5.3 Multivariate and cluster analyses

A principle component analysis is first implemented as a multivariate analysis tool to construct and use a reduced set of new variables called principle components, which contain most of the information, i.e., the measure of variance, within the initial variables. A detailed discussion of the principle component method can be found in Abdi and Williams (2010). The analysis is performed by determining a set of eigenvectors and the associated eigenvalues for the covariance matrix of the dataset. Principle components that describe the highest variability in the data are selected for further analysis, including clustering.

Hierarchical cluster analysis is performed as an initial screening method to visualize the distinct clustering patterns in the geothermal brine properties based on the well locations, after the methods of Lindsey et al. (2018). The potential clusters are visualized by overlaying the distribution of principle components on a map. A cluster dendrogram obtained from the hierarchical cluster analysis can further demonstrate the more robust clustering structures.

Finally, K-means clustering, a clustering method that evaluates the relationship between numbers of observations (i.e., wells representing the samples) without being trained by a dependent variable, is implemented to partition the objects into K number of groups (Lindsey et al., 2018). In our case, the Hierarchical cluster analysis and the robust cross-validation methods helped determine the optimal number of clusters, K, a predetermined number of clusters for the K-means clustering. The clusters are plotted in relation to the principle components to identify the influential components in each group and displayed spatially on Alberta's map to visualize their locations. Both the principle component analysis and cluster analysis are done in the environment of the programming language R.

5.4 Precipitation models

We used the results of the cluster analyses to speciate aqueous geochemical models in the Geochemist Workbench® (GWB). Models were based on equilibrium thermodynamics around the principle of Gibb's Energy minimization. The GWB is an industry-leading softrware, although programs, notable PHREEQc, may be able to replicate these models, albeit with less sophistication. The modeling process in the GWB

is a follows: Representative samples from each group in the four formations, as derived from the cluster analysis, were carefully selected based on the availability of temperature data and consistency with the median distributions. The GWB application is set to React in the launch window of the GSS's analysis tab, and the 'precip = off' is deleted from the trailer command. In the subsequent basis tab of the React window, the temperature is selected for the sliding temperature option. The initial temperatures are set to the measured values for each of the sample/groups, and the slide temperatures are put for the ambient air temperature (0 ºC). If the initial temperature is greater than 100 ºC, the H_2O on the Basis tab is set to 1 kg of solvent instead of 1kg of free solvent to eliminate the loss of water to a vapour phase. The model is then run to calculate the mineral precipitation. The model is also configured to suppress the dolomite, as the reaction kinetics of dolomite are slow enough to prevent it from precipitating from a solution.

5.5 Geochemistry Results

5.5.1 Distribution of the chemistry and reservoir properties in the Devonian formations

Results showing the ionic concentrations within the investigated geothermal brines are shown in Table 7. The major chemical components found in the four formations' fluids are sodium, potassium, calcium, magnesium, chloride, bicarbonate, and sulfate. The fluids' total dissolved solids range from ~7 g/l (Leduc) to ~345 g/l (Granite Wash). The mean total dissolved solids ± standard deviation for the Leduc, Swan Hills, Granite Wash, and Gilwood Formation are 158.04 ± 68.86, 151.98 ± 51.39, 215.26 ± 36.36, and 216.35 ± 41.79, respectively. The fluids' pH range from 4.2 (Gilwood) to 9.0 (Swan Hills). The average pH for each of the four formations is near neutral to weakly acidic. The total dissolved solids are dominated by sodium and chlorine. Chlorine concentrations range from 0.87 g/l (Leduc) to 215.6 g/l (Granite Wash), with averages ± one standard of 96.78 ± 43.75 g/l, 92.83 ± 32.32 g/l, 133.55 ± 22.78 g/l, and 133.9 ± 25.98 g/l for the Leduc, Swan Hills, Granite Wash, and Gilwood, respectively. Sodium concentrations for the Leduc, Swan Hills, Granite Wash, and Gilwood, respectively, are 42.32 ± 16.98 g/l, 45.64 ± 15.60 g/l, 56.28 ± 9.70 g/l, and 59.29 ± 12.82 g/l, with a low of 1.11 g/l (Leduc) and a high of 117 g/l (Granite wash). The remainder of the cations required to charge balance are supplied by calcium, potassium, and magnesium. In addition to alkali and alkali earth metal chloride salts, the fluids also contain consequential amounts of various anions. Bicarbonate is found in concentrations ranging from 0.002 g/l (Leduc) to 7.81 g/l (also Leduc). The mean and standard deviation of bicarbonate concentrations for the Leduc, Swan Hills, Granite

Wash, and Gilwood, respectively are 0.75 ± 0.68 g/l, 0.39 ± 0.59 g/l, 0.09 ± 0.09 g/l, and 0.15 ± 0.12 g/l. Another important contributing anion is sulfate. The mean and standard deviation of sulfate concentrations for the Leduc, Swan Hills, Granite Wash, and Gilwood, respectively are 1.16 ± 1.93 g/l, 1.05 ± 1.12 g/l, 0.79 ± 0.53 g/l, and 0.69 ± 1.49 g/l. The distribution of the available temperature values depends primarily on the depths. The four formations' median temperatures are 60 ºC for the Leduc, 55.6 for the Swan Hills, 48 ºC for the Granite Wash, and 64 ºC for the Gilwood. The maximum temperature of 146.1 ºC in the Leduc corresponds to the deepest sample at 4447.65 m among the four formations.

Table 7 Summary of ion concentrations found Western Canadian Sedimentary Basin Brine

	Values (g/l)	Na^+	K^+	Ca^{2+}	Mg^{2+}	Cl^-	HCO_3^-	SO_4^{2-}	TDS	pH	Density (g/cm^{3+})	Depth (m)	Temp (°C)
Leduc	Median	45.54	1.65	15.60	2.40	111.59	0.63	0.62	181.51	6.7	1.128	1741.70	60.0
	Min	1.11	0.01	0.004	0.01	0.87	0.002	0.001	7.07	5.5	1.004	297.20	17.94
	Max	91.75	6.11	33.74	17.74	177.00	7.81	26.42	278.16	8.4	1.335	4447.65	146.1
	Mean	42.32	1.83	14.10	2.54	96.78	0.75	1.16	158.04	6.7	1.109	1857.30	61.9
	STD	16.98	1.38	9.30	1.64	43.75	0.68	1.93	68.86	0.6	0.048	754.25	23.1
Swan Hills	Median	46.00	0.45	8.65	1.65	95.10	0.20	0.79	154.71	6.6	1.108	1734.00	55.6
	Min	89.38	0.004	0.68	0.05	10.17	0.005	0.002	22.87	5.0	1.006	598.05	11.1
	Max	5.92	3.75	28.33	11.42	187.63	5.85	12.23	304.01	9.0	1.214	4609.05	143.3
	Mean	45.64	0.60	10.11	1.71	92.83	0.39	1.05	151.98	6.6	1.105	2014.97	63.2
	STD	15.60	0.47	6.03	0.96	32.32	0.59	1.12	51.39	0.7	0.035	688.89	26.7
Granite Wash	Median	54.26	0.75	20.10	2.62	128.90	0.06	0.72	206.85	6.0	1.145	1596.85	48.0
	Min	28.67	0.05	2.43	0.07	87.50	0.002	0.0042	140.28	4.2	1.039	1264.00	11.1
	Max	117.00	3.47	48.37	10.68	215.60	0.98	5.51	344.71	8.1	1.273	3579.10	98.9
	Mean	56.28	0.95	21.03	2.85	133.55	0.09	0.79	215.26	6.0	1.149	1753.28	50.81
	STD	9.70	0.53	6.64	1.17	22.78	0.09	0.53	36.35	0.7	0.027	392.85	14.1
Gilwood	Median	58.07	1.18	18.54	2.41	133.39	0.13	0.50	214.17	5.8	1.150	1945.75	64.3
	Min	30.80	0.10	1.69	0.22	64.40	0.003	0.004	106.74	4.2	1.050	1347.35	19.0
	Max	99.35	4.88	39.64	7.78	184.14	1.12	23.42	298.55	7.7	1.213	3588.70	135.6
	Mean	59.29	1.45	18.81	2.65	133.90	0.15	0.69	216.35	5.8	1.148	2084.80	67.4
	STD	12.82	0.95	6.17	1.21	25.98	0.12	1.49	41.79	0.6	0.029	454.08	19.6

5.5.2 Principle component and Cluster analyses

Principle component analysis (PCA) was performed on the nine compositional variables that describe the brine chemistry. The continuous variables are major ions (sodium, potassium, calcium, magnesium,

chloride, bicarbonate and sulfate), and the corresponding pH. Figure 18 shows the proportion of the variance represented by each principle component. For example, the percentages of variance accounted for by principle component 1 in the Leduc, Swan Hills, Granite Wash and Gilwood formations are 46.1%, 42.9%, 37.5% and 33.7 %, respectively. The number of variables needed to account for the variation in the original dataset adequately can be evaluated from these variance percentages. In Figure 4, for the Leduc Formation, the first three principle components account for 72.2% of the total variance present in the dataset. Figure 4 also shows that the first three principle components for the other formations contribute as much as 70.3% of the total variability for the Swan Hills, 66.5% for the Granite Wash and 63.1% for the Gilwood.

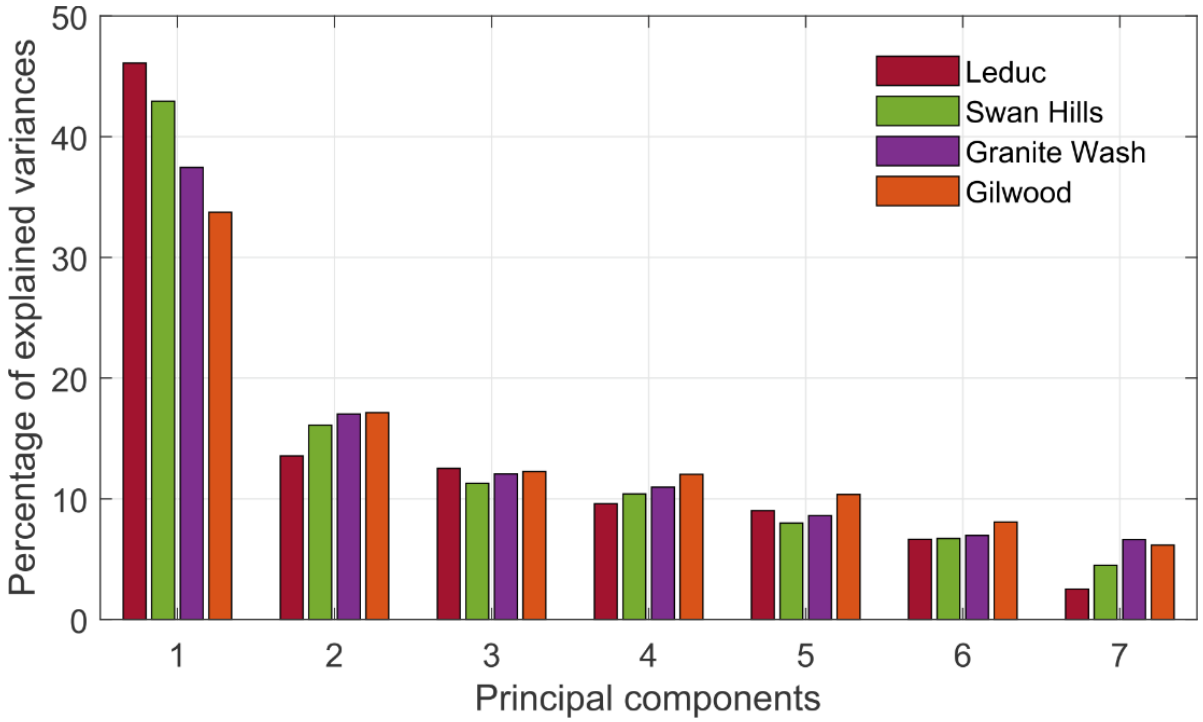

Figure 16: The percent of variance for the principle component ordinations in the Leduc (red), Swan Hills (green), Granite Wash (purple), and Gilwood (orange) formations. The seven components account for ~99.8% of the variance.

The correlations of the predictor variables on the first three principle components are often referred to as weighting or factor loading. The higher the absolute value of the loading, the more likely the three components are to be a significant contributor to the behaviour of the dataset. Thus, the loadings and correlations of the variables on the first three principle components assist in having a better understanding

of the hydrogeochemical clusters. A final number of clusters for each formation are identified after implementing various algorithms dedicated to this purpose. The number of groups for the Leduc and Swan Hills formations are three and for the Granite Wash and Gilwood formations are two. Table 8 shows the median values of the distribution for the eight variables used in the analyses, along with the total dissolved solids, density and depth in each group. Only the non-zero elements of the variables were used for the determination of the median values.

Table 8: The median values of the distribution of the variables used for the analyses, and TDS, density and depth of the groups in the Leduc, the Swan Hills, the Granite Wash and the Gilwood formations.

	Leduc			Swan Hills			Granite Wash		Gilwood	
	Grp 1	Grp 2	Grp 3	Grp 1	Grp 2	Grp 3	Grp 1	Grp 2	Grp 1	Grp 2
Sodium (mg/l)	9286	54584	30478	48830	51793	28299	51745	64859	52597	68234
Potassium (mg/l)	350	3113	930	513	0	331.5	665	1355	890	2004
Calcium (mg/l)	1240.5	21635	4925	10160	16484	5081	17633	26200	16212	22500
Magnesium (mg/l)	415.5	3368	1488.5	2066	1547	1003	2549.5	2916	2234	2746
Chloride (mg/l)	13865	132030	61046	103713	112900	54560	121223	158260	121800	157900
Bicarbonate (mg/l)	1698	506	675	135	977	437	59	73	163	75
Sulfate (mg/l)	3826.5	460	1078	135	241.5	1284.5	911	397	593	360
pH	7.2	6.5	6.9	6.3	6.7	7	6.2	5.6	6.1	5.6
TDS (mg/l)	33302	213431	101606	168575	184351	92800	194029	255233	196867	254683
Density (g/cm^3)	1.0275	1.146	1.071	1.1175	1.126	1.065	1.135	1.173	1.135	1.175
Depth (m)	1406.6	2256.5	1197.2	1796	3242.9	1513.5	1542.5	1850.5	1839	2163

As mentioned earlier, the most important parameters associated with the variability in the data set are correlated with principle component 1 and principle component 2. However, principle component 3 contributes ~12% of the variability. Figure 19 represents the three-dimensional biplots of the clusters that include all of the first three principle components axes. The points (circles) are the observations (i.e. wells). The different colours indicate separate groups. The blue lines represent the variables. The correlations of the variables on the principle components and their relationships with one another can be visualized in Figure 19 It also indicates the relationships between all the variables contained in the first three components. The variables are grouped if they are positively correlated. They are positioned on the opposite sides if the

correlation is negative. The clusters analyses in Figure 19 do not use the principle component scores. Rather, the clustering was done on the original dataset without reducing the dimensionality of data. The lines reveal the variables that have the most influence on any particular group.

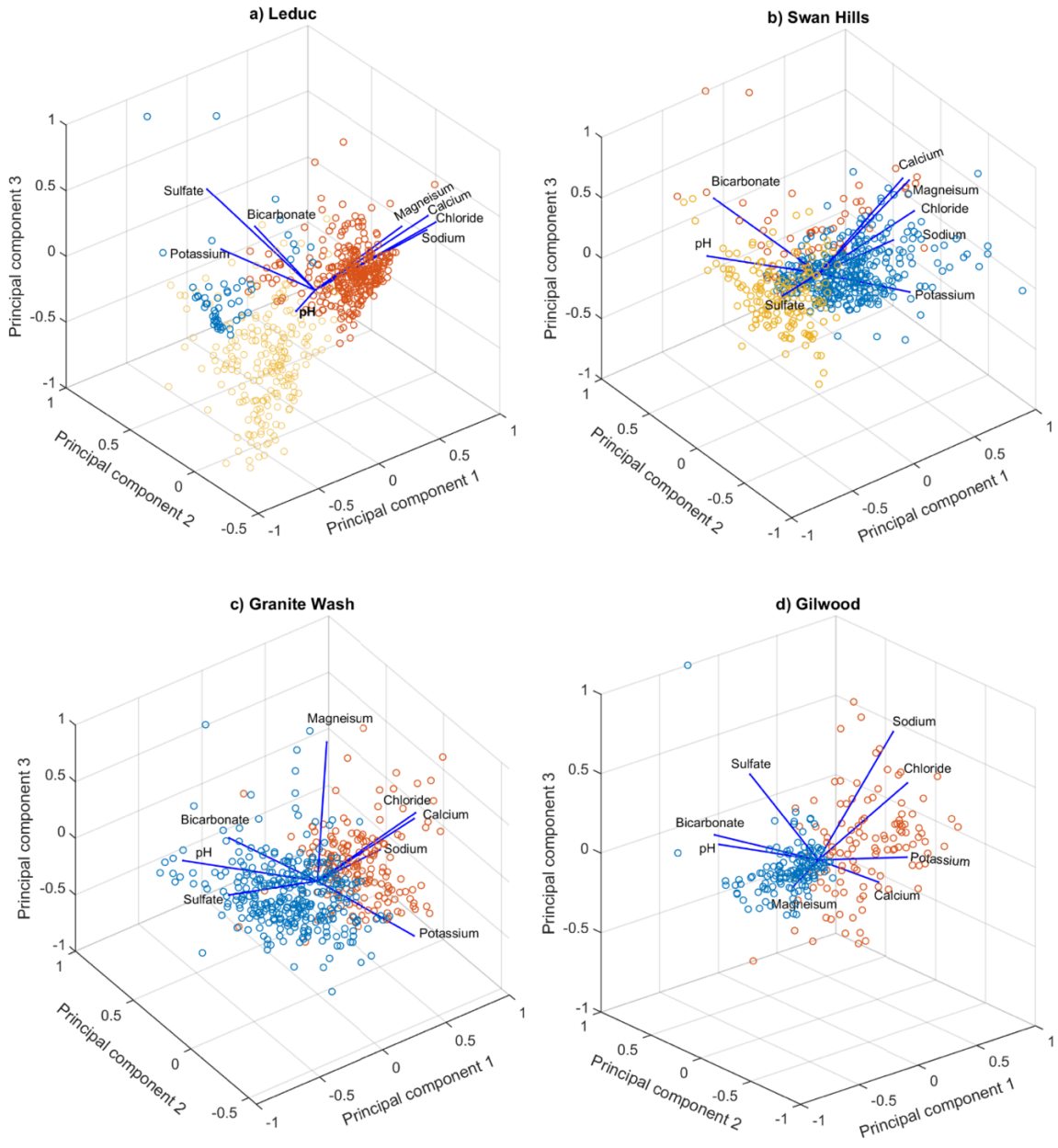

Figure 17: Three dimensional biplots showing the clusters of the samples in relation to the first three principle component axes for the a) Leduc (blue: group 1, orange: group 2, yellow: group 3), b) Swan Hills (blue: group 1, orange: group 2, yellow: group 3), c) Granite Wash (blue: group 1, orange: group 2) and d) Gilwood (blue: group 1, orange: group 2) formations. Case groupings were based on the clustering from the k-means cluster analyses.

Well clusters 2 and 3 in the Leduc Formation, (Figure 19a) are distributed along with the principle component 1 axis. Group 2 shows substantial influence from magnesium, calcium, sodium and chloride, and group 3 is mostly influenced by bicarbonate, sulfate, and the brines' pH. Group 1, on the other hand, shows a strong contribution from bicarbonate.

Out of the three distinct well clusters in the Swan Hills Formation (Figure 19b), variations in groups 1 and 3 are better explained by principle component 1. In contrast, group 2 is more represented by principle components 2 and 3. The blue lines show that group 1 is more associated with chloride salt of alkali and alkali earth metals. Group 3 is mostly associated with sulfate and pH. Wells in group 2 have substantial influence from bicarbonate as well as sodium, calcium, and chloride.

There are only two optimal groups for Granite Wash and Gilwood formations. Group 1 in the Granite Wash Formation (Figure 19c) shows a strong association with pH, sulfate, and bicarbonate, whereas group 2 shows associations with the aforementioned chloride salts. The Granite Wash and Gilwood formations are not spatially as prevalent as the Leduc and the Swan Hills formations. Figure 19d shows the group distribution for the Gilwood Formation. Group 1 exhibits a strong association with pH, as well as influences from bicarbonate, sulfate and magnesium. Group 2 possesses a higher correlation with chloride, sodium, calcium, and potassium.

5.5.3 Precipitation models

The precipitation models include the measured values for dissolved sodium, potassium, calcium, magnesium, chloride, bicarbonate, sulfate, and total dissolved solids, as well as the fluids' pH (Table 9). The depths in Table 9 were not involved with the geochemical modelling, but showcase that the deeper the samples are, the higher the temperature and the larger the TDS.

Table 9: The measured values of the ions, TDS, pH, and temperature used for the geochemical modelling for each group in the Leduc, the Swan Hills, the Granite Wash, and the Gilwood formations.

	Leduc			Swan Hills			Granite Wash		Gilwood	
	Grp 1	Grp 2	Grp 3	Grp 1	Grp 2	Grp 3	Grp 1	Grp 2	Grp 1	Grp 2
Sodium (mg/l)	16998	80258	53832	41913	55632	24828	46528	73600	43607	77828
Potassium (mg/l)	0.0	0.0	0.0	0.0	0.0	0.0	944	0.0	0.0	0.0
Calcium (mg/l)	3628	20527	2382	7866	17519	6000	22980	24424	6200	20360
Magnesium (mg/l)	949	1618	352	1227	983	608	5482	2454	899	2360
Chloride (mg/l)	32800	163949	84600	81284	119122	50410	128700	163600	80585	162700
Bicarbonate (mg/l)	1425	1153	170	792	688	454	90	200	415	82
Sulfate (mg/l)	2411	249	4854	523	158	4.0	704	206	16	240
pH	7.2	6.5	6.9	6.3	6.7	7	6.2	5.6	6.1	5.6
TDS (mg/l)	58211	267754	146190	133605	194102	82304	205428	264484	131722	263570
Temperature (°C)	65.56	122.22	51.1	83.3	132.22	60	62	98.89	73.33	104.4
Depth (m)	1921.8	3518.9	1440.2	1598.7	3090.7	1397.5	1465	2926.1	2191	2818.7

Figure 20 shows the mineral precipitation required to re-equilibrate 1 kg of the modeled fluids as the initial temperature (varies with groups) decreases to the ambient air temperature (0 °C) during geothermal power production. The oversaturated mineral phases before any suppression are dolomite ($CaMg(CO_3)_2$) for all the four formations. After dolomite and quartz are suppressed, as seen in Figure 21, the primary oversaturated mineral is calcite ($CaCO_3$) and can be found in each of the formations. The group 2 sample from the deeper depth in the Leduc Formation (Fig 20a) shows brucite ($Mg(OH)_2$) precipitation as the initial temperature of 122°C drops to 0°C during geothermal production. Figures 20a-b and 21a-b show that dolomite and calcite precipitation for the group 1 and 2 in the Leduc are three to five-fold larger than that from the Swan Hills' first two groups. However, group three in the Swan Hills Formation displays more than five times mineral deposition than group 3 in the Leduc. Group 1 in the Granite Wash Formation, Fig 20c and 21c, does not exhibit any mineral precipitation. Although both of the groups in the Gilwood formation show dolomite and calcite precipitation, the values of minerals for group 2, despite the deeper formation, are significantly smaller than that of group 1.

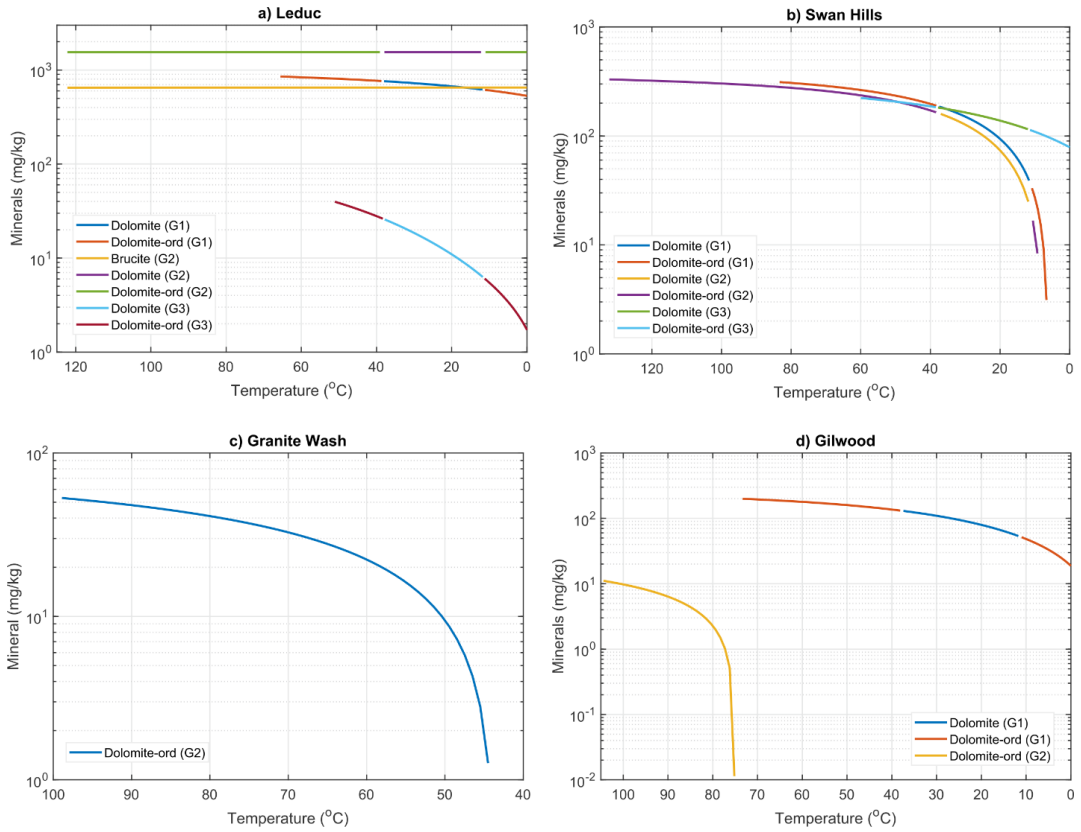

Figure 18: The maximum minerals precipitations from 1kg of composition water as the initial temperature of the samples decreases to ambient air temperature for the Leduc, Swan Hills, Granite Wash, and Gilwood formations. 'G1/2/3' represents the groups in each formation.

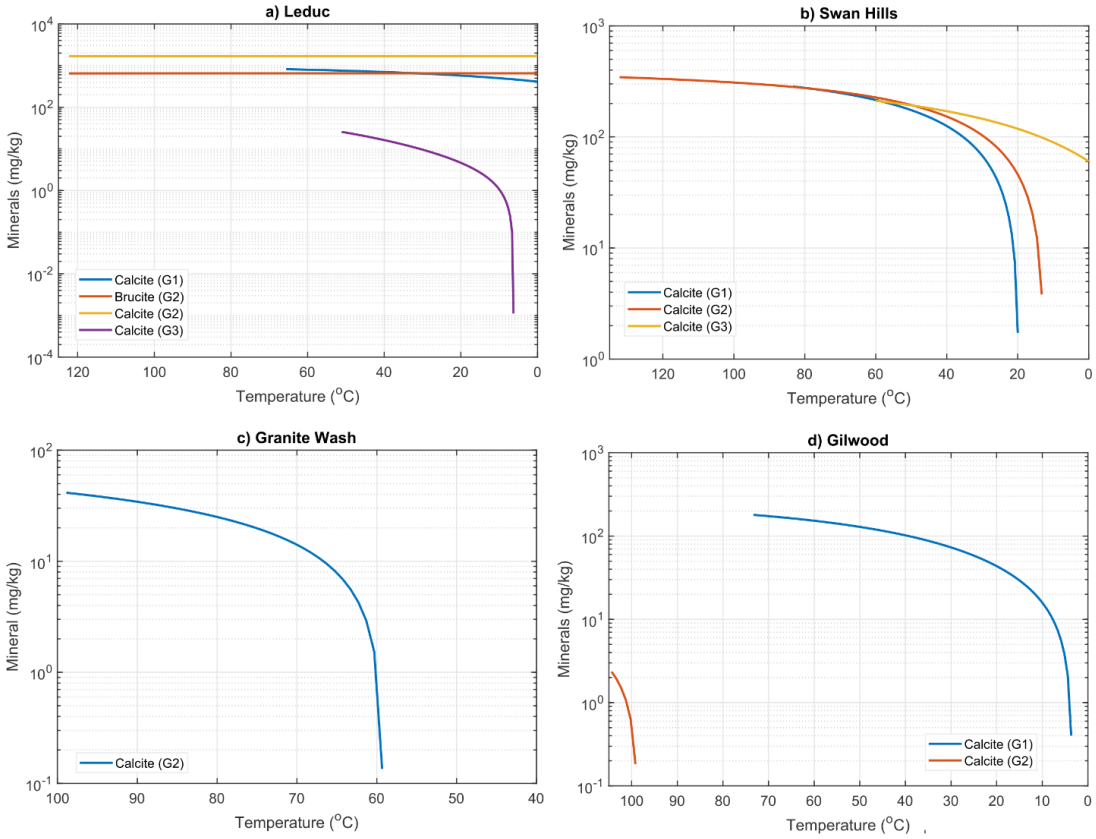

Figure 19: The maximum minerals precipitations from 1kg of composition water as the initial temperature of the samples decreases to ambient air temperature for the Leduc, Swan Hills, Granite Wash, and Gilwood formations (Dolomites and Quartz are suppressed). 'G1/2/3' represents the groups in each formation.

The results of the geochemical analysis show that calcite is the main scale-forming mineral presenting a geochemical risk in the production of geothermal power throughout the Western Canadian Sedimentary Basin. Calcite is a well-known scaling risk associated with geothermal systems (Siega *et* al, 2005; Yanagisawa *et al*, 2008; Wanner *et al*, 2017; Zotzmann *et al*, 2018). Calcite may be precipitated through decompression, reaction with pipe walls, boiling, and degassing of CO_2 (Zotzmann *et al*, 2018). In higher-temperature geothermal systems, boiling is often a major concern (Pereira, 2014; Zotzmann *et al*, 2018). Due to its retrograde solubility, i.e. becoming increasingly less soluble with increasing temperatures, calcite will tend to precipitate upon reinjection into the reservoir.

Several methods exist currently to deal with calcite scaling issues. One of these methods is controlling wellbore pressures with a deep pump. This method reduces calcite scaling and allows for control over the

depth of scale deposition (Pereira, 2014; Zhao & Zhao, 2015). Additionally, chemical techniques have been developed which include the use of phosphate molybdenum inhibitors (Zhao & Zhao, 2015; Zotzmann *et al*, 2018). These treatments carry environmental concerns. Inhibitors based on polycarboxylates are also known to be effective at reducing calcite scaling risks under geothermal conditions (Pereira, 2014; Zotzmann *et al*, 2018). Chemical inhibitors have been shown to be cost effective because they mitigate the need for mechanical cleaning of the wellbore. Thus, they are a popular method of controlling calcite scaling (Siega *et al*, 2005; Pereira, 2014).

Overall, mineral scaling does not appear to be a major concern with the circulation of oil field brines in the context of geothermal power production.

6 Performance of deep borehole heat exchangers

6.1 Introduction

Converting whole hydrocarbons fields for geothermal power production involves utilizing conventional geothermal production technology, i.e. production and injection wells, and the circulation of formation fluids from the reservoir, to the surface, and back into the reservoir. We also investigated the feasibility of extracting geothermal energy from suspended and abandoned petroleum wells using coaxial borehole heat exchangers (BHE). Such heat exchangers are created using retrofitted single sealed wellbores.

A coaxial BHE is a closed circulating system consisting of two concentric pipes for working fluid circulation (Wang et al, 2014; , Kujawa et al., 2006) The working fluid is continuously injected through the annulus space and produced through the center tube, without direct contact with the surrounding geothermal reservoir (Caulk and Tomac, 2017). Cold working fluid is heated by the increasingly higher temperature of surrounding rocks as it flows down the annulus of the BHE. The heated fluid eventually returns to the surface with the heat loss due to heat transfer from the hot produced flow to the cooler injected flow (Kujawa et al., 2006). Utilizing wells in the Hinton, AB area as exemplars, we developed a simulation model that combines the fluid flow field, heat transfer, and their coupling. Data for these wells were collected through GeoSCOUT. These wells are spread out around Hinton in an area of approximately 108 km^2. The model was created in established in COMSOL Multiphysics and verified with an analytic solution used two independent statistical validation methods. Developers can adapt the method presented below to suit the site-specific parameters of their wells.

6.2 Methods

6.2.1 Data sources and processing

6.2.1.1 Geothermal gradient

The formation temperature in Hinton was fitted linearly based on well logging data of the fourteen individual wells. Formation temperatures are obtained by oil/gas well logs and are described by many researchers as a linear function (e.g. Wight and Bennet, 2015):

(eq. 16) $$T(z) = az + b$$

where z is the formation depth, m; $T(z)$ is the formation temperature at depth z, °C; a is the geothermal gradient, °C/m; b is the surface temperature, °C.

6.2.2 Material properties

In addition to geothermal gradients, material properties strongly affect the performance of borehole heat exchangers. These materials include the well's casing steel, a thermally insulated pipe/tube, the working fluid (e.g. water), and the reservoir rock. Based on previous studies, the relevant properties of the casing steel and insulating pipe, as shown in Table 10, are assumed to be temperature independent. On the other hand, most heat transfer related properties of the working fluid or the reservoir rock are temperature-dependent, thereby affecting well performance during the extraction of geothermal energy. Historically, little attention has been paid to the effect of the temperature dependence of heat transfer related properties in BHEs. A significant advance in this study is that the main temperature-dependent properties of the working fluid (water) and the reservoir rocks are considered.

The thermodynamic properties of water are imported from the Material Library of COMSOL [50]. The temperature-dependent properties of water relating to flow field and heat transfer have been extensively investigated and detailed in previous studies (e.g. Strauss and Schubert, 1977).

Table 10: Thermal physical properties of rock matrix and pipes of the simulation model.

Physical parameter	Rock matrix	Thermal insulating tube	Casing steel
Density (kg/m^3)	2,600	1,150	7,850
Thermal conductivity (W/(m·K))	$\frac{770}{0.929(350+T)}+0.7$	0.26	44.5
Specific Heat capacity (J/(kg·K))	824.8+0.9343·(T-21)	1700	475

The specific heat of the reservoir rock is a linear function of the temperature over a wide temperature interval), where the specific heat at a given temperature (T) is:

(eq. 17) $$C(T) = C(T_i) + \beta(T - T_i)$$

where T_i is the initial temperature, °C; $C(T_i)$ is the specific heat at initial temperature, J/(kg·K) ; and β is the coefficient, J/(kg·°C^2).

The lithology of the geothermal reservoir in Hinton under investigation is described as f-grained sandstones, f-m sandstones, a matrix of f-m sands, mudstone, siltstone and conglomerates. In this study, the formation is assumed as a homogeneous sandstone. The specific heat of sandstone is defined by the following equation experimentally derived from Eppelbaum et al. (2014) at 21 °C:

(eq. 18) $$C(T) = 824.8 + 0.9343 \cdot (T - 21)$$

The thermal conductivity of the rock is another temperature-dependent property of the formation. Haenel et al. [58] summarized the average temperature dependence of thermal conductivity for different rocks as:

(eq. 19) $$k(T) = \frac{770}{B(350+T)} + 0.7$$

where $k(T)$ is the thermal conductivity at temperature T, W/(m·K), and B is the thermal conductivity coefficient of the rock in question. This general equation has been experimentally verified by Vosteen and Schellschmidt (2003).

According to Majorowicz et al. (2010), the average thermal conductivity of the Western Canadian Sedimentary Basin (WCSB) is 2.94 W/(m·K) at laboratory temperature (20 °C). Therefore, the relationship between thermal conductivity and temperature in Hinton can be generally expressed by the following equation:

(eq. 20) $$k(T) = \frac{770}{0.929(350+T)} + 0.7$$

6.3 Borehole heat exchangers

6.3.1 Borehole heat exchanger geometry

The deep coaxial borehole heat exchanger concept employed in this study is shown in Figure 22. A coaxial BHE is composed of an injection annulus and a production pipe/tube. The existing well casing of the petroleum well is used as the outside frame of the exchanger. A second, smaller, thermally insulated pipe is located concentrically to the well casing and acts as the inside channel of the exchanger. A segment of

thermally insulated pipe is installed along the top of the well casing to prevent heat loss from the warm injected fluid to the cooler ground.

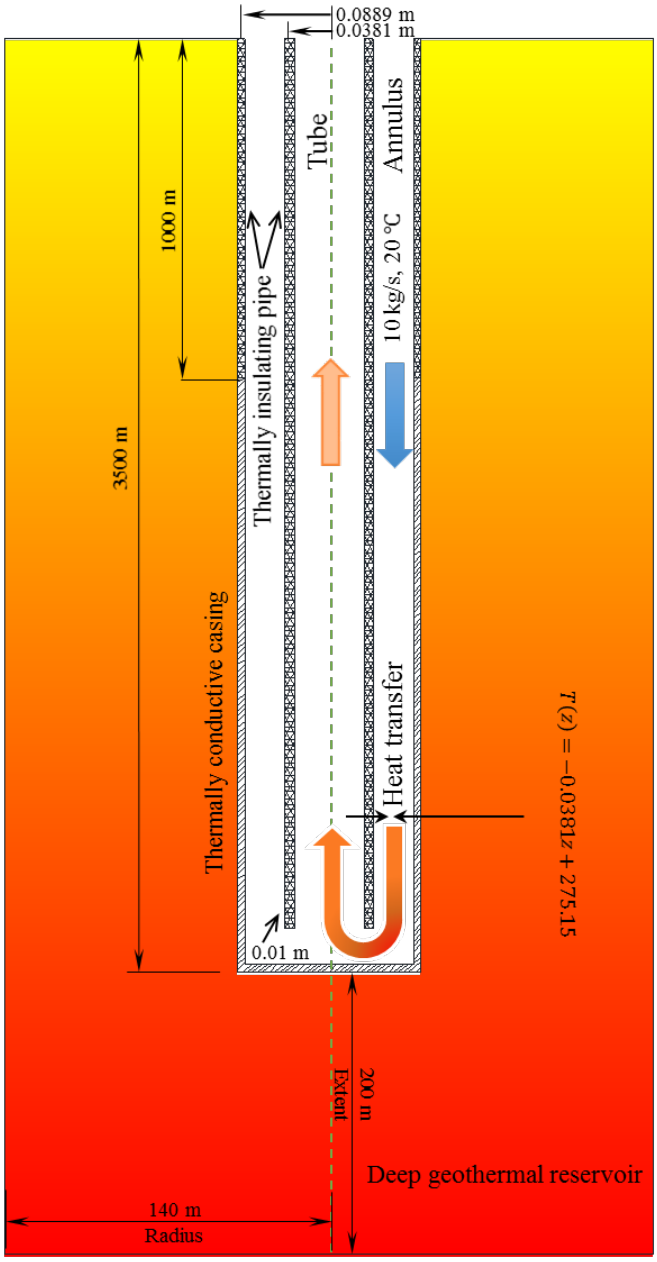

Figure 20: Schematic diagram and boundary conditions of a coaxial BHE for geothermal production from petroleum well in the Hinton, AB area [18, 19, 29, 30].

6.3.2 Model Geometric Configuration

Based on information obtained through geoSCOUT, the radius of the abandoned well is set as 0.0889 m (3.5 inches). The BHE tube's radius is set to 0.0381 m, allowing it to fit in the 0.0889 m well radius. The thermally insulated steel pipe and annulus were modeled as 0.01 m in thickness. End-users may utilize whatever borehole radii and tubing sizes are relevant to their assets. Most abandoned wells in Hinton range between 2,500 m and 4,000 m [57]. The depth of the well was set as 3,500 m, according to the reports from Hinton (e.g. Banks and Harris, 2018). As discussed in section 6.7.2, below, the lateral extent of the reservoir surrounding the wellbore was determined to be 140 m. The extent of the geothermal production zone beneath the bottom of the wellbore was selected as 200 m. The length of insulated section of the annulus was set as 1,000 m. All of these parameters are summarized in Table 11 and are shown to scale in Figure 22, above.

Table 11: Geometry of the geothermal coaxial BHEs exemplar used in this study.

Parameter	Value
Well depth, m	3,500
Radius of the tube, m	0.0381
Radius of the annulus, m	0.0889
Insulation length of the annulus, m	1,000
Thickness of the tube and the annulus pipe, m	0.01
Radius of the geometry, m	140
Extent of the deep geothermal reservoir, m	200

6.3.3 Heat transport within the system

Thermal conduction occurs in the reservoir rocks surrounding the abandoned well, through the well bore casing, and into the working fluid. Heat is transferred within the working fluid via forced convection. Heat is transferred through the thin layer (tubing) between the injected and the produced fluid, as well as between the surrounding rock and the injection flow (through well casing) via conduction.

Heat transfer through the rock is described as

(eq. 21) $$\rho_r C_r \frac{\partial T}{\partial t} = \nabla \cdot (k_r \nabla T) + Q$$

where ρ_r is the density of the rock, kg/m^3; C_r is the specific heat of the rock, J/(kg·K); T is the temperature, K; k_r is the thermal conductivity, W/(m·K); and Q is the heat flow, W/m^2.

Water was used as the working fluid for geothermal energy exploitation because of its high specific heat and thermal stability [63]. Heat transfer in water circulating through the tube and annulus is via forced convection. The conservation of energy equation for water in a pipe is

(eq. 22) $$\rho_w C_w \frac{\partial T}{\partial t} + \rho_w C_w \boldsymbol{u} \cdot \nabla T = \alpha_w T \left(\frac{\partial p}{\partial t} + \boldsymbol{u} \cdot \nabla p\right) + \nabla \cdot (k \nabla T) + \tau : \nabla \boldsymbol{u} + Q_c$$

where ρ_w is the density of water, kg/m^3; C_w is the specific heat of water, J/(kg·K); u is the velocity vector, m/s; p is the pressure, Pa; α_w is the coefficient of thermal expansion, 1/K; τ is the viscous stress tensor, Pa; and Q_c are heat sources other than viscous dissipation on a W/m^3 basis.

Heat transfer across the inner tube and the outer well casing was computed using a thermally thick layer boundary condition. In this case, the tangential heat flux is neglected and only the heat flux across the layer's thickness is considered:

(eq. 23) $$\boldsymbol{q_2} = \frac{T_{il} - T_{ol}}{d_{tl}/k_l}$$

where T_{il} is the temperature on the inside of the layer, K; T_{ol} is the temperature on the outside of the layer, K; d_{tl} is the thickness of the thin layer, m; k_l is the thermal conductivity of the thin layer, m; q_2 is the heat flux vector on the outside of the layer, W/m^2; and q_1 is the heat flux on the inside of the layer, which is simply the opposite of q_2, W/m^2.

6.4 Modeling methods

Two modeling methods are used in this study: numerical simulation and analytical calculation. Numerical modeling was first conducted using COMSOL Multiphysics. Then, the widely used mathematical model

proposed by Ramey [43, 64] was employed to verify the accuracy of the COMSOL results, following the examples conducted by previous researchers (e.g. Hagoort, 2004).

6.4.1 Numerical modeling

The first method used in this study is numerical modeling with COMSOL Multiphysics. It is used in geothermal modeling due to its superiority in multi-physics coupling [66], for example solving heat transfer problems in fluid and rocks with a finite element method. For numerical simulation, the most widely used k-epsilon (k-ε) turbulence model (e.g. Zhao and Ghidaoui, 2006) was chosen to calculate the fluid flow field in the tube and the annulus. The Conjugate Heat Transfer module was selected to solve thermal transport equations in the system. We made the heat transfer related properties of the water and the rock temperature-dependent and coupled the temperature field and the fluid field variations in the simulation model with COMSOL.

The BHE's performance in terms of production temperature and geothermal well power was evaluated using numerical simulations. The production temperature can be directly exported from the COMSOL results. The geothermal well power is a function of the injection flow rate, the specific heat of the circulating fluid, and the temperature difference between the injected and the produced working fluid, as shown in the following equation:

(eq. 24) $$P = WC_w(T_p - T_i)$$

where P is the geothermal well power, W; T_p is the production temperature, °C; and T_i is the injection temperature, °C.

6.4.2 Analytical modeling

Due to the lack of field data real-world deep coaxial boreholes, an analytical equation developed by Ramey (1962) was used to determine the validity of the COMSOL model developed. Ramey's equation is widely employed to describe temperature distribution in wellbores (Ramey, 1962). Assuming the flow inside the well is a single-phase flow, Ramey's equation can be used to calculate temperature distribution in a wellbore fluid as a function of wellbore depth and geothermal gradient:

(eq. 25) $$T(z,t) = az + b - aA + (T_{inj} - b + aA)e^{z/A}$$

where $T(z,t)$ is the temperature of fluid in wellbore, °C; T_{inj} is the injection temperature, °C; and z is the depth of the fluid in wellbore, m.

A is defined as (Satman and Tureyen, 2016):

(eq. 26) $$A = \frac{WC_w f(t)}{2\pi k_r}$$

where W is the mass flow rate, kg/s; k_r is the thermal conductive coefficient of the surrounding rock, W/(m·K); and $f(t)$ is a dimensionless time function representing the transient heat transfer to the formation, defined as (Satman and Tureyen, 2016):

(eq. 27) $$f(t) = -ln\left(\frac{r_w}{2\sqrt{\alpha t}}\right) - 0.29$$

where r_w is the radius of the well, m; and α is the thermal diffusivity of the rock, m^2/s.

6.4.3 Boundary conditions

The first group of boundary conditions are the operational conditions, which include the operational parameters of the working fluid and the running time. In the proposed geothermal production model, water is continuously circulated in the closed coaxial BHE system. Geothermal well performance is controlled by the operating parameters of circulating water, as shown in Figure 22, above, and Table 12, below.

Table 12: Operational parameters of geothermal production model with coaxial BHEs.

Parameter	Value
Injection rate, kg/s	10
Injection temperature, °C	20
Running time, years	25

Deep BHE injection rates usually range from 2 kg/s to 15 kg/s, and injection temperatures range from 10 °C to 50 °C. We used an injection rate of 10 kg/s and an injection temperature of 20 °C. The time duration of long-term geothermal production prediction is usually between 10 to 30 years, because geothermal production ability will stabilize after running for several years. In this study, a running time of 25 years was used.

Another group of boundary conditions are the initial conditions. In long-term simulations, the initial conditions are key to obtaining reliable transient results. Initial temperatures of the working fluid and the rocks were set equal to that of the geothermal reservoir. The radiation and the heat transfer to and from the ground are neglected; the ground is seen as a thermally insulating boundary without radiation and heat transfer. Boundary conditions of other borders are regarded as temperature boundaries determined by the geothermal gradient of the geothermal reservoir.

6.4.4 Model verification

The model was verified by comparing the COMSOL results to the analytical results. Verifying the model requires agreement between the operational parameters of the simulation and the analytical model. Using Ramey's equation described in section 6.4.2 for verification, the thermal properties of the water and the rock are taken as constants. All the properties of the rock and the water are taken as temperature independent properties, as listed in Table 13. As Ramey's equation does not consider heat transfer from the production tube to the injection annulus, the tube in the center is regarded as perfectly insulated. Under these conditions, heat exchange between the water on either side of the tube does not occur.

Table 13: Thermal properties of the rock matrix and water at 20 ºC for verification

Physical parameter	Rock matrix	Water
Density (kg/m3)	2,600	998.2
Thermal conductivity (W/(m·K))	2.94	0.60
Heat capacity (J/(kg·K))	823.87	4,184.4

Root-mean-square error (RMSE) and mean absolute percentage error (MAPE) were used to measure the difference between simulated results and analytical results. These two indices are the most common metrics widely adopted in measuring the discrepancy between different results. MAPE measures the deviation

between analytical results and simulation results in terms of percentage. RMSE is the square root of the variance of the residuals. This metric indicates the absolute fit of simulation results to analytical results. These two indices are given by:

(1) RMSE

(eq. 28) $$RMSE = \sqrt{\frac{\sum_{i=1}^{n}(T_s - T_a)^2}{n}}$$

where n is the number of predicted temperature; T_s is the simulated temperature, °C; and T_a is the analytical temperature calculated by Ramey's equation, °C.

(2) MAPE

(eq. 29) $$MAPE = \frac{1}{n}\sum_{i=1}^{n}\frac{|T_s - T_a| * 100}{T_a}$$

6.5 Parametric sensitivity analysis

The operational parameters of the water (i.e. injection rate and injection temperature) and the parameters of the insulation pipe (i.e. the thermal conductivity and the insulated length along the well casing) affect the geothermal well performance. To investigate the influence of these parameters, sensitivity studies were carried out by parametric sweeping in COMSOL. The simulations were performed for the mass flow rates of water from 2.5 kg/s to 10 kg/s, and for the injection temperatures from 20 °C to 40 °C, with increments of 1.5 kg/s and of 2.5 °C, respectively. In addition, the thermal conductivity of the insulating pipe was changed from a perfect insulator to 0.5 W/(m·K), with increments of 0.002 W/(m·K). The insulated length along the well casing was varied from 100 m to 1,600 m, at 100 m increments.

6.6 Modeling Procedure

Figure 23 presents the flow chart demonstrating the numerical modeling method on a coaxial BHE in an abandoned petroleum well. First, the influence range of temperature drawdown around the coaxial BHE was investigated by parametric sweep after the model converged. Second, the geometry radius was determined.

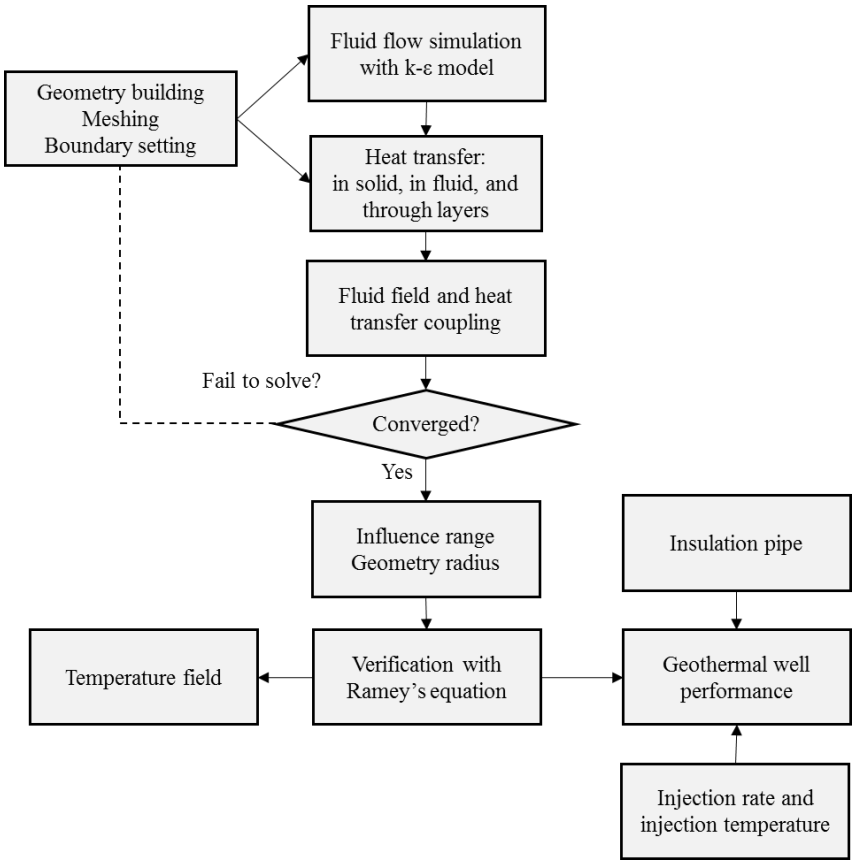

Figure 21: Flow chart of numerical modeling on a coaxial BHE to exploit geothermal energy from the abandoned petroleum well.

Then, the model was verified with analytical results calculated by Ramey's equation. After analyzing the variation of heat transfer related properties of the water and reservoir rock on long-term geothermal energy production, sensitivity studies were conducted to investigate the influence of operation parameters and insulation pipe on the BHE's performance for 25 years. As the production temperature and geothermal well power of deep coaxial BHE plummet in the beginning and then decline gradually, the time interval of the simulation should be short in the beginning and can be longer afterwards to make more accurate descriptions of the trend. The coaxial BHE performance was simulated for 25 years with an increment of 0.001 years between 0 and 0.1 years, 0.05 years between 0.1 years and 0.95 year, and 1 year from 1 year to 25 years.

6.7 Results

6.7.1 Temperature

6.7.1.1 Calculated geothermal gradient and surface temperature

The surface temperature and geothermal gradient form a linear function that describes the temperature distribution of a geothermal reservoir. The formation temperature in Hinton was linearly fitted based on well logging data of fourteen individual wells, as shown in Figure 24. The geothermal gradient was calculated as ~35 °C/km, which is higher than global averages (20-30 °C/km). The geothermal gradient in Hinton is confirmed, for example, by Lam et al. (1982), who published a geothermal gradient of 36 °C/km in Hinton area. The average air temperature between 2014 and 2019 of Hinton was 2.33 °C, calculated based on statistics in a weather station for Hinton obtained through the Alberta Climate Information Service (ACIS). The calculated surface temperature of 2.29 °C in the linear fitting correlates well with these reported temperatures. The fitted geothermal gradient and surface temperature are used in this study's numerical and mathematical models.

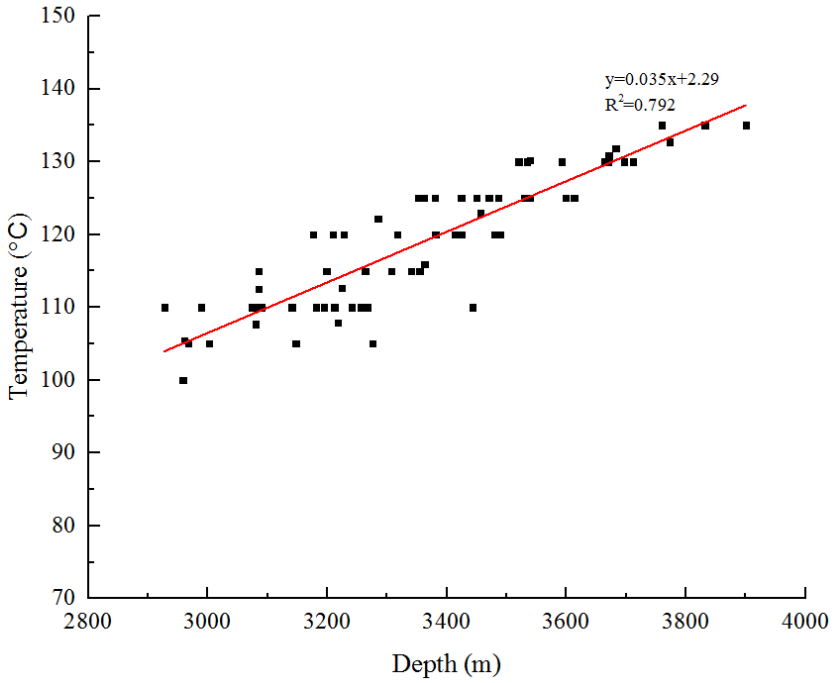

Figure 22: Logged depth and temperature from fourteen abandoned petroleum wells around Hinton, Alberta, Canada.

6.7.2 Spatial extent of temperature change

To investigate the spatial extent of the temperature change in the reservoir during geothermal production, a parametric sweep of the model's radius was conducted using the basic operational parameters listed in Table 12 and 13. Figure 25 shows the relationship between the model's radius and the production temperature of the coaxial wellbore heat exchanger after the model runs for 25 years. The production temperature decreases as the radius of the model increases up to ~80 m. The production temperature remains stable at a distance from the wellbore greater than 80 m. The maximum temperature influence range is defined as a distance from the geothermal well center to the boundary of the domain where the production temperature of the model remains constant. As such, 80 m is determined to be the maximum influence range of the model for 25 years. Beyond 80 m, the lateral extent of the modeled reservoir has little effect on the outlet temperature. Reporting extends to 140 m from the wellbore to better show the results and provide a sufficient buffer between the maximum influence range and the boundary of the simulation domain.

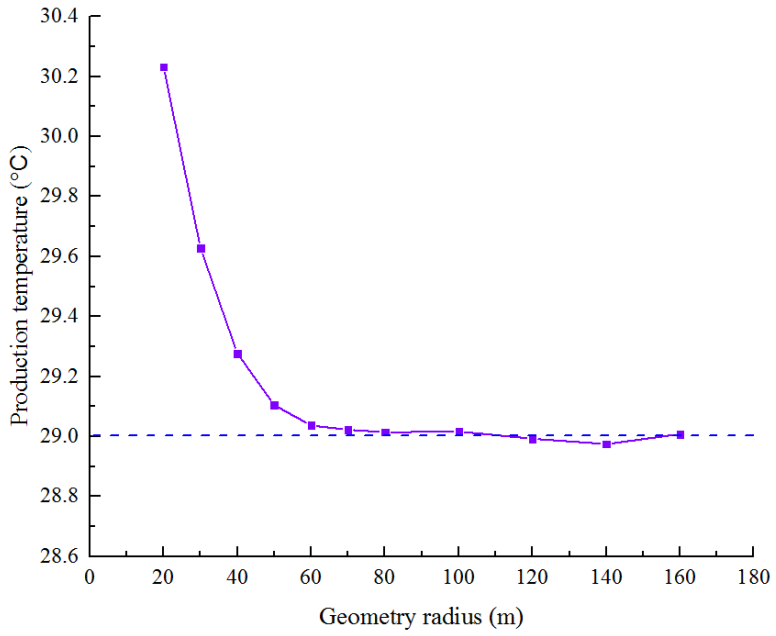

Figure 23: The production temperature over the geometry radius of the coaxial BHE after 25 years of operation, with an injected flow rate of 10 kg/s at 20 °C.

6.7.3 Temperature field changes in the reservoir

Changes to the temperature field were simulated over 25 years of geothermal energy production through the coaxial BHE, as shown in Figure 26. The temperature field cones around the geothermal well. The reservoir's temperature field has two distinct regions. In the shallow reservoir, the temperature of the reservoir rock immediately surrounding the well bore slightly increases, leading to a slight concave-down coning of the iso-surfaces. Deeper in the reservoir, geothermal energy production leads to a sharp concave-up coning, as the temperature in the well bore's immediate vicinity is drawn down. The inflection point between these two zones is at about 500 m, if the injection temperature is 20 °C. The impact of geothermal extraction becomes less pronounced in the reservoir as one moves away from the wellbore.

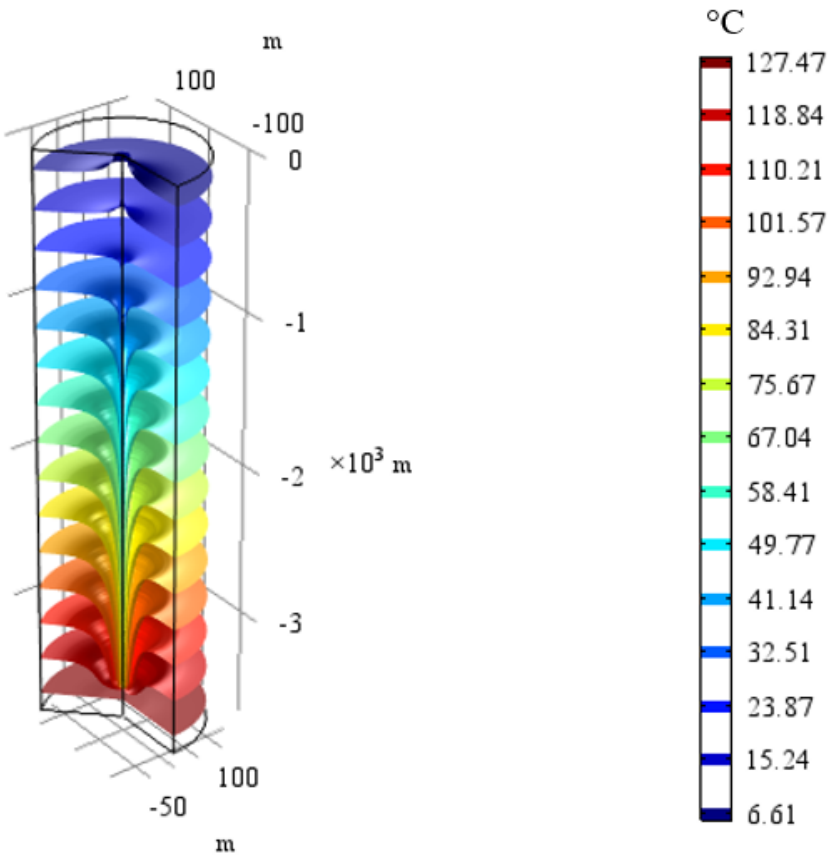

Figure 24: The production temperature over the geometry radius of the coaxial BHE after 25 years of operation, with an injected flow rate of 10 kg/s at 20 °C.

6.7.4 Temperature distribution in the wellbore

Temporal changes in the water temperature within the coaxial BHE are shown in Figure 27. The water temperature increases with depth along the annulus, gradually at the beginning and rapidly afterwards, before peaking at the bottom of the well. The maximum water temperature at the bottom decreases from ~36 ˚C to ~30 ˚C over the 25-year simulation. The water in the production tube, after being heated in annulus, continually loses heat to the injected water in the annulus. The temperature of produced water decreases from ~32 ˚C to ~ 29 ˚C over the 25-year simulation.

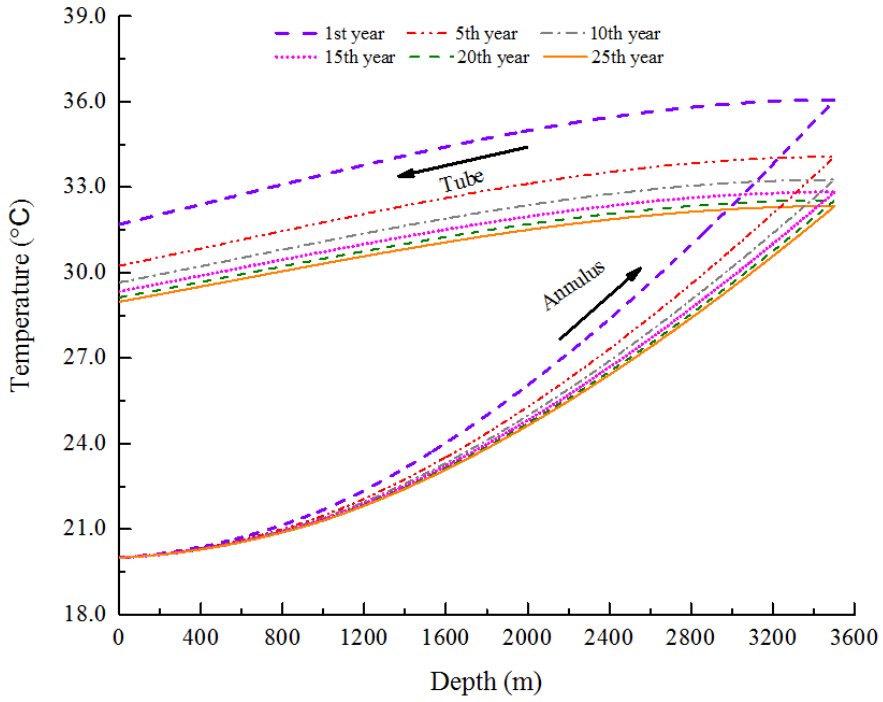

Figure 25: The temperature distribution along the tube and the annulus in the coaxial BHEs at different operating times.

6.8 Model verification in COMSOL

To verify the simulation model, simulated and analytical results for the temperature distribution in the annulus after 25 years were compared, as shown in Figure 28. Figure 29 shows the corresponding MAPE and RMSE as a function of well depth. The analytical temperature is slightly higher than the corresponding COMSOL results. MAPE and RMSE increase with well depth. Although greater well depths result in

greater variance, the difference between the simulated result and the analytical result is still marginal. This conclusion is supported by the MAPE and RMSE shown in **Error! Reference source not found.**. After r unning for 25 years, the MAPE and RMSE of a 3,500 m coaxial BHEs are only 1.74 % and 0.59 °C at 3,500 m, respectively. These results suggest that the simulation model fits well with the analytical model and can be used for long-term geothermal well performance evaluation.

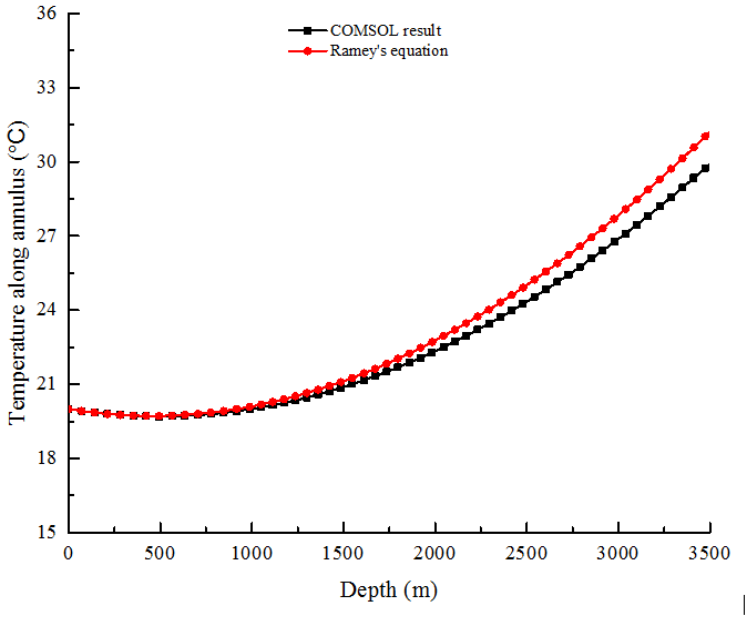

Figure 26: The comparison of the water temperature distribution along the annulus between the COMSOL result and Ramey's equation after running for 25 years.

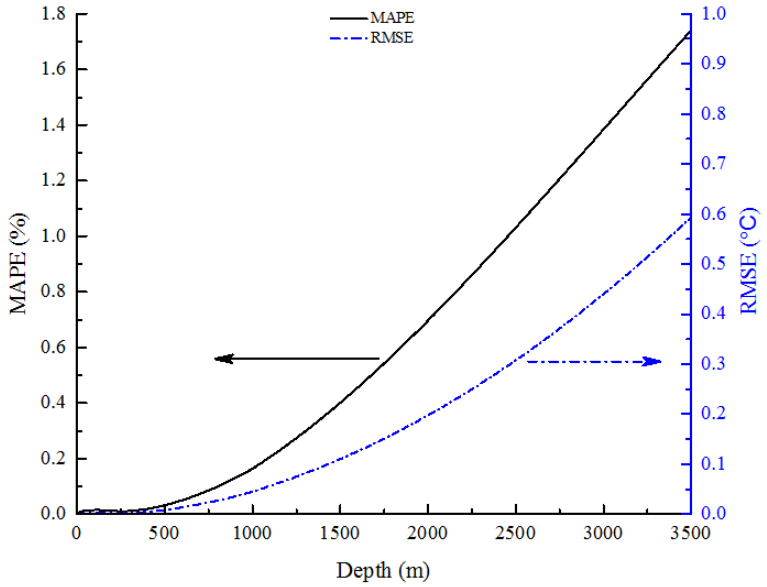

Figure 27: MAPE and RMSE over well depth between COMSOL result and Ramey's equation on the temperature distribution along the annulus after running for 25 years.

6.9 Borehole heat exchanger performance

6.9.1 Production temperature and production power

To assess the performance of the coaxial BHE, regression curves for the production temperature and the geothermal well power data were calculated, as shown in Figures 30 and 31, respectively. The fitted results show that both production temperature and well power follow a negative power function trend with time, plummeting quickly in the beginning, before leveling off. Within the initial 5 years, both the output temperature and the geothermal well power drop substantially. After that, both values decrease gently, stabilizing at around 30 °C and 0.4 MW, respectively. After running for 25 years, the production temperature decreases to 28.97 °C, and the corresponding geothermal well power is 0.38 MW. These numbers speak directly to the low-enthalpy geothermal power potential of abandoned petroleum wells. Due to the quick drop of the production temperature and the geothermal well power in the initial running time, long-term evaluation should be considered in geothermal well performance prediction.

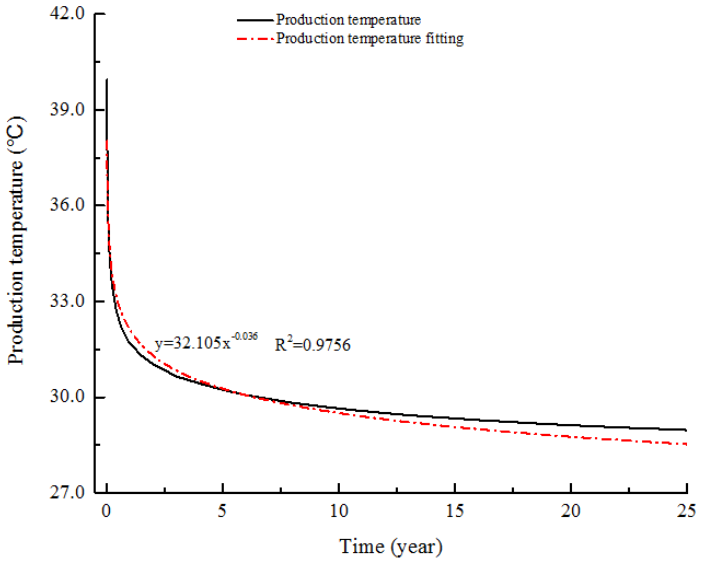

Figure 28: The production temperature over the operation time of the coaxial BHE, with an injection flow rate of 10 kg/s at 20 °C.

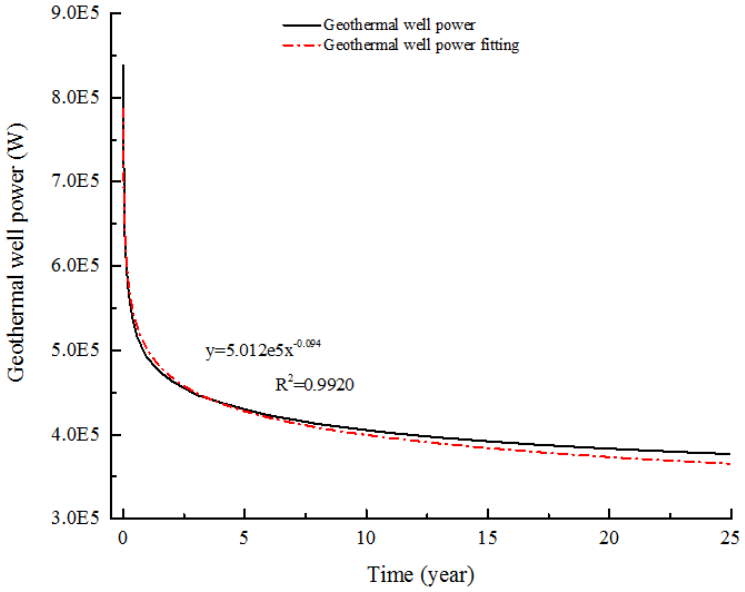

Figure 29: The geothermal well power over the operation time of the coaxial BHE, with an injection flow rate of 10 kg/s at 20 °C.

6.9.2 Effects of transient temperature-dependent properties

To investigate the influence of the temperature dependence of thermodynamic properties, a production temperature comparison taking thermal properties as constants (at 20 °C) and using temperature-dependent variables was conducted. The results of this comparison are shown in Figure 32. After 25 years, the temperature of the injected water increases by ~9 °C and ~10 °C using transient and constant variables, respectively, with an injection temperature of 20 °C. The temperature discrepancy between the two models is ~1 °C, corresponding to ~11 % relative error between the two cases. If the heat transfer related properties of the coaxial BHE are taken as temperature-independent variables, the output capacity will be overestimated.

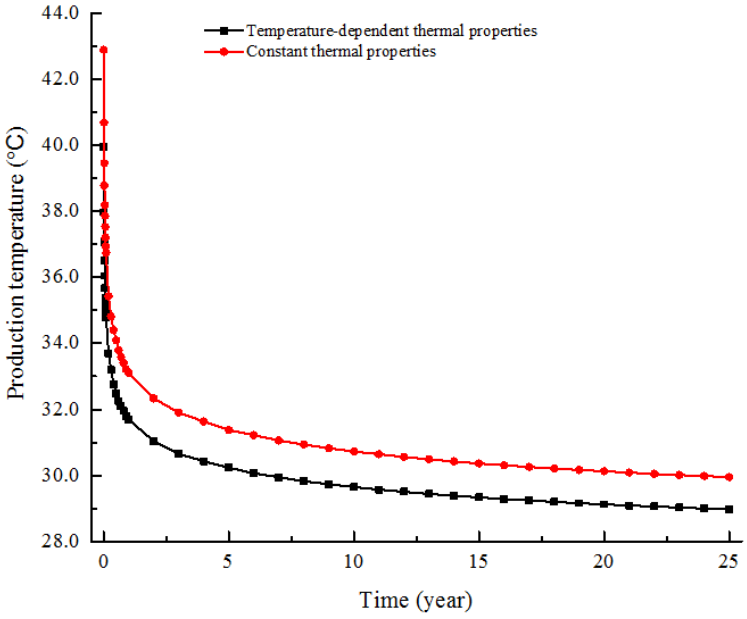

Figure 30: The comparison of the production temperature between using constant (red line) and transient (black line) thermodynamic properties at 20 °C, with an injection flow rate of 10 kg/s at 20 °C.

6.10 Sensitivity analysis

6.10.1 Injection flow rate

A key operating parameter of a coaxial BHEs is the injection rate. Regression curves were calculated to analyze the effects of varying injection rates on the production temperature over time. Figure 33 presents the production temperature and the fitted curves over time at different injection rates with an injection temperature of 20 °C. The results show that all the production temperatures have a negative power relation with the production time. The higher the injection rate, however, the lower the scaling factor. Likewise, as geothermal well power is determined by the difference between the injection and production temperatures (Eq. 24), the geothermal well power as a function of varying injection rates is also represented by negative power functions over time.

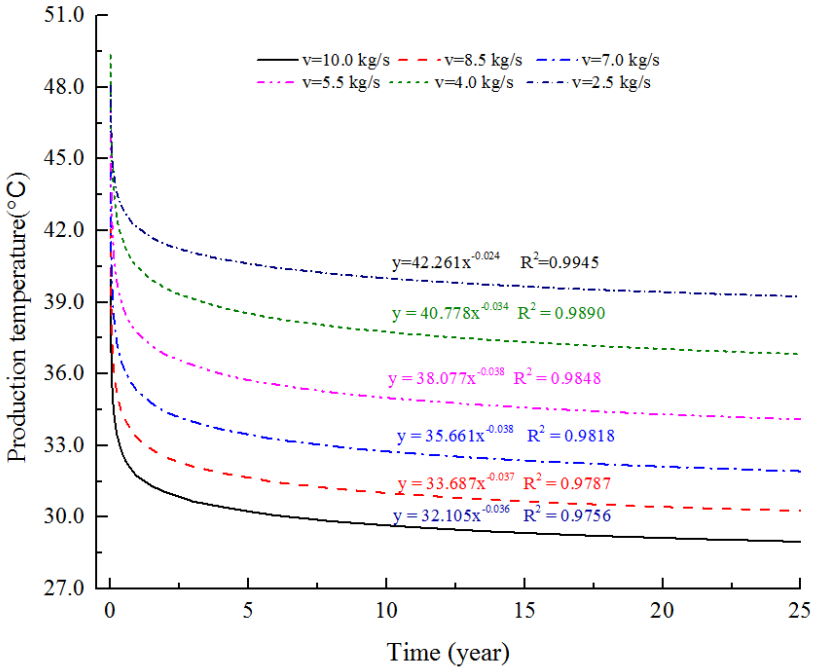

Figure 31: The production temperature over time of the coaxial BHE affected by injection flow rates with an injection temperature of 20 °C.

The effect of injection rates on the long-term performance of a coaxial BHE was analyzed via parameter fitting. The fitted relationships between the geothermal well performance and the injection rate after running the model for 25 years are demonstrated in Figure 34. Different trends were observed in the production temperature and geothermal well power versus injection rate plots. The output temperature decreases linearly from ~39 ˚C to ~29 ˚C with an increasing injection rate from 2.5 kg/s to 10 kg/s. The geothermal well power increases logarithmically from ~250 kWt to ~400 kWt with the same increase in injection rates.

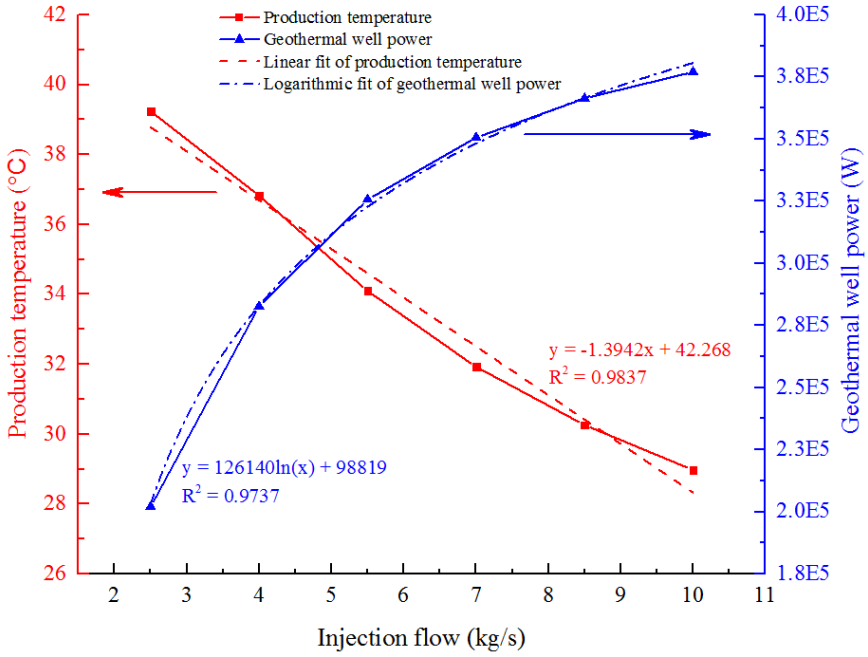

Figure 32: The performance of the geothermal well affected by injection flow rates after running the model for 25 years with an injection temperature of 20 °C.

6.10.2 Injection temperature

Another important operational parameter of a coaxial borehole heat exchanger is the injection temperature of the working fluid (water). At an injection flow rate of 10 kg/s, the production temperature and the geothermal well power were both fitted to the injection temperature as shown in Figures 35 and 36, respectively. The fitted results indicate that both the production temperature and the geothermal well power are linearly dependent on the injection temperature, albeit with opposing trends. The higher the injection temperature, the higher the production temperature and the lower the geothermal well power.

The slopes of the fitted lines increase and the intercepts decrease slightly over time. As opposed to the injection rate, higher injection temperatures are needed for higher temperature production. Lower injection temperatures should be used if more geothermal power is desired.

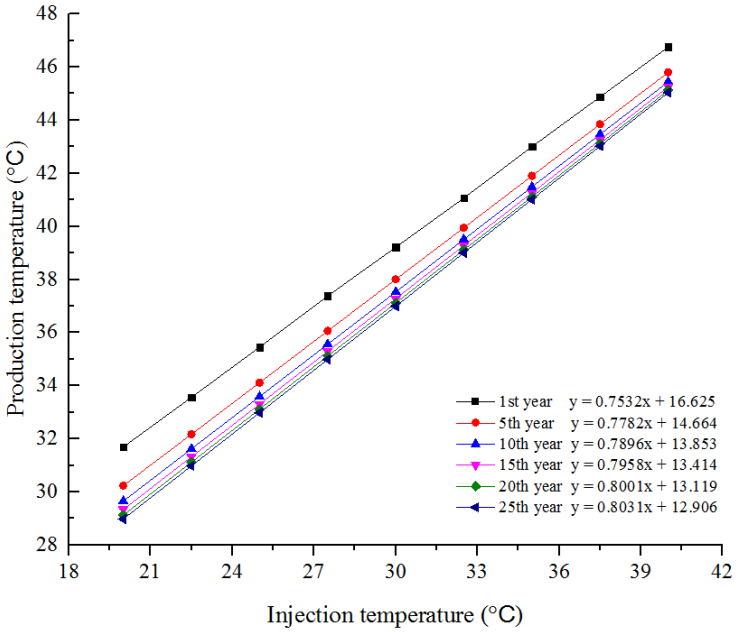

Figure 33: The linear relationship between the production temperature and the injection temperature of the coaxial BHE with an injection flow rate of 10 kg/s.

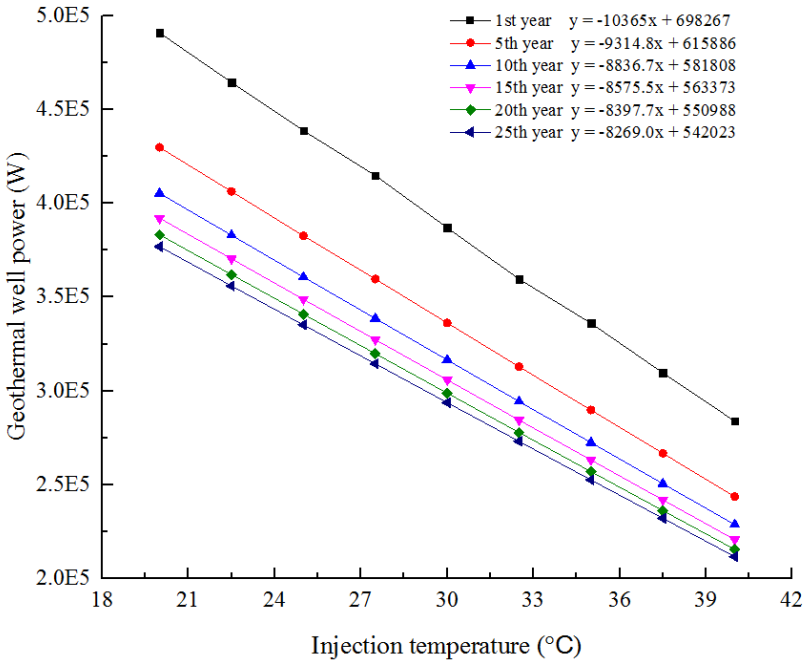

Figure 34: The linear relationship between the geothermal well power and the injection temperature of the coaxial BHE with an injection flow rate of 10 kg/s.

6.10.3 Thermal conductivity of the insulating pipe

Linear fitting was also employed to investigate the influence of the insulated pipe's thermal conductivity on the geothermal well's performance, as shown in Figures 37 and 38. The fitting lines show that both the production temperature and the geothermal well power decrease linearly with an increase of the insulated pipe's thermal conductivity. The slopes of these lines gradually increase while the intercepts gradually decrease. Therefore, the lower the thermal conductivity of the insulated pipe, the better the geothermal well performance. These results indicate that a better insulator reduces the heat loss, not only from the injected flow to the ground, but also to the produced water in the annulus.

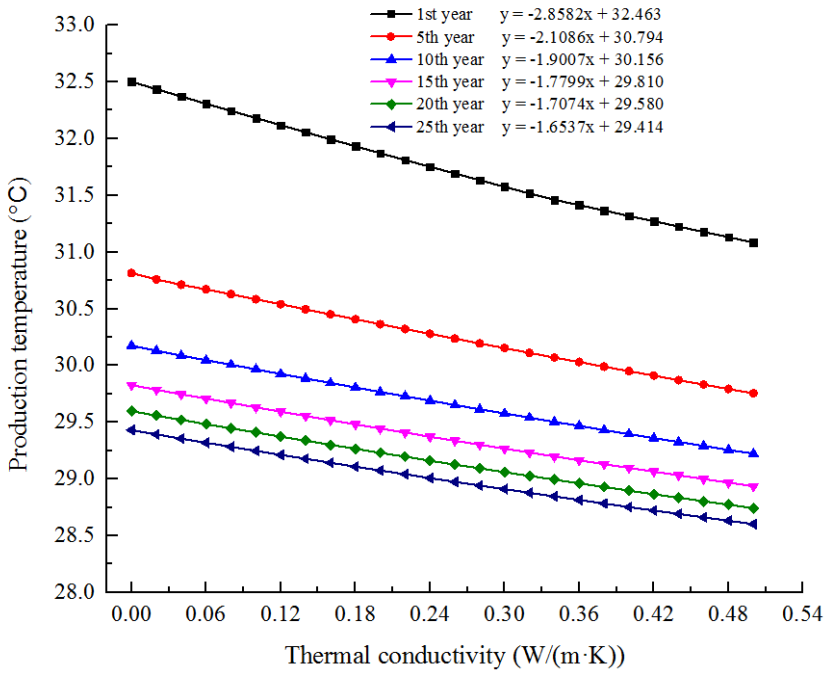

Figure 35: The production temperature of the coaxial BHE influenced by thermal conductivity of the insulating pipe with an injection flow rate of 10 kg/s at 20 °C.

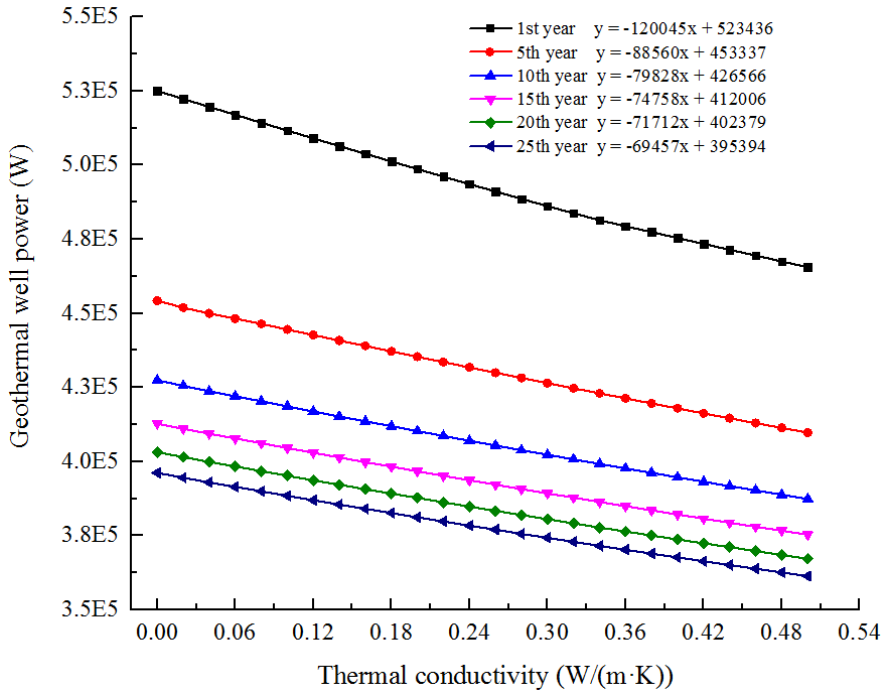

Figure 36: The geothermal well power of the coaxial BHE influenced by thermal conductivity of the insulating pipe with an injection flow rate of 10 kg/s at 20 °C.

6.10.4 Insulated segment of the well casing

The thermally insulated segment of the well casing on the top of the coaxial BHE prevents heat loss from the injected water flow to the surrounding rocks. Figure 39 shows the relationship between production temperature and the length of the insulated casing at different run times. Overall, there is no significant difference in the production temperature associated with varying lengths of insulated well casing. At most, only ~0.2 °C difference was generated, regardless of run time.

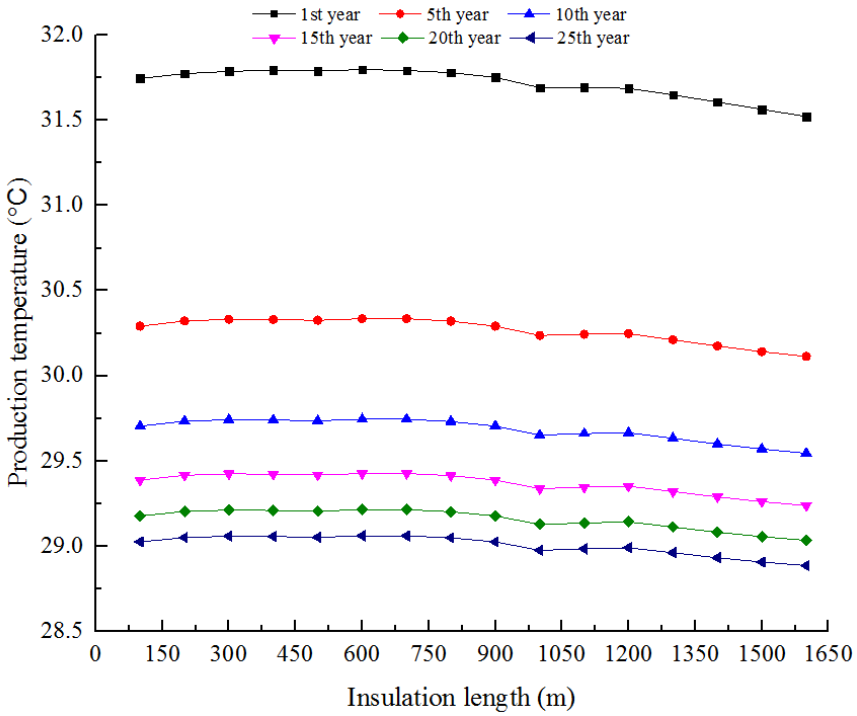

Figure 37: The production temperature influenced by the insulating length of the annulus with an injection flow rate of 10 kg/s at 20 °C.

6.11 Discussion

The results of this modeling study indicate that reliably simulating geothermal energy production through a coaxial BHE requires careful consideration of the model's lateral extent and temperature-dependent thermodynamic properties during the model's run time. The simulated coaxial BHE did not disturb the reservoir temperature beyond a distance of ~80 m from the well bore. The temperature dependence of the water and reservoir rock's heat transfer related properties can lead to a ~11% (~1 ˚C) relative error over the temperature-independent case.

Abandoned petroleum wells have a great potential for geothermal exploitation using coaxial BHE, but this potential is affected by the operational parameters of the water and the insulating pipe. The production temperature and the geothermal well power can be controlled by adjusting the injection temperature, the injection rate and the thermal conductivity of the insulating pipe.

The output temperature of the coaxial BHE is not affected by an increase of the lateral extent of the model, if the lateral extent is greater than the maximum influence range of temperature drawdown. Heat-flux, or

temperature boundaries are often employed in BHE models. This convention, however, can produce models with inappropriately small radii, leading to unreliable final results, as shown, for example by Caulk et al. (2017). This study addresses this issue by establishing the maximum influence range of temperature drawdown in an iterative process before designing the final model. Initial iterations of the model showed no temperature changes in the reservoir at a distance greater than ~80 m from the wellbore; the final model had a lateral extent 140 m from the wellbore. Time-dependent radii of interactions are another convention commonly used to define the lateral extent of a coaxial BHE model. Although this approach considers the time effect and thermal diffusivity, the operating parameters of the working fluid are still neglected. This study is the first in the literature that considers transient thermodynamic properties and operating parameters of the BHE when establishing the lateral extent of the simulation model.

This study shows that heat transfer between the water in the BHE and the surrounding rock leads to temperature field changes in the reservoir and in the working fluid. The reservoir temperature field can be divided into two zones. In the shallow zone, the temperature of the injected fluid is higher than the surrounding ground temperature. Due to a greater temperature difference across the production tubing, however, heat transferred from produced flow is greater than heat loss to the surrounding rock . Consequently, the water temperature in the annulus increases slowly with the depth (**Error! Reference s ource not found.**), as does the temperature in the surrounding reservoir. In the deep zone, the temperature of surrounding rock exceeds the temperature of the water in the annulus. Therefore, both the surrounding geothermal reservoir and the produced water in tube transfer heat to the injected water, leading to the temperature drawdown shown in **Error! Reference source not found.**'s coned isothermal surfaces.

As the temperature field changes in the reservoir and in the working fluid of the coaxial BHE during geothermal energy production, the thermodynamic properties of the geologic media (i.e. reservoir rocks and working fluid) vary because of these properties' temperature-dependence. Accounting for these property variations changes the performance of the coaxial BHE. A production temperature difference was observed that is attributable to transient properties controlling heat transfer in the coaxial BHE. This finding is confirmed by Bu et al. (2012), who noted that a geothermal well's power is over-estimated if the temperature variation is neglected in the reservoir. In another comparative study conducted by Kohl et al. (2000), the real output temperature of a 1,213 m BHE was up to 2.0 °C lower than the modeled output. The variation of properties caused by temperature field changes can explain the production temperature difference between the simulated output temperature and measured data.

In this study, considering the temperature dependence of the geologic media's thermodynamic properties led to a ~11% (~1 ˚C) relative error over the static case. This result confirms that failure to consider these transient properties will lead to the over-estimation of a BHE's power generation capacity. In previous geothermal well performance studies on abandoned petroleum wells, heat-transfer related properties were usually considered invariable with temperature; the effects of the variation of heat transfer related properties during geothermal production were not considered (e.g. Sui et al., 2018). These omissions call into the question the accuracy of such geothermal production models using abandoned petroleum wells. Therefore, the temperature dependence of heat-transfer related properties should be considered, especially in deep wells with high bottom temperatures.

Both the production temperature and the geothermal well power will change with time and are affected by the injection temperature, injection rate, and thermal conductivity of the insulating pipe. The production temperature and the geothermal well power are negatively correlated with the running time of the coaxial BHE model. This relationship is in accordance with the pseudo-steady-state described by Nalla et al. (2005). Linear relationships were found between the production temperature and the injection flow rate, injection temperature, and the thermal conductivity of insulating pipe. Geothermal well power also has a linear relationship with the injection temperature and the pipe's thermal conductivity, but increases logarithmically with an increasing injection rate. If the density and specific heat of water are both temperature-independent, geothermal well power versus injection flow rate should show an opposite linear trend compared with the production temperature affected by the injection rate. This study's result again confirms the necessity of treating thermodynamic properties as transient when modeling the performance of a coaxial BHE in an abandoned petroleum well. An exception to this is the insulated segment along the top of the well casing. The variation of this length has little effect on the final performance of the well. This observation substantiates the claims made by other researchers that the thermal resistance of casing can be neglected (e.g. Satman and Tureyen, 2016).

By optimizing the operating parameters, the production temperature and the geothermal well power of the studied 3,500 m coaxial BHE in Hinton can reach ~40 °C and ~0.45 MW, respectively after 25 years. The production temperature and the geothermal well power will be higher if the well is deeper, e.g. 4,000 m. However, the production temperature and geothermal well power of the coaxial BHE are still low in comparison with the output capability of the enhanced geothermal system (Zhang et al., 2017). Further

studies, which utilize enhanced geothermal system to exploit geothermal energy through abandoned petroleum wells in the Western Canadian Sedimentary Basin need to be undertaken.

In summary, this study shows that using abandoned petroleum wells to extract geothermal energy with coaxial BHEs is feasible in the Hinton area of the Western Canadian Sedimentary Basin. The performance of the coaxial BHEs is affected by the temperature dependence of heat transfer related properties of the water and the reservoir rock and are controlled by the injection temperature, the injection flow rate and the thermal conductivity of the insulating pipe. The proposed simulation model can not only be used to investigate geothermal energy producing feasibility in Hinton, but also can be expanded to geothermal production evaluation using coaxial BHEs other areas.

7 Well Retrofit Costs

7.1 Introduction

In this section, a cost model is detailed for retrofitting a wellbore as a deep wellbore heat exchanger, the geometry and performance of which were described in the previous section. Cost data for this model was obtained from the 2019 PSAC report. The PSAC study is a bi-annually published guide that predicts the prices of oilfield services, equipment, and materials in Western Canada. This study uses the data from Alberta's Foothills region. Up-to-data cost can be obtained by applying the most recent PSAC report data for the most appropriate region to the methodology detailed below.

7.2 Planning / Lease Preparation Costs

Planning and lease preparation costs include licencing and permits; engineering design and planning; preparing the lease for heavy equipment; and miscellaneous and overhead cost components. Table 14 contains an itemized list of these costs from the Winter 2019 PSAC Well Cost Study. The miscellaneous costs are calculated as an 8% surcharge on the other expenses to provide protection against cost overruns and unanticipated expenses, while overhead is an additional 2% surcharge applied to cover administrative staffing and materials. End-users may adjust these figures based on their own internal metrics. Although the expenses in this category may vary based on well location and ease of access to the well site, they are independent of existing wellbore characteristics, so we consider them as fixed costs.

7.3 Well Equipment Costs

Well Equipment costs include the cost of a new wellhead at the surface and a packer installed downhole to seal off the old producing zone. These costs are also included in Table 14.

Table 14: Itemized list of fixed costs for retrofit of an oil and gas well for geothermal energy production.

Planning and Lease Preparation	Item Cost ($)	Description
Well License / Applications	500	Regulatory permit
Preparation & Roads	8,700	1 day of lease cleanup + supervision
In-house Engineering (Drilling)	16,000	100 hrs of engineering work
Equipment Inspection	3,500	Casing inspection log
Misc. Costs	2,296	8% Cost overrun buffer
Overhead	574	2% Administrative addition
Subtotal	31,570	
Well Equipment		
Packer	12,750	To seal wellbore from oil or gas producing zone
Wellhead	18,000	To replace old wellhead
Misc. Costs	2,460	8% Cost overrun buffer
Overhead	615	2% Administrative addition
Subtotal	33,825	

7.4 Service Rig Costs

Service Rig costs include the use of a rig and crew for three days, along with the materials needed to replace the tubing and test the newly retrofitted well. Within their service rig costs, the PSAC Well Cost Study includes items, such as hauling of equipment, that are not directly part of the service rig but are necessary for the service rig to complete its work. This study categorized costs in the same manner. Three days of rig time was chosen based upon discussion with oil and gas industry professionals. This includes two days to set up the rig, install tubing up to 2500m depth, and dismantle the rig, plus a third day to replace the wellhead, install a packer, and conduct cementing and pressure tests. A depth of 2500 meters was chosen as a representative value for wells that may be under retrofit consideration. Actual field time will vary depending on the depth of the well. Service rig costs include both one-time expenditures (fixed costs) and items charged on a per-day basis (variable costs). As seen in the breakdown of costs in Table 15, the variable expenses add up to $24,088 of additional cost for each additional day of service rig time. This marginal day cost will be considered in the scenarios and sensitivity analysis.

7.5 Tubing and Casing Costs

Tubing and casing are per metre variable costs that depend upon the depth of the wellbore. This study used 73.0 mm 9.67 kg/m J-55 tubing and 114.3 mm 17.26 kg/m P-110 production casing. According to the PSAC

2019 Well Cost Study, these classifications of pipe are commonly used in this geographic region. Several wells already have casing in place to their bottom depth and so only require tubing installation.

Table 15: Itemized list of service rig cost components and tubing/casing costs. Note: an * denotes a cost item that is charged at a day-rate and is dependent upon the number of days the service rig is employed.

Service Rig Costs	Item Cost/Day or Unit ($CDN)	Total Three-Day Cost ($CDN)	Description
Service Rig*	7,750	23,250	Rig and crew
Transportation*	2,500	7,500	Hauling of equipment
Other Services*	4,500	13,500	Vacuum truck
Completion Fluids*	4,500	13,500	Water and trucking
Logging (Cement Bond Log)	4,250	8,500	Run two CBL (check quality of cement job)
Slickline/Wireline (Other)	4,250	4,250	Gauge ring, run and pull recorders (confirm diameter/uniformity of internal wellbore)
Remedial Cementing	13,500	13,500	A run of remedial cementing (to repair existing cement plug deficiencies)
Wellsite Supervision*	1,400	8,400	Service rig days+3
Inspection / Safety	1,500	3,000	2 site inspections
Environmental*	1,000	3,000	Environmental technician cost per day
Lease & Road Maintenance*	500	3,000	Service rig days+3
Misc. Costs*	1550	8,112	8% Cost overrun buffer
Overhead*	388	2,028	2% Administrative addition
Subtotal		111,540	
Per Addl Day (Total Variable)		24,088	
Tubing and Casing Costs	**Price of Pipe ($/m)**	**Attachments & Accessories ($/m)**	**Description**
73.0 mm 9.67 kg/m J-55	20.75	-	Tubing Pipe
114.3 mm 17.26 kg/m P-110	35.75	2.00	Production Casing Pipe, Tongs, and Accessories
Misc. Costs			8% Cost overrun buffer
Overhead			2% Administrative addition

7.6 Calculating the Suspended Well Retrofit Expense

As described above, the cost of retrofitting an oil and gas well for geothermal energy production can be broadly broken into four components:

(eq. 30) $C_{RS} = PLP + WE + SR_T + CT_T$

Where C_{RS} is the total cost of a suspended well retrofit, PLP is planning and lease preparation cost, WE is well equipment cost, SR_T is total service rig cost, and CT_T is the total casing and tubing cost.

(eq. 31) PLP = sum of the item costs seen in Table 14

(eq. 32) WE = sum of the item costs seen in Table 15

(eq. 33) $SR_T = SR_F + SRV*D$

Where SR_F is the fixed cost or amount attributed to one day of service rig time, SR_V is the cost for each additional day, and D is the number of additional days the rig is required.

(eq. 34) $CT_T = (T*TVD + C_P*TVD) * (1.1)$

Where T is tubing cost in $/m, C_P is the cost for production casing and accessories in $/m, and TVD is the total vertical depth or the meters of pipe required and 10% is added for miscellaneous and administration costs.

7.7 Retrofitting an Abandoned Well

Abandoned wells would incur the same costs as above, as well as additional time and expense to remove plugging fluid, mill out a cement plug, and reattach surface casing. These additional steps are considered by conservatively adding two days of service rig time, plus the cost to purchase one standard 10m length of surface casing pipe and weld it to the existing surface casing. Table 16 provides an itemized list of additional costs incurred for retrofitting an Abandoned well.

Table 16: Itemized breakdown of additional costs incurred to retrofit an Abandoned well. Note: an * denotes a cost item that is charged at a day-rate and is dependent upon the number of days the service rig is employed.

Additional Costs for an Abandoned Well	Cost Per Day/Unit	Total Two-Day Cost	Description
Cut & cap replace	870	870	10m of 244.5 mm 53.57 kg/m J-55
Welding	1,500	1,500	Day rate
Service Rig*	7,750	15,500	Rig and Crew
Transportation*	2,500	5,000	Hauling of equipment
Other Services*	4,500	9,000	Vacuum truck
Completion Fluids*	4,500	9,000	Water + trucking
Logging (cement bond log)	4,250	4,250	Additional CBL (check old cementing)
Wellsite Supervision*	1,400	2,800	Extra days of site supervision
Environmental*	1,000	2,000	Environmental technician per day
Lease & Road Maintenance*	500	1,000	Service days
Misc. Costs*		6,254	8% Cost overrun buffer
Overhead*		1,564	2% Administrative addition
Subtotal		$58,738	

7.8 Calculating the Abandoned Well Retrofit Expense

The additional cost to retrofit an Abandoned well is as follows:

(eq. 35) $AWC = SRA*2 + \text{welding day rate} + C_S*10\text{metres}$

Where AWC is abandoned well cost and C_S is the $/m cost for 244.5 mm 53.57 kg/m J-55 surface casing. The welding day rate is a fixed value for one day of welding obtained from the PSAC Well Study Report.

Total cost to retrofit an Abandoned well will be calculated using the formula:

(eq. 36) $C_{RA} = PLP + WE + SR_T + CT_T + AWC$

or

(eq. 37) $C_{RA} = C_{RS} + AWC$

The overall economic performance of such a wellbore retrofit is not only a function of the cost of retrofitting the wellbore, but also on the economic gain achieved by the utilization of the refurbished geothermal system. Such gains are dependent on the specific end-use of the geothermal system. In the following section, detailed analysis of the economics of using retrofitted hydrocarbon wells to heat cattle field water in the winter as an example of a full life-cycle techno-economic assessment of this process.

8 Case Study: Cattle Feed Water Heating at Tomahawk Ranch

8.1 Introduction

Tomahawk Ranch consists of 14,500 acres of land located in Parkland County, Alberta, approximately 100 km west of the provincial capital Edmonton, as shown in Figure 40. The ranch sits directly above the heart of the Western Canadian Sedimentary Basin. The ranch is home to approximately 2000 head of cattle and 33 petroleum wells of varying age and status.

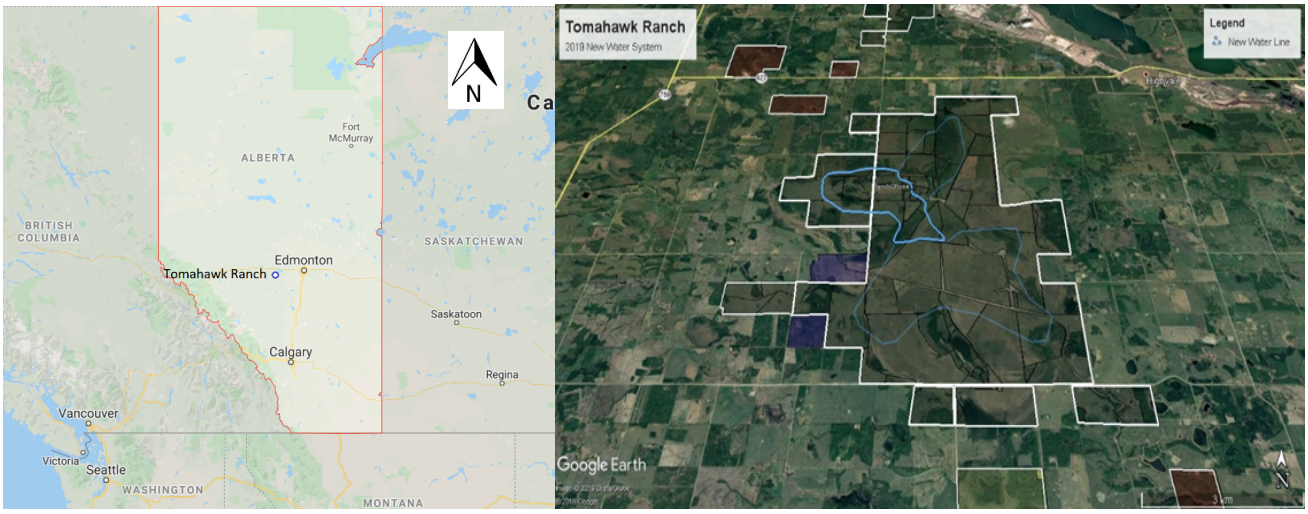

Figure 38: Location and geometry of Tomahawk Ranch in central Alberta, ~100km West of the provincial capital.

One of the major challenges for the ranch is providing drinking water for the cattle during the cold winter months. Ambient temperatures from November until March have averaged a daily high of -1.7 °C and daily low of -11.6 °C over the past 10 years, including a low of -39.27 °C during January 2020 (Alberta Agriculture and Forestry, nd). Such temperatures are cold enough to freeze standing water. The water wells on Tomahawk's land were originally able to service only 5-10% of the property's total area. A recent 9.6 km installation of 75 mm high density polyethylene pipe in a circuit has connected four water wells, allowing them to charge the water system from multiple locations and use a 1.12 kW pump that keeps the water flowing and prevents freezing. At various points, the water flows into an insulated tank where the cattle can drink from small holes. Although these holes often develop an icecap during the winter when water temperature can drop to 1 ˚C, they are tapered in a manner that allows the cows to easily dislodge the cap and access drinking water. With this system in place the ranch is now able to provide 5-6 l/s (~90 gal/min) of liquid water to about one third of the total acreage.

Although the cattle now have access to drinking water, the temperature of that water is often near freezing, and the Ranch owner believes that this may be causing weight loss or increased feed costs during the winter months. A literature review was unable to confirm this hypothesis but does suggest a link between ambient temperature and cattle health. Peterson et. al. (2016) found that water intake decreases as ambient temperature drops, but that animals offered warmer water will drink larger volumes. Other studies have also found that cattle dry matter intake tends to increase with cooler ambient temperature (Fox and Tylutki, 1998) and that the ratio of water intake to dry intake increases with warmer drinking water (Osborne, 2002. Collectively, these studies infer that cold water leads to decreased liquid intake along with increased dry feed intake. Intuitively, it is understood that any ingested water must be warmed to the cow's internal body temperature. Every joule of energy used to warm their drinking water is a unit lost to maintenance or growth. Thus, cattle must consume greater quantities of feed to make up this deficit. Furthermore, the rancher has also noticed an increased mortality rate among birthed calves during the winter months and believes access to warmer water may lower that rate. If increasing the cattle's drinking water temperature decreases the amount of feed required or the mortality rate of calves, it would be a direct economic benefit of using a well retrofit for geothermal heat production at Tomahawk Ranch.

8.2 Calculating the Benefit

There are two anticipated benefits from heating the cattle drinking water. First, the cattle will need to expend fewer joules of energy to warm the consumed water internally, thereby requiring less feed to maintain their body weight. The ranch owner has provided the following data:

- Average daily water consumption per animal during the winter months is 20-40 litres
- The cattle are predominantly fed Hay, which is purchased at a cost of $0.11/kg
- A system which records the current water temperature was installed in February 2020; from mid-February to mid-April 2020 the average drinking water temperature was approximately 2.5°C

Given that it takes 4.184kJ of energy to increase the temperature of 1L of water by 1°C and that the digestible energy present in 1g of hay is 11,087.6 J (Merck Veterinary Manual, 2020), it requires 7.55g of hay to increase 20L of ingested water by 1 °C. Using a hay price of $0.11/kg and 2000 head of cattle, the cost of feed that goes towards internally warming drinking water is $1.66/day/1°C. The region around

Tomahawk Ranch typically experiences 5 months of average air temperature at or below freezing (Alberta Agriculture and Forestry, 2020) and 103 days with snow cover of at least 5cm (Environment Canada, Dec 2019). The study assumed 4 months (122 days) where the cattle are subject to winter temperatures and unable to forage. This provides a yearly benefit of $202.52 ($1.66/day * 122 days) in reduced feed costs for every 1°C the drinking water temperature is warmed by the retrofit well. Scaled-up calculations for the total water consumption per cow are found in the results.

The second benefit of warmer drinking water is a possible increase in birthed calves. It is difficult to attribute any loss directly to cold drinking water, but the ranch owner estimates that he loses 3-5% of his calves due to the cold and typical calf value is $700. If we assume that 5 additional calves will survive because of access to warmer drinking water, this presents a $3500 annual benefit.

The base economic analysis included the estimated decrease in feed costs and no change to calf mortality rate; the best-case scenario will use a higher Hay price and include increased calving success of 5 additional calves. The techno-economic assessment of retrofitting an oil or gas well for geothermal energy production at Tomahawk Ranch property combines the deep borehole heat exchanger model described in Chapter 6 with the wellbore retrofit cost model described in Chapter 7 to evaluate the feasibility of using such retrofits for heating cattle feed water. The inputs for the deep borehole heat exchanger model are found in Table 17 below.

Table 17: Parameters for the 1D numerical model to calculate thermal power available for single phase fluid (water) from the five suspended wells at the operational conditions

Model Parameters	Values
Well length (m)	See Table X
Injection pressure (psia)	9000
Mass flow rate (kg/s)	1 to 10
Temperature (geothermal) gradient (°C/m)	See Table X
Injection temperature (°C)	5
Length increment for model (m)	5
Inner well radius (m)	0.03896
Pipe thickness (m)	0.0054864
Insulation thickness (m)	0.01
Diffusivity thickness of rock (m)	0.05
Pipe conductivity (W/m.K)-stainless steel	54
Cement conductivity (W/m.K)	0.55
Insulation conductivity (W/m.K)	0.04
Thermal conductivity of rocks (W/m.K)	2.5 (3.3 for well #5)
Surface air temperature T_o (ºC)	-10
Simulation time (days)	9132 (25 years)
Time increment for model (days)	5
Rock density (kg/m^3)	2630 (2500 for well # 5)
Rock specific heat capacity (J/kg.K)	910 (920 for well # 5)
Water specific heat capacity (J/kg.K)	4198

The inputs for the cost model are predominantly found in the previous section. Due to the specific nature of the case study, a few additional costs come into play. These costs include surface infrastructure costs, abandonment and reclamation costs, and operation costs, as described below.

8.3 Surface Infrastructure & Connection

Water flow from the existing drinking water supply must be diverted to reach the retrofit well so that it can be heated. Upon reaching the well, the water will be injected down the wellbore and heated using the coaxial borehole heat exchanger model. It is assumed that the water supply will be diverted and connected to the wellbore using the same 75mm high density polyethylene pipe used in the existing water circuit. The owner

of Tomahawk Ranch reported a price of $16.40-$32.80/metre, which includes pipe, all fittings and valves, and excavation for in-ground installation. Changes in topography and vegetation, which affected the excavation and installation, were primarily responsible for the range in reported cost. The base estimate uses the mid-range value of $24.60/metre, while the low and high-end values will feature in the best and worst-case scenarios.

By using a map of the water system (Figure 41) and plotting the relative location of each well based on its Unique Well Identifier (UWI), a reasonable approximation of the geographic distance between each well and the nearest point of the existing water flow system was created. This distance will inform the length of pipe required for connecting water flow to the retrofit well.

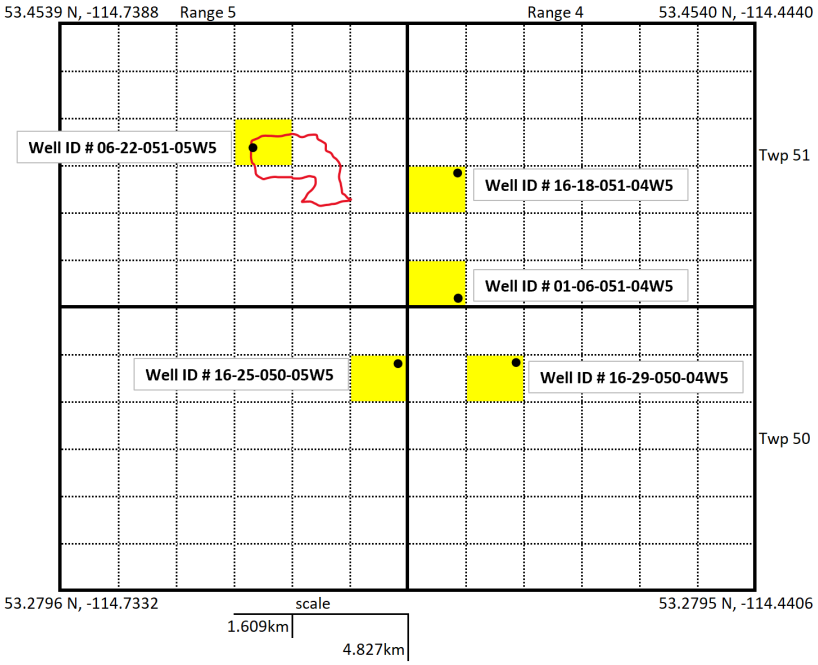

Figure 39: A plot of the Tomahawk water supply system(red line in upper left quadrant) and Suspended wells (black dots) on Tomahawk property on a grid representing the Dominion Land Survey for the area. Each square in the grid represents 1 square mile (1.6 square kilometres).

8.4 Calculating the Surface Infrastructure & Connection Cost

The surface infrastructure cost is calculated using the following equation:

(eq. 38) $SI = P * d$

Where SI is the surface infrastructure cost, P is the $/m cost for high density polyethylene pipe and installation, and d is the distance between the well and water flow system.

8.5 Abandonment and Reclamation Costs

AER Directive 011 provides guidance for oil and gas operators regarding both abandonment costs and reclamation costs. Abandonment costs are broken down into one of six regions in Alberta and further delineated by vertical depth and downhole completion characteristics. Reclamation costs are separated into seven provincial regions. Well age also has a significant impact on these costs. Correspondence a with a remediation firm based in Calgary, AB suggests that wells drilled prior to 1996 incur the highest cleanup costs, while those wells drilled more recently than 2003 incur the lowest cleanup costs. The abandonment and reclamation costs used in this paper reflect the values suggested by AER guidance while accounting for the age factor by adding 25% to the expense for wells drilled prior to 1996 subtracting 25% for wells drilled after 2003. To reflect the uncertainty in clean-up costs, the abandonment and reclamation expense will be increased or decreased by a further 50% in the worst and best-case scenarios.

The Tomahawk Ranch property is located within Regional Abandonment Area 2 and the Regional Reclamation Parklands Area as outlined in AER Directive 006. A well in this location with depth between 1200-1999 metres has a listed abandonment cost of $56,505 and a reclamation cost of $27,350 (AER Directive 011) for a combined $83,755 base case expense which was adjusted based on well age. Additionally, these numbers reflect the cost today; in the calculation the expense will be incurred at the conclusion of the project. As such, the costs seen in Table 18 will be adjusted for inflation and applied at the end of year 25.

Table 18: AER Abandonment and Reclamation costs adjusted by 25% for well age in the base scenario and adjusted again by 50% for best and worst-case scenarios

Well Age	Base Case	Best Case (-50%)	Worst Case (+50%)
1996-2003 Well	$ 83,755	$ 41,878	$ 125,633
Newer Well (-25%)	$ 62,816	$ 31,408	$ 94,224
Older Well (+25%)	$ 104,694	$ 52,357	$ 157,041

8.6 Operational Costs

Once the initial retrofit has been completed and the infrastructure is in place, ongoing operational costs are expected to be minimal. The installed infrastructure has a life expectancy exceeding that of the geothermal energy project, so no repair or replacement is anticipated. Yearly operational costs will be subject to inflation and discount rates based on when they occur.

A 25-year project lifetime was assumed. The full lifecycle economic evaluation was completed using a custom-built Excel spreadsheet that includes a comprehensive list of inputs, as described in section 2.3, below.

8.7 Results

8.7.1 Well data

Figure 42 displays the distributions of the wells on Tomahawk property by bottom hole temperature, depth below surface, smallest casing size, and year drilled all sorted by regulatory status. Of the 33 (13 active, 15 abandoned, and 5 suspended) petroleum wellbores on Tomahawk Ranch, 26 (including 4 of the Suspended wells) terminate in the Banff formation. These wells possess vertical depths between 1500-1750 m from the surface. Six other wells, including the 1 remaining suspended well, were drilled to the Cardium formation, with depths between 1000-1250m. The remaining well reaches the Nisku formation at a depth of 2065m.

Twenty-four of the wellbore records (including all the suspended wells) contained the data needed to calculate a corrected bottom hole temperature. The corrected temperature values range from 58.91°C to 80.68°C.

The oldest well was drilled in 1981, and the most recent was drilled in 2013. There is a barbell distribution of well ages as the majority were either drilled in the 1980s or after 2005, with minimal activity during the intervening years. Most, including all of the suspended wells, possess a smallest casing diameter of 139.7mm, although a handful of currently producing wells have 177.8mm intermediate casing as their smallest casing size. Some of the abandoned wells have no casing at all.

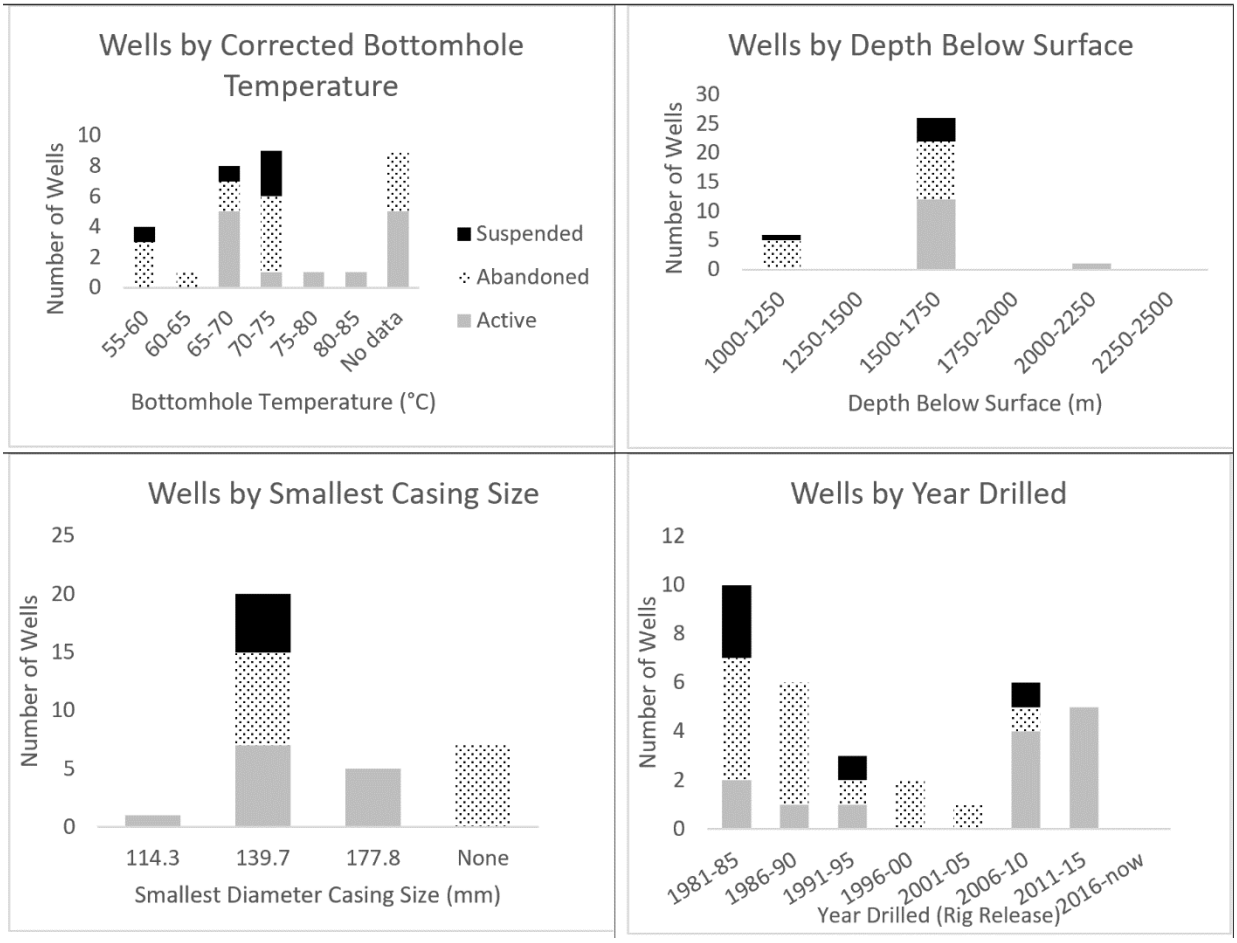

Figure 40: Distribution of the number of wells on Tomahawk property, sorted by regulatory status, for bottomhole temperature, vertical depth below earth surface, smallest diameter installed casing size, and year of drilling.

8.8 Geothermal Power Potential

Figure 43 shows the calculated thermal power for mass flow rates from 1 kg/s to 10 kg/s over 25 years for the five suspended wells. These graphs show that the thermal power outputs become steady within the first

few weeks of the production period. The power increases linearly with the rise of mass flow rate, as expected. The 25-year thermal power projections are more than 150 kW with >1 kg/s mass flow rate for the first three wells (Figure 43 a-c). For well # 4, the projection is around 100 kW with a 1-10 kg/s flow rate (Figure 43d). Due to the shallower depth, well # 5 is projected to produce 46 to 62 kW of thermal power over 25 years (Figure 43e). Figure 6f shows the produced temperature for well #5. The values of the fluid's produced temperature at 1 kg/s and 10 kg/s are 16 ºC and 6.5 ºC, respectively, revealing the influence of the flow rate on the temperature and, ultimately, on the thermal power. A lower flow rate produces fluid with higher temperatures, but decreases the thermal power output. The costs described below in Section 8.9.1 highlight that well #5 (00/06-22-051-05W5/0) is the least expensive to be retrofitted for the geothermal energy.

The thermal power required to raise the water temperature from 2 ºC to 10 ºC, flowing at a rate of 5-6 l/s (~90 gallons/min), is ~190 kW. In order to achieve this power with a sustainably low flow rate (~1 to 3 kg/s), Figure 43 suggests that at least three wells, including #5, need to be retrofitted to supply geothermal power to the entire volume of cattle feed water.

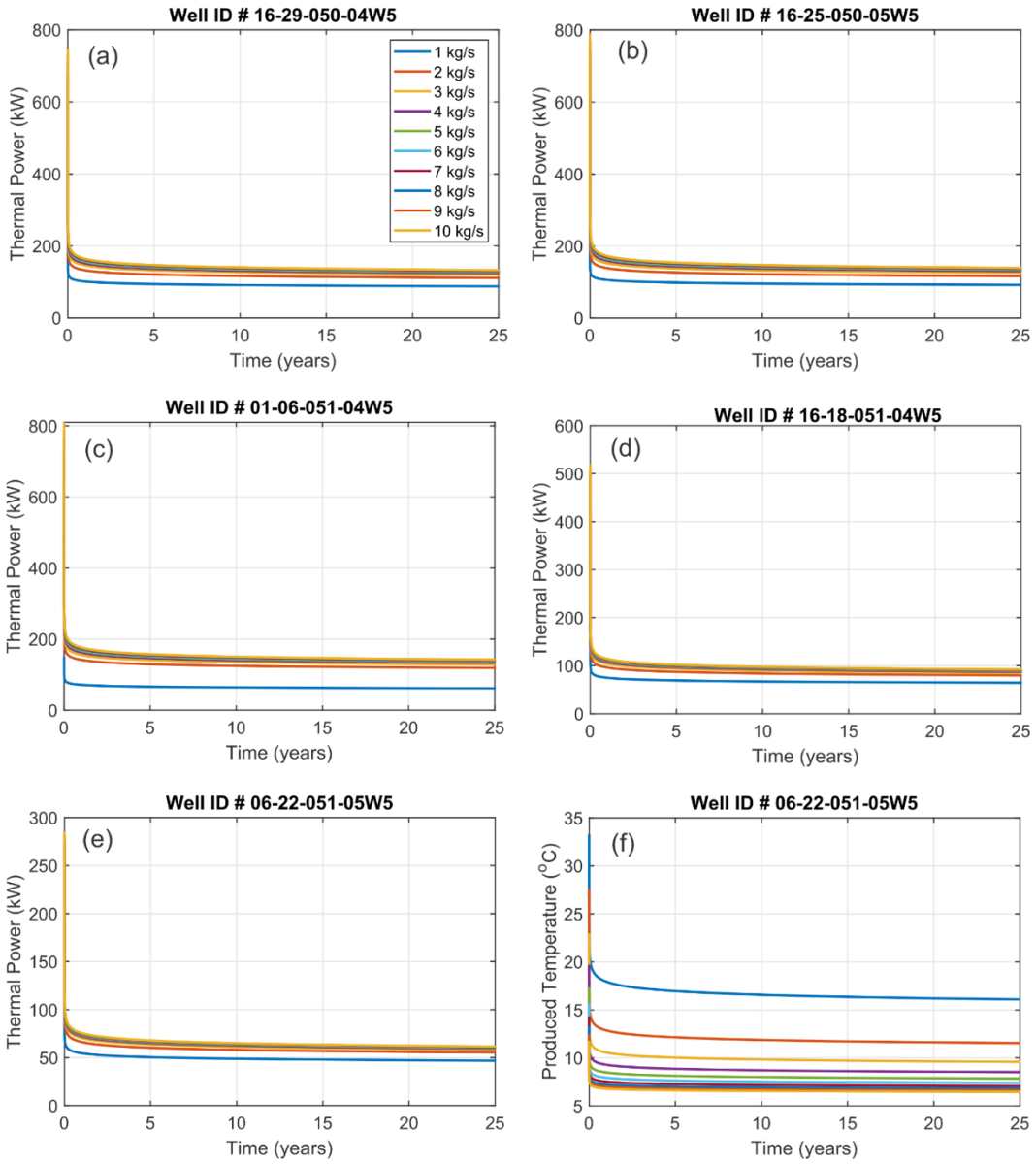

Figure 41: (a-e) 25 years projections of the thermal power, at 1 kg/s to 10 kg/s mass flow rate, for the five suspended wells at the Tomahawk Ranch Area, and (f) The produced temperature for the well # 5 at the same scenario.

8.9 Well Retrofit Costs

8.9.1 Suspended Wells

Using updated PSAC Winter 2019 Well Cost Study data, the average estimated cost to retrofit one of the five suspended Tomahawk wells for geothermal heat production is $212,999 (note: all dollar figure values

are presented as Canadian dollars), ranging from a low of $204,645 to a high of $215,281. This narrow cost range reflects the similarity of wellbore depth and geographic location. Table 19 outlines the breakdown of retrofit costs for each suspended UWI. Casing is currently installed in these wellbores, so the tubing and casing expense consists of tubing only.

Table 19: Breakdown of retrofit costs for Suspended wells on Tomahawk Ranch property

UWI	TVD (m)	Planning & Lease Prep	Well Equipment	Service Rig	Tubing and Casing	Total Cost ($CDN)
100/16-29-050-04W5/0	1665	$ 31,570	$ 33,825	$ 111,540	$ 38,004	$ 214,939
100/16-25-050-05W5/0	1670	$ 31,570	$ 33,825	$ 111,540	$ 38,118	$ 215,053
100/01-06-051-04W5/0	1680	$ 31,570	$ 33,825	$ 111,540	$ 38,346	$ 215,281
100/16-18-051-04W5/0	1671	$ 31,570	$ 33,825	$ 111,540	$ 38,141	$ 215,076
100/06-22-051-05W5/0	1214	$ 31,570	$ 33,825	$ 111,540	$ 27,710	$ 204,645

Approximately half of the expected retrofit cost, $104,671, are fixed costs. The relative homogeneity of the wellbores on the Tomahawk Ranch has resulted in the variable portion of service rig costs remaining constant. Thus, tubing and casing accounts for 100% of the retrofit cost variance

8.9.2 Abandoned Wells

The average estimated cost to retrofit one of the 15 abandoned wells on the Tomahawk Ranch is $301,421, or approximately $86,000 greater than a suspended well. There is also greater variation in retrofit cost, ranging from a low of $262,150 to a high of $346,018. This range is largely due to six of these wellbores requiring casing installation in addition to tubing. Table 20 displays the estimated retrofit cost for each Abandoned well.

Table 20: Breakdown of retrofit costs for Abandoned wells on Tomahawk Ranch property. Highlighted Tubing and Casing costs indicate those wells that required production casing installation in addition to tubing.

UWI	TVD (m)	Planning & Lease Prep	Fixed Well Equipment	Service Rig	Tubing and Casing	Addl Cost for Aban Well	Total Cost ($CDN)
100/10-31-050-04W5/0	1634	$ 31,570	$ 33,825	$ 111,540	$ 37,296	$ 58,738	$ 272,969
100/16-31-050-04W5/0	1665	$ 31,570	$ 33,825	$ 111,540	$ 38,004	$ 58,738	$ 273,676
100/08-18-051-04W5/0	1655	$ 31,570	$ 33,825	$ 111,540	$ 37,775	$ 58,738	$ 273,448
100/14-18-051-04W5/0	1626	$ 31,570	$ 33,825	$ 111,540	$ 104,999	$ 58,738	$ 340,671
102/16-18-051-04W5/0	1160	$ 31,570	$ 33,825	$ 111,540	$ 26,477	$ 58,738	$ 262,150
100/06-12-051-05W5/0	1670	$ 31,570	$ 33,825	$ 111,540	$ 107,840	$ 58,738	$ 343,513
102/06-12-051-05W5/0	1693	$ 31,570	$ 33,825	$ 111,540	$ 109,325	$ 58,738	$ 344,998
100/03-13-051-05W5/0	1673.9	$ 31,570	$ 33,825	$ 111,540	$ 38,207	$ 58,738	$ 273,879
100/08-14-051-05W5/0	1680	$ 31,570	$ 33,825	$ 111,540	$ 108,486	$ 58,738	$ 344,159
100/02-22-051-05W5/0	1208.6	$ 31,570	$ 33,825	$ 111,540	$ 27,586	$ 58,738	$ 263,259
100/13-22-051-05W5/0	1708.8	$ 31,570	$ 33,825	$ 111,540	$ 110,346	$ 58,738	$ 346,018
100/08-23-051-05W5/0	1185	$ 31,570	$ 33,825	$ 111,540	$ 76,521	$ 58,738	$ 312,194
100/14-23-051-05W5/0	1708	$ 31,570	$ 33,825	$ 111,540	$ 110,294	$ 58,738	$ 345,967
100/08-24-051-05W5/0	1161	$ 31,570	$ 33,825	$ 111,540	$ 26,500	$ 58,738	$ 262,172
100/14-24-051-05W5/0	1164.3	$ 31,570	$ 33,825	$ 111,540	$ 26,575	$ 58,738	$ 262,248

Most of the additional expenses required for retrofitting an abandoned well are due to the extra two days of service rig time and the installation of production casing, as needed. There is also an additional $2,370 to replace and reattach the top portion of surface casing. As with the suspended wells, all retrofit cost variance for abandoned wells is attributed to the tubing and casing cost component.

8.10 Total Capital Expenses

Any well that undergoes the retrofit process will also need to be connected to the cattle's water supply and properly plugged and reclaimed at the end of the project's 25-year life. These expenses must also be considered when calculating which wellbores present the least capital expenditure.

Table 21 outlines the total capital investment expected for each suspended wellbore including the retrofit expense, the present value of the abandonment and reclamation cost, and the installation of high-density polyethylene pipe. Based on these values, the 100/06-22-051-05W5/00 UWI requires the least capital investment.

Table 21: Summary of capital cost inputs for each suspended well on Tomahawk property.

UWI	Retrofit Cost	Year Drilled	Aban/ Rec Cost	Distance (m)	Pipe & Install Cost	Total Cost
100/16-29-050-04W5/00	$ 214,939	1983	$ 25,080	5000	$ 123,000	$ 363,019
100/16-25-050-05W5/00	$ 215,053	1985	$ 25,080	4800	$ 118,080	$ 358,213
100/01-06-051-04W5/00	$ 215,281	2007	$ 15,048	3400	$ 83,640	$ 313,969
100/16-18-051-04W5/00	$ 215,076	1981	$ 25,080	3200	$ 78,720	$ 318,876
100/06-22-051-05W5/00	$ 204,645	1995	$ 25,080	100	$ 2,460	$ 232,185

Tables 22 and 23 show the change to each capital expense component and the total expected capital investment required for each suspended well in a best or worst-case scenario. UWI 100/06-22-051-05W5/00 remains the lowest cost option in all scenarios and provides the smallest differential between best and worst-case scenarios. UWIs 100/01-06-051-04W5/00 and 100/16-18-051-04W5/00 are the next best choices in terms of total cost and variance despite having the two highest costs for the retrofit itself.

Table 22: Capital cost component values for each Suspended well under the Best and Worst-Case scenarios

	Best Case			Worst Case		
UWI	Retrofit Cost	Aban/ Rec Cost	Pipe & Install Cost	Retrofit Cost	Aban/ Rec Cost	Pipe & Install Cost
Variable Adjustment	20% less	50% less	$ 16.40/m	20% increase	50% increase	$ 32.80/m
100/16-29-050-04W5/0	$ 171,951	$ 12,540	$ 82,000	$ 257,927	$ 37,620	$ 164,000
100/16-25-050-05W5/0	$ 172,042	$ 12,540	$ 78,720	$ 258,064	$ 37,620	$ 157,440
100/01-06-051-04W5/0	$ 172,225	$ 7,524	$ 55,760	$ 258,337	$ 22,572	$ 111,520
100/16-18-051-04W5/0	$ 172,061	$ 12,540	$ 52,480	$ 258,091	$ 37,620	$ 104,960
100/06-22-051-05W5/0	$ 163,716	$ 12,540	$ 1,640	$ 245,574	$ 37,620	$ 3,280

Table 23: Total capital investment expected for each wellbore for each scenario

UWI	Base Case	Best Case	Worst Case	Variance
100/16-29-050-04W5/0	$ 363,019	$ 266,491	$ 637,303	$ 370,752
100/16-25-050-05W5/0	$ 358,213	$ 263,302	$ 624,973	$ 361,613
100/01-06-051-04W5/0	$ 313,969	$ 235,509	$ 510,896	$ 275,346
100/16-18-051-04W5/0	$ 318,876	$ 237,081	$ 525,270	$ 288,150
100/06-22-051-05W5/0	$ 232,185	$ 177,896	$ 319,523	$ 141,626

8.11 Full Lifecycle Project Economics

The geothermal power potential model indicates that three wells are needed to provide sufficient power to increase the drinking water to 10°C. UWI's 100/06-22-051-05W5/00, 100/16-18-051-04W5/00, and 100/01-06-051-04W5/00 have the lowest expected capital investment and present the least financial risk of the five Suspended wells evaluated for the Tomahawk Ranch geothermal energy retrofit project. As such, selection of these three wellbores provide the greatest chance for economic feasibility over a 25-year project lifecycle. Table 24 shows the input values used for calculating each of the scenarios.

Table 24: Input variables used in each project scenario

Revenue	Base Case	Worst Case	Best Case
Hay Price ($/kg)	$ 0.11	$ 0.09	$ 0.13
Yearly savings per 1°C Water Temp Increase	$ 202.57	$ 129.64	$ 291.70
Increase in drinking water temp (°C)	7.5	7.5	7.5
Calf deaths	0	0	5
Value per Calf	$ 700	$ 700	$ 700
Total Yr 1 Benefit	$ 1,519	$ 972	$ 5,688
Initial Capital Investment			
Well retrofit cost	Base	Plus 1 rig day and 20% increase	Minus 1 rig day and 20% decrease
Total Retrofit (3 wells)	$ 635,002	$ 848,719	$ 450,190
HDPE Install ($/m)	$ 24.60	$ 32.80	$ 16.40
HDPE Total	$ 164,820	$ 219,760	$ 109,880
Total Initial Capital Investment	$ 799,822	$ 1,068,479	$ 560,070
Abandonment and Reclamation	Base	50% increase	50% decrease
Present A&R cost (1 newer well, 2 older wells)	$ 272,204	$ 408,306	$ 136,102
Future A&R cost (in year 25: 2% inflation)	$ 446,580	$ 669,869	$ 223,290

Using the base case assumptions, including an 8% discount rate on all future cash flows, the expected net present value of the project is negative $845,775. Expenses include the up-front capital investment of $635,002 for the three well retrofits and high-density polyethylene pipe installation and the future $446,580 cost for abandonment and reclamation of the wells in year 25 ($272,204 subject to 2% inflation for 25 years). Warming the cattle's drinking water temperature to 10°C (a 7.5°C increase) creates a present value lifetime benefit of just $19,255. The calculated overall net present value drops to -$1,153,969 in the "worst-case" scenario, while improving to -$520,588 in the "best-case" scenario. Figure 44 shows the present value of lifetime benefits and overall net present value for each scenario. In both the base and worst cases, despite a decrease in benefits, the project's overall value increases. This counter-intuitive result is due to the accumulated benefits being less than the expected abandonment and reclamation expense at the conclusion of the project.

In all scenarios at all assessed discount rates, the projected net present value of this retrofit project is negative. The expected benefit from reduced feed costs is insufficient to justify the investment. In the base

case, reduced feed costs create $1,519 of benefit in year one, while feed cost savings of $68,252 (rising with inflation each year) would be required to break even. In the best-case estimate, the addition of improved calf-birth rates decreases that gap, but still fails to make this a profitable project.

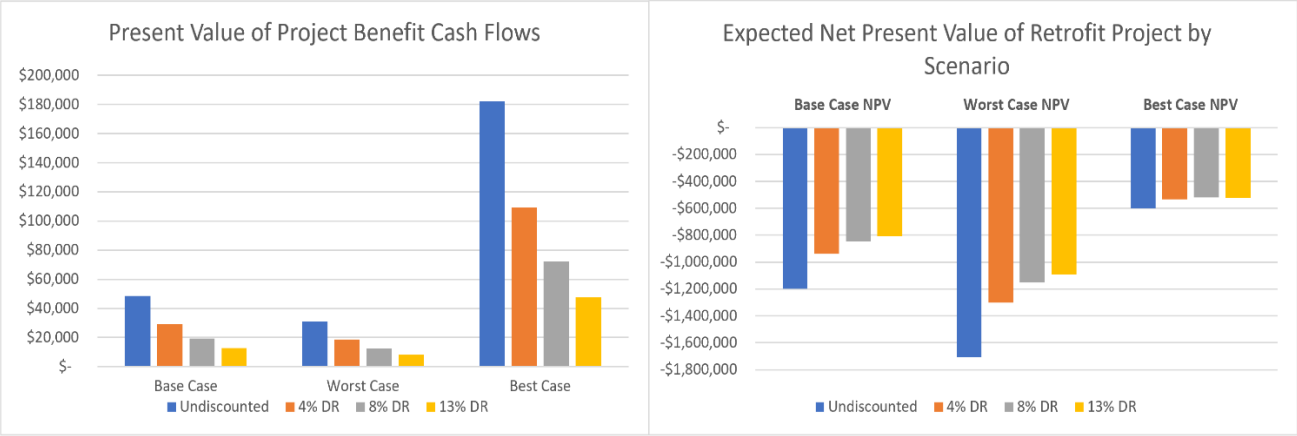

Figure 42: Left - Present value of all benefit cash flows. Right - Net present value of all project cash flows

8.11.1 Sensitivity Analysis

For the final step of the economic evaluation, a sensitivity analysis was conducted to better understand which variables have the greatest impact on projected net present value. Beginning with the base case scenario inputs, each variable was adjusted by 20% to calculate the change in expected net present value. Recognizing that the benefits to cattle are unlikely to make a geothermal energy retrofit project feasible, the break-even annual revenue value of $68,252 in year one was used. Figure 45 shows the results of the analysis. Choosing a break-even revenue means that this variable must equal all expenses, so a 20% change on revenue has the largest impact on net present value. A 20% change to initial capital expenditure, the largest project expense, alters the project's financial outcome by nearly $160,000. Lowering the retrofit cost or finding an alternative revenue source will be the most effective means of making this project economically feasible. The discount rate is the next most influential factor on the project's net present value. Inflation rate has a relatively minor impact on project economics. Abandonment and reclamation costs have the least economic impact due to the discounting of this expense that occurs over 25 years' time.

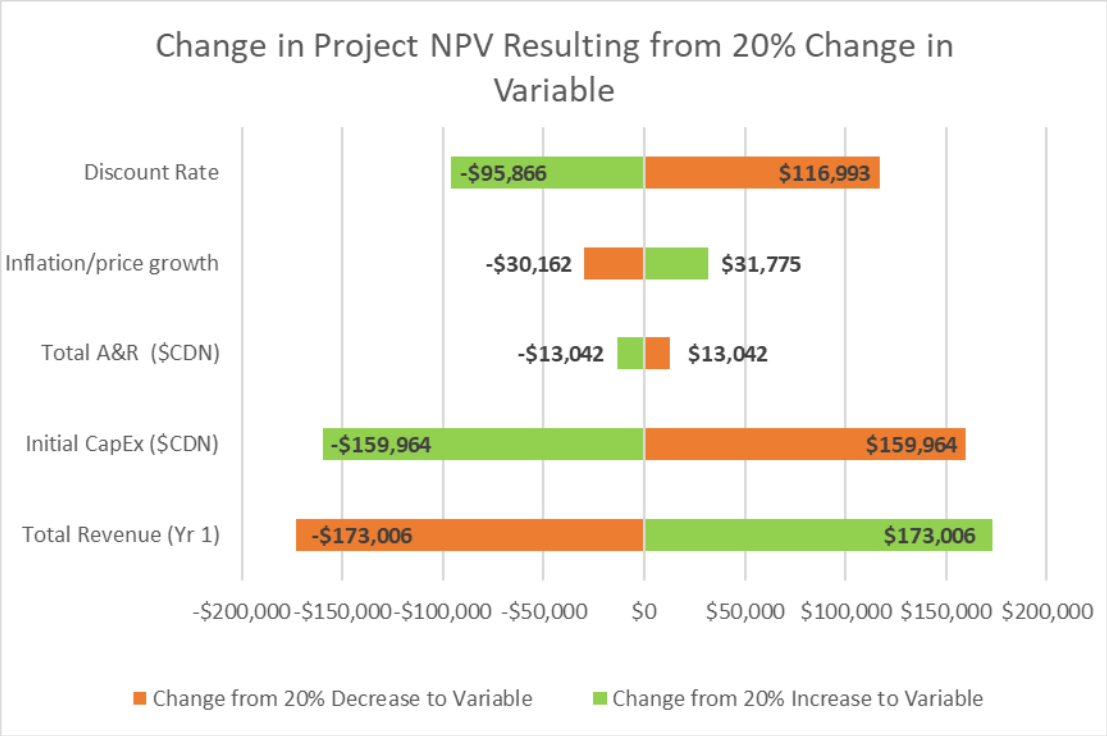

Figure 43: Sensitivity analysis showing change to project net present value resulting from 20% change to inputs

Based upon the ranch owner's experience of increased cattle feed costs during the winter months and the intuition that an animal will need to expend some joules of energy to warm ingested drinking water to body temperature, it was hypothesized that being able to warm drinking water by a matter of degrees may reduce the animal's caloric intake and reduce overall feed costs. The ranch owner has also noticed fewer successful calf births during cold weather periods and suggested that warmer drinking water may improve the birth rate.

The calculated net present value of retrofitting inactive oil and gas wells to geothermal wells for warming the drinking water for 2000 head of cattle, however, is negative $845,775. This figure includes $865,030 of expenses and $19,255 of benefits. The expected reduction in feed costs of just over $1,500 per year are too small to justify significant capital spending.

The well retrofit project at Tomahawk Ranch is likely not economically feasible unless an alternative use for the heat is found. The study analysis, however, does provide valuable insight for future well retrofit evaluations. First, suspended status wells are the optimal retrofit target because they are likely easier to

acquire the lease rights for and will have a lower retrofit price than an abandoned well with the otherwise same characteristics. Second, a reliable estimate of both the thermal power potential and well retrofit costs can be estimated based on knowledge of two factors, well location and vertical depth. Third, surface infrastructure expenses are the greatest source of variance in an overall project cost. These costs increase with increasing distance between the well (heat source) and water (heat recipient) and these distances can vary by kilometres. Fourth, abandonment and reclamation costs are relatively unimportant to the overall project economics because of discounting and the long lifespan of a geothermal energy source. Finally, the choice of discount rate for future cash flows plays a significant role in a project's economics. The long lifespan of a geothermal energy project, coupled with offset carbon emissions and the potential for reducing abandonment and reclamation liability from retrofit oil and gas wells, may make this type of project particularly appealing entities concerned with social welfare.

9 The Geothermal Atlas of the Western Canadian Sedimentary Basin

9.1 Introduction

The Geothermal Atlas of the Western Canadian Sedimentary Basin is an interactive, map centric, web application that developed and partnership between the University of Alberta and the Alberta Geological Society. The beta-version was completed within the context of this study, and the final version will be hosted by the Alberta Geological Survey. It will consist of a comprehensive geologic model of every geothermal reservoir ≥ 40˚C in the Western Canadian Sedimentary Basin. These models will contain geospatial, hydrogeological, geomechanical, and thermodynamic incorporated into a interactive, GIS – enabled software product. The purpose of this atlas is to enhance exploration and development of geothermal resources and reduce costs by providing salient information upfront to both industry and policy makers. It will provide the tools required for preliminary project planning which will reduce upfront research and development costs. The data contained in this atlas could reduce geothermal project development costs on the order of $100,000s to $1,000,000s per project. The atlas may also be used to inform a long-term (50 + years) geothermal energy development strategy in the WCSB.

The beta-version of atlas contains full functionality for the Swan Hills region of Alberta. The atlas will eventually expand the from this initial study to a much wider geographic area and to lower temperature reservoirs, covering all resources in the WCSB, i.e. Saskatchewan, Alberta and NE British Columbia, as well as the Yukon and Northwest Territories. To date, this information has been restricted to academic and government use and has not yet been consolidated in any useful manner pertaining to geothermal energy exploration. It will provide services to the energy sector along with the academic community, as well as the general public and municipal, provincial, and federal governments. Market segments span many industries and include: entrepreneurial start-ups, oil and gas producers, oil and gas service providers, drillers, regulatory and legislative bodies, municipalities, academics, data management firms, and the general public.

The Western Canadian Sedimentary Basin (WCSB) contains enormous amounts of energy in undeveloped geothermal resources, worth billions of dollars. Although several high-level assessments of this resource base have been performed (e.g. CanGEA's Canadian National Geothermal Database, GSC's Geothermal Energy Resource Potential of Canada, Chapter 30 of the Geologic Atlas of the WCSB), these assessments have not led to the commercial development of any of these resources. In part, the lack of development is because these assessments, while scientifically sound, do not provide information detailed enough to inform

commercialization – focused decision-making within Canada's fledgling geothermal industry. Geothermal energy developers require actionable information regarding the:

- rock properties of basin – hosted geothermal reservoirs
- hydrodynamic and thermodynamic reservoir parameters
- specific location and depth of suitable reservoirs
- energy and power production estimates for these reservoirs
- pre-designed schematics and process flow diagrams for various types of geothermal energy projects (both direct – use and electricity generating)
- accurate cost projections based on reservoir parameters, project locations and project types.

The creation and upkeep of the Geothermal Atlas of the Western Canadian Sedimentary Basin has many steps utilizing many different computer programs. It requires the acquisition of data from existing oil and gas wells that have geophysical properties associated with them. Relating all of these properties geospatially allows an inverse distance weighted interpolation to fill in areas where data is scarce. Data can be organized and cleaned in a spreadsheet in excel before importing it into ArcMap to be displayed geospatially. Once in ArcMap, maps can be created using tools such as Geospatial Analyst (GA) and Raster Calculator.

Each map is saved as separate .mxd files and "shared" as a "service" on ArcGIS Online. These hosted feature layers are then added to a web map that serves as the map containing all of the layers of the atlas. Custom pop-ups are configured for each layer depending on which data fields should be displayed. This web map is linked to the web app that is created using the Environmental Systems Research Institute's (ESRI) Web AppBuilder Developer Edition. The web map is used by the web app as the base of all geospatial and geophysical data. The web app utilizes ready-made configurable widgets such as Layer List and Query to interact with the data hosted in the web map in addition to custom widgets created from scratch using Javascript programming language along with ESRI and Dijit APIs. The open source API Plotly is also utilized in creating the histograms of the results in both the Volumetric Monte Carlo Simulation and Wellhead Monte Carlo Simulation widgets. The Developer Edition of Web AppBuilder also allows for the complete customization of the appearance of the Atlas interface. For example, custom colour schemes and widget button size and icon.

9.2 Methods

9.2.1 Spreadsheets and importing data into ArcMap:

Software programs such as geoSCOUT, ArcMap, ArcGIS Online, and ESRI's Web AppBuilder are required to get all of the necessary data into a useable format inside the Atlas web application. Each map layer of the atlas requires geological and geophysical data acquired through geoSCOUT that is organized as an Excel spreadsheet which is then imported into ArcMap to be displayed geospatially. Table 25 contains a list of the data required for a map layer of oil and gas wells to be uploaded to ArcGIS Online. Formation thickness is added to the dataset using rasters calculated from formation top and base grid files from the Alberta Geological Survey. The resulting collection of well point shapefiles is uploaded to ArcGIS Online as a Hosted Feature Layer.

Table 25: List of required data for the creation of map layers

Data	Location
UWI	from geoSCOUT in the Well Data export
Temperature	BHT from geoSCOUT in the DST Data export as well as corrected BHT from raster logs
Flow Rate	from geoSCOUT in the Individual Production export
Porosity	from geoSCOUT in the Core Data export
Bulk Formation Thickness	from AGS grid files. Thickness calculated from the difference between the tops and bases. Extract Value to Points tool used to add the thickness values to individual wells
Net Pay Thickness	from geoSCOUT in the Reservoir Evaluation sheet of the Well Data export
Easting/Northing	from geoSCOUT Well Data export calculated from latitude/longitude
UTM Zone	from geoSCOUT Well Data export calculated from latitude and longitude
Formation	from geoSCOUT corresponds to producing/injection formation and DST formation
Field	from geoSCOUT Well Data export
Unit	from geoSCOUT Well Data export
Current Operator	from geoSCOUT Well Data export
Well Status	from geoSCOUT Well Data export
TVD	from geoSCOUT Well Data export
MD	from geoSCOUT Well Data export
KB	from geoSCOUT Well Data export
Latitude/Longitude	from geoSCOUT Well Data export

Other maps are created using ArcMap tools such as Raster Calculator and Geostatistical Analyst and are described in more detail below. Each map is uploaded to ArcGIS Online as a separate file to be added to a Web Map as Hosted Feature Layers.

9.2.2 Temperature and porosity maps:

Temperature and porosity maps of each formation are made from the map of oil and gas wells by using the Geostatistical Analyst tool. It uses all data present and interpolates values spatially between the points. Definition Queries are applied to the layer of oil and gas wells before using the Geostatistical Analyst tool to remove any value that should not be included in the interpolation. For example, any zeros that result from blank cells in the spreadsheet by using simple "greater than" logic equations.

With the Definition Query applied, the Geostatistical Analyst tool will only use values that fit the definition. For the Swan Hills case study, an Inverse Distance Weighted interpolation is used to create the maps for the Atlas. A Mean value is used in the case of multiple data points existing from the same location. This ensures that if there are multiple entries from the same well for the same formation, they aren't over represented in the interpolation. After the Geostatistical Analyst tool is complete, the extent of the resulting layer is changed to the extent of the shapefiles with which the interpolated layer will later be clipped with. In the case of the Swan Hills Formation, these are the shapes of the carbonate reefs defined by the oil and gas Field. Each reef shapefile is created using the Aggregate Points tool with an 800m buffer around the outermost wells of the Field which assumed to be the maximum extent of the reservoir.

9.2.3 Geothermal Gradient maps:

Geothermal gradient maps display the subsurface temperatures at regular intervals. They are calculated using Bottom Hole Temperatures and measurement depths taken from DSTs. The DST data is acquired from geoSCOUT and organized in a spreadsheet that is added to ArcMap. This table is "Joined" to the oil and gas well layer using UWIs before the Geostatistical Analyst tool interpolates data points spatially between wells. Like the temperature and porosity maps, the geothermal gradient maps use an Inverse Distance Weighted interpolation. The DST depths are measured depths not true vertical depths and thus only data from vertical wells are used. Geothermal gradients are calculated by using this formula:

(eq. 39) (([DST BHT (°C)] – [Average Annual Surface Temp (°C)]) / (DST Depth (m))

An average annual surface temperature of 1.8°C is used for the Swan Hills case study. The gradient calculated at each well location is then be applied to calculate the temperature for depth interval:

(eq. 40) (Geothermal Gradient (°C/m)) * (Specific Depth Interval (m))

A custom symbology is applied to all of the geothermal gradient layers to demonstrate a cohesive colour scheme across depth intervals. For example, an equal interval for every 5°C from the coldest to hottest temperatures present across the layers. These layers are exported to vectors using the Geostatistical Analyst tool to Contour tool before being uploaded to ArcGIS Online.

9.2.4 Processing Bulk Formation Thickness from AGS Rasters

The AGS has open source tops and bases for a number of formations within the WCSB in the form of ASCII rasters. The thickness of the formations across the basin are calculated by importing the rasters into ArcMap and using the Raster Calculator tool to calculate the difference between the base and top of each formation. The "Extract Values to Points" tool uses both a shapefile and a raster input to create a new shapefile with all of the data from the shapefile input as well as all of the cell values of the raster that correspond to each point geospatially.

9.2.5 Favourability Maps:

The geothermal favourability maps are designed to locate favourable sites within existing oil and gas fields for the development of geothermal energy resources. They are produced by geospatially overlapping bottom hole temperature and flow rate data taken from drill stem tests (DSTs). This case study focuses on four known oil and gas fields within the Swan Hills Formation.

9.2.6 Favourability mapping procedure

The favourability mapping procedure is identical to that described in Chapter 3, above.

9.2.7 Favourability mapping input data

Bottom hole temperature and flow rates are derived from DSTs in known oil and gas fields using geoSCOUT software. Data is filtered for the Kaybob, Kaybob South, Virginia Hills, and Swan Hills fields within the Swan Hills Formation. The data is exported as Excel files and then processed through geographic information system software (i.e. ArcMap). Well data for each field is exported from geoSCOUT and processed through ArcMap software to produce the final favourability maps. Only data from active and suspended wells were collected. Abandoned wells are neglected due to the difficulty of bringing these wells

back into operation. Bottom hole temperature corrections were calculated using a time since circulation method (Corrigan, 2003). Water flow rates from the last 12 months of production were taken from available DSTs.

9.3 Structure

Once all the maps are created, they can be shared to ArcGIS Online as Hosted Feature Layers. Each of these layers is added to a Web Map which serves as the base of the Geothermal Atlas. Each layer is configured for custom pop-up and attribute table displays that are carried over to the Web Application. The atlas uses ESRI's Web AppBuilder to create a web-based application that uses custom maps from ArcMap and ArcGIS Online, custom widgets using JavaScript code, and configurable out of the box widgets created by ESRI. Table 26 summarizes the widgets used in the development of the atlas. The web map of the Western Canadian Sedimentary basin consists of multiple layers that contain geological, hydrogeological, geophysical, and geochemical properties that will aid in the enhancement of exploration and development of geothermal resources. Each property can be viewed in an attribute table or in pop-up windows with configured data that appear when a well or polygon in a map layer is clicked on.

Table 26: Out of the box widgets that are incorporated into the Atlas

Widget	*Description*
Attribute Table	Displays multiple wells at a time in a spreadsheet style table
Coordinate	Displays the latitude and longitude of the mouse cursor
Extent Navigate	Can easily switch between extent views – much like a back and forth button
Full Screen	Switches to a full screen view, removing the browser window
Home	Returns to the original extent view
My Location	Finds the user's location and zooms to it
Overview Map	Displays a pop-up of an overview map with the current extent box
Scalebar	Displays a scalebar directly in the map
Search	Searches for locations by name or address and zooms to that location
Splash	A pop-up window appears when the atlas is initially opened. This is the introduction to the atlas and is completely customizable to include a description and how to use the atlas.
Zoom Slider	Simple navigation buttons to zoom in or out of the map
Basemap Gallery	A selection of ESRI's basemaps
Layer List	A list of searchable layers that are contained within the map. These include: • Well layers (by formation) • Favourability maps • Temperature maps (by formation/area) • Porosity maps (by formation/area) • Geothermal gradient maps (500m intervals) • Lithofacies maps (by formation)
Query	A widget that applies configurable queries to any selected layer within the map. The queries can highlight which wells have either temperature or net pay data. Some of the queries use inputs defined by the user such as Well Status or setting a filter to show which wells have BHT greater than a given temperature.
Screening	A polygon can be created by drawing a shape, applying a radius to a location, or uploading a shapefile. All of the well data from within the polygon is returned and can be printed with a map view.
Select	Returns a list of wells within a drawn square for which statistics can be calculated
Measurement	Measuring tool for distance, area, or location (latitude/longitude)
Print	Print the current map view
About	A sidebar to display information about the atlas and where to contact support

9.3.1 Custom Widgets:

There are two custom widgets, the Volumetric and Wellhead Monte Carlo Simulations, which host the main functionality of the Atlas. They process a series of inputs and results from queries of the map layers to produce heat and power outputs that will aid in the initial stages of geothermal energy exploration. The inputs for both of these simulations are detailed in Chapter 3, above. A screenshot of the volumetric simulation input screen is shown in Figure 46.

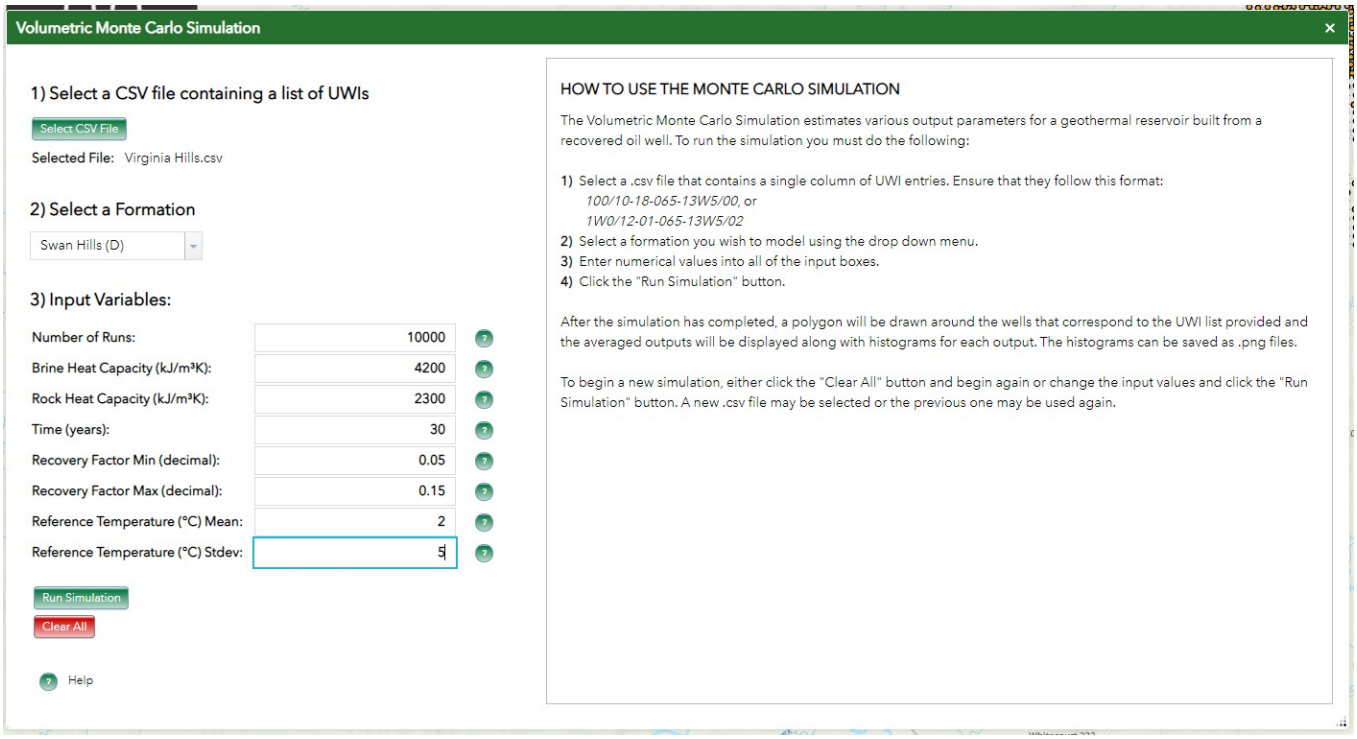

Figure 44: Screenshot of the Volumetric Monte Carlo Simulation Widgets

The results of each simulation are displayed in a separate window as average output values along with histograms of each output that can be cycled through. The results window, shown in Figure 47 can be printed as a group of sheets. Multiple simulations can be run one after the other with each new results section appearing in a new tab so the results can be easily compared. Otherwise, all results can be cleared and the process can be started over. If there is insufficient data in the map layer to be queried, a unique window appears explaining the error and next steps to be taken.

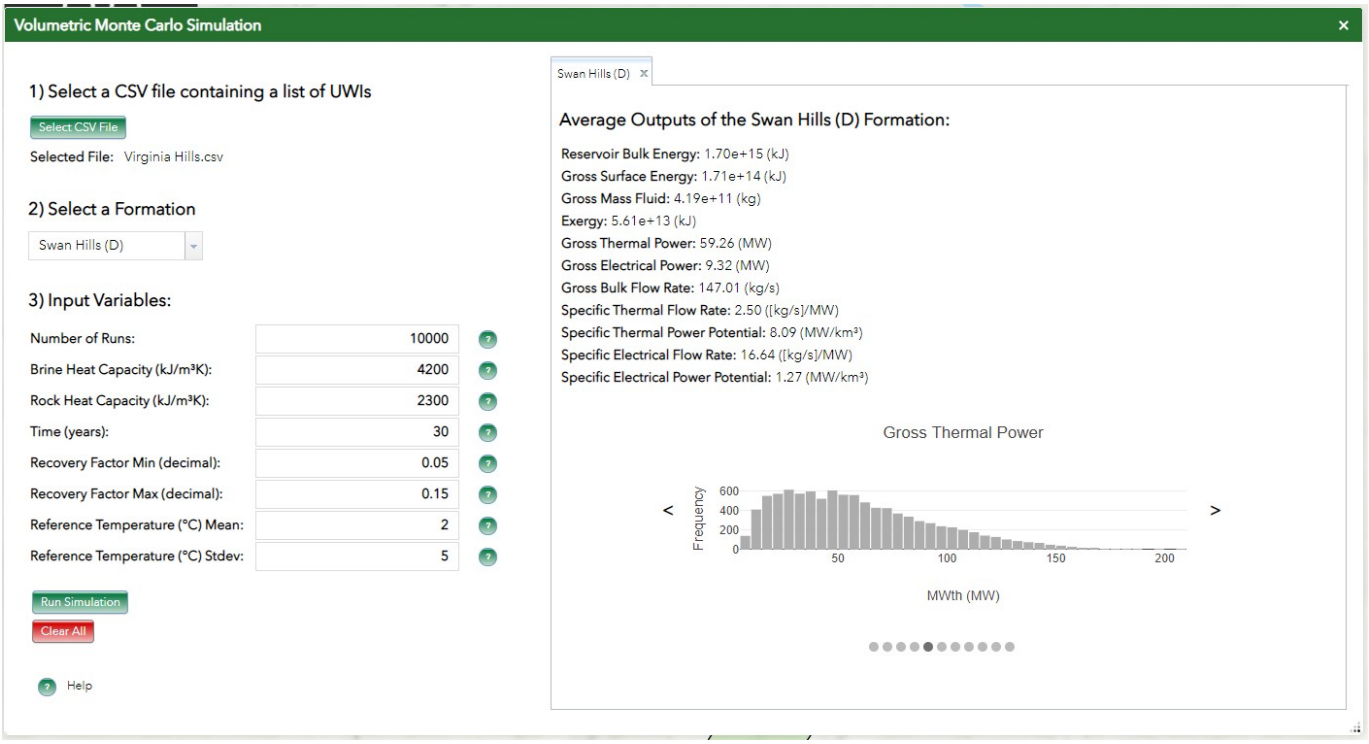

Figure 45: Volumetric Monte Carlo Simulation widget with averaged outputs and histogram

The Volumetric and Wellhead widgets utilize Monte Carlo simulations that require only a few user inputs. The rest of the data is contained within each map layer and is automatically queried and used in each set of calculations. All that is required is a list of wells using Unique Well Identifier (UWI) format, a geological formation selected from a drop-down menu, and a list of inputs found in Figure 46 Step-by step-instructions for using the widget are found below in Table 27.

Table 27: Step by step instructions on how to run the Volumetric Monte Carlo Simulation Widget

A csv file containing a list of 16-digit UWIs is uploaded and be the basis of all queries into the layer
A formation is selected from a drop-down menu
Values are filled in as inputs which vary depending on what simulation is being run
The "Run Simulation" button is clicked and the simulation runs through various functions before displaying the output results as averaged values and histograms.
The csv file is analyzed and each UWI is extracted
The map layer based on the selected formation is queried and a buffered polygon is drawn around the wells to give an area for calculating the reservoir volume
The map layer is queried again for other input values which vary depending on what simulation is being run
Each output (see Table # - with the variables, symbols, types) is calculated using a combination of the user inputs and the results from the queries, then displayed as averaged values and histograms.
A new simulation can be run and the results will appear in a new tab so results can be easily compared, or
The "Clear All" button can be clicked to start over

The functionality of the well-head based simulation is broadly similar to that of the volumetric simulation.

9.4 Conclusion

The Geothermal Atlas of the Western Canadian Basin is an accessible online tool that provides an entry point to the development of geothermal projects in Alberta. This technology can play an important role in the field of renewable energy and the development of related technologies. This project has the potential to have cascading effects throughout the Canadian economy with the creation of jobs in the research sector as well as the development and implementation of geothermal projects, including the conversion of legacy oil and gas wells for the use of producing electricity and the installation of new geothermal energy plants. It will create jobs for those involved in the research and development of renewable energy resources and related technology and will provide additional work for those in the drilling and resource extraction industries and has the potential to bring in investors from countries who have existing geothermal energy programs.

10 Socio-political roadmap for large-scale adoption of brown-field geothermal power development in Alberta

10.1 Overview of transformation frameworks

Industry transformation is multidimensional. In this section, we outline various frameworks for understanding industrial transformation and describe how these frameworks may be integrated in the context of transitioning from hydrocarbon production to geothermal power production. A comparative case study was performed detailing why the hydrocarbon-to-geothermal transition has been slow to take root in Alberta, whereas other jurisdictions, such as France, has seen greater success.

Several frameworks can be used to understand the socio-political conditions required for transformation, which focus on various dimensions and policy prescriptions (Garud & Gehman. 2012). The first framework is evolutionary, as exemplified by the multi-level perspective (Geels & Schot, 2007). Small clusters of actors (individuals and organizations) generate ideas within a market niche. As their innovations evolve, some are picked up by others and adopted more broadly, given environmental selection processes, triggering a contest amongst competing designs, until a new design becomes victorious and locked into the institutional system (revised market categories, regulation, etc.). This evolutionary framework sensitizes researchers to the interdependencies between multiple actors and levels (local, regional, national, international), varying rates of change (slow/fast, continuous/bursty), and the co-evolution of technologies, practices, and regulation.

The second framework is relational, as typified by the continuously negotiated networks of 'socio-material' associations (Callon, 1999; Pinch & Bijker, 1984; Garud, Kumaraswamy, & Karnøe, 2010). People, organizations, and things (technologies, objects, etc.) are all actors, entangled in ongoing identity recreation (who are we?), meaning-making (what does this mean?), and translations into practice (what do we do?). In the area of stakeholder relationships, there is emergent scholarship on bridging stakeholder groups for long-term value creation (Strebel, Cossin, & Khan, 2020) and social licence to operate (Gehman, Lefsrud, & Fast, 2017). This framework alerts researchers to examine phenomena - like geothermal energy - in the making and the involved actors, their meanings, interactions, and practices.

The third framework is durational, as exemplified by inter-temporal narratives (Bartel & Garud, 2009). Actors are constantly creating, rationalizing, coordinating, and recategorizing language repertoires to direct our memories of the past, attention to the present, and anticipations of the future. By appealing to transcendental ideals of what is sacred, narratives can create social solidarity, even among those from very different institutional systems and logics (e.g. Voronov & Weber, 2017;). Outside the domain of energy,

Reagan et al. (2016) have explored how narratives develop among stakeholder groups through emotional arcs. Lawrence & Phillips (2004) explore the role of macro-cultural discourse in the structuring of new fields. Oberg, Lefsrud & Meyer (2021) examine how climate change policy debate and invest-divest discussions are interacting and influencing each other at the macro-global level. This durational framework sensitizes researchers to actors' choice of words, subjects, and storylines; temporal orientations; and forward- and backward-looking narratives.

Each framework suggests differing policy, strategic, and research levers for energy transitions (Garud & Gehman, 2012). Evolutionary frameworks suggest that niche innovations must be protected and promoted, say with feed-in tariffs to provide an incentive for developing renewable energy. Conversely, top-down 'moon-shot' initiatives promote path-breaking innovations. Evolutionary pathways can also be managed - such as with regulatory changes - to reconfigure the selection environment and direct evolution. Relational frameworks examine how regulators and other evaluators (investors, market analysts, consumers) are active co-creators of the energy supply and demand system. This suggests that governments must share data, host forums to bring all the players together, support active piloting and experimentation, and continuously adapt market mechanisms to support transition. Durational frameworks focus on the creation of narratives. This suggests that change is enabled through groups like task forces that host discussions to reflect on past actions, coordinate current activities, and enact possibilities.

Duygan et al. (2019) incorporate all three frameworks - evolutionary, relational, and durational – to examine the resources, social networks, and discourses required for industrial transformation (See Figure 48). They leverage institutional entrepreneurship: "the strategic action exerted by actors who have an interest in a particular set of institutional arrangements and use their agency to pursue them" (Duygan et al., 2019, p.15). Institutional entrepreneurship specifically examines the collective action of many actors who play diverse and partisan roles in the network that emerges around a technical innovation.

10.2 The modern geothermal industry

Many jurisdictions around the world have also started realizing the benefits of using geothermal energy directly as heat (i.e., 'direct use'; Reber, Beckers, & Tester, 2014; Francesco, et al., 2016; Hähnlein, Bayer, Ferguson, & Blum, 2013; Harrestrup & Svendsen, 2014; Kubota, Hondo, Hienuki, & Kaieda, 2013; Purkus & Barth, 2011). Space heating in various industrial, commercial, and residential projects can contribute up to 50% of the project's total energy demand (Seyboth and Beurskens, 2008). Furthermore, the potential for

non-electric applications of geothermal energy has been found to far outweigh the electricity production market. Lavigne (2018), for example, showed that both economic and environmental performance of a proposed direct use geothermal system near Hinton, Alberta was ten times greater than an electrical system powered from the same reservoir. Houldsworth & McDevitt (1982) examined the market potential for non-electric applications of geothermal energy in the USA, finding that, while most resources are not adequate for generating electricity using conventional flash or binary technologies, many of these resources are adequate for non-electric applications such as space and water heating, and even for various production process requirements. These authors acknowledge that maximum exploitation of these low-enthalpy geothermal resources requires effective marketing and additional research concerning the roles of consumer acceptance and public policy in developing a heretofore untapped resource.

Clearly, geothermal heating is a viable and valuable form of renewable energy, but studies show that sociotechnical factors such as supportive public policies and public perception can significantly limit its development. For example, the exploitation of low-enthalpy geothermal resources requires better understanding of changes to groundwater aquifers, especially regarding geothermal production's influence on the long-term environmental health of such systems. For Japanese projects, societal acceptance by local stakeholders is the fundamental barrier to geothermal energy development, trumping all other barriers such as financial, technological, and political (Kubota, Hondo, Hienuki, & Kaieda, 2013). Purkus & Barth (2011) echo this finding, stating that the unprecedented growth in Germany's geothermal sector in the last decades has been tied to extensive political support and favourable market conditions. Finally, Malafeh & Sharp (2015) show that government royalties for geothermal energy need to better incorporate the rate of heat extraction, because this can be a leading factor leading to the project's long-term economic sustainability.

As mentioned, converting oil and gas wells to geothermal production is not technically simple or inexpensive. First, the suspension and abandonment of oil and gas wells involves several steps that make conversion increasingly difficult. These steps are: 1) temporary suspension of production; 2) abandonment of the reservoir, well integrity evaluation, and placing of primary and secondary barriers to prevent flow to the surface; 3) retrieval of the casing, installing primary and secondary barriers to isolate the intermediate hydrocarbon and water-permeable zones, and a placement of a surface 'environmental' plug; and 4) removal of all surface structures, wellhead, and reclamation of the site (Kurnia et al., 2021). Conversion is easiest during well suspension and highly impractical after permanent abandonment. Second, as the

integrity of the well-bore degrades through time, newer wells are better candidates for conversion than older wells. Third, the geothermal potential of a well is a function of the bottom-hole temperature, permeability of the rock formation to pump water in or out to extract the heat, and the potential for nearby users. Fourth, volatility in commodity prices and development policy make investments less certain. In sum, the economic favourability of conversion will decrease with stage of suspension/ abandonment, age, lower temperatures, permeability, and more distant users.

In jurisdictions including France, New Zealand, Germany, Japan, the Adriatic Region, and certain U.S. states with recent low-temperature geothermal development, proponents have employed cross-sectoral collaboration, entrepreneurial support systems, and public support to significantly improve the chances of project success (Reber, Beckers, & Tester, 2014; Francesco, et al., 2016; Kubota, Hondo, Hienuki, & Kaieda, 2013; Purkus & Barth, 2011; Malafeh & Sharp, 2015). In Alberta, however, despite robust geothermal potential and interest by multiple proponents, complementarities between the established oil and gas sector and the emergent geothermal sector have been under-leveraged (Leitch et al., 2019).

10.3 Hydrocarbon to geothermal transition in Alberta

Alberta has had a prominent oil and gas industry since the 1914 discovery of oil in Turner Valley, although the industry mainly developed after WWII following discovery in Leduc. Unlike France, there is minimal history of geothermal development in Alberta, except for sparse hot springs in the Rocky Mountains. In 2012, academic research demonstrated the availability of significant low-enthalpy geothermal energy. Three different projects were attempted between 2010 and 2019 to extract geothermal heat from idle oil wells but have so far stagnated.

In 2015, a newly elected government announced an ambitious Climate Leadership Plan, and despite implementing various renewable electricity carve-outs the program made no mention of low-carbon heat. Furthermore, persistently low natural gas prices made the deregulated heating energy market unfavorable to new entrants like geothermal power. In 2016, an academic study by the Canadian Geothermal Energy Association identified over 60,000 wells with bottom hole temperatures hot enough for heating applications, with 500 well-suited for power generation. The same year, the Town of Hinton initiated a Front-End Engineering Design (FEED) study with an industry partner to evaluate the viability of a geothermal district heating system but found that complex subsurface re-engineering would be required and revenue from heat production alone would not cover these capital costs.

Between 2015 and 2017, the provincial climate-progressive government received opposition to renewables, especially in rural regions. The same year, a second oil-to-geothermal initiative called the Living Energy Project emerged amidst concern from entrepreneurs and policymakers about the rising number of inactive oil wells. In the 2019 provincial election, the incumbent government lost to a new government who swiftly cancelled the province's carbon tax and Renewable Energy Program. Low global oil prices resulted in over 84,000 oil and gas wells becoming inactive, with some being considered for geothermal energy retrofitting. Numerous academics and think tanks continued promoting geothermal heat, with one think tank citing in a report that "the cost of retrofitting an idle well into a geothermal heat source being roughly half the cost of reclaiming the idle well." Despite this, industry proponents remained reluctant to invest capital into geothermal projects, with some citing an oversight of geothermal regulation in the provincial Oil and Gas Conservation Act and Public Utilities Act. Some entrepreneurs identified that the Canadian tax code failed to recognize geothermal heat as a renewable energy source. When the provincial government announced a multi-million-dollar program for cleaning up abandoned and idle oil and gas wells in 2020, it made no mention of geothermal conversions. As of June 2020, a low-enthalpy geothermal project from an inactive oil well has yet to come online in Alberta. Eavor Technologies, an Alberta-based startup specializing in low-enthalpy geothermal technology, announced a demonstration using its Eavor-Lite product in Rocky Mountain House, Alberta, but has no linkages to oil and gas wells. The South Swan Hills project associated with the study received research and development subsidies from the provincial and federal governments but is yet to be completed.

This 10-year process of Alberta's activities in oil-to-geothermal innovation is shown in Figure 48. Overall, actors have failed to strategically mobilize the three elements of agency in Alberta, resulting in a divergence that has impeded oil-to-geothermal development. With regards to the mobilization of networks, Alberta's initiatives have operated in silos, without major multi-sectoral and institutional partnerships. The Hinton project failed due to lack of funding to support the creation of district heating infrastructure. The Renewable Energy Program, while active, offered no subsidies to renewable heat resources, making it difficult for geothermal heat to compete with natural gas. The most recent inactive well cleanup program by the provincial government still makes no mention of the geothermal power opportunities. Overall, the low-enthalpy geothermal resource in Alberta has been consistently undermined by a lack of government support, and proponents have acted in silos from one another and end-use partners. In terms of resources, Alberta's quest has been to mobilize idle, suspended, or orphaned oil wells requiring complex subterranean

engineering to convert the moving fluid from oil to water. On the other hand, since the Western Canadian Select (WCS) price is volatile to global fluctuations in oil markets, geothermal co-production too may be economically unfeasible in many Albertan wells which are either idle, abandoned, or orphaned.

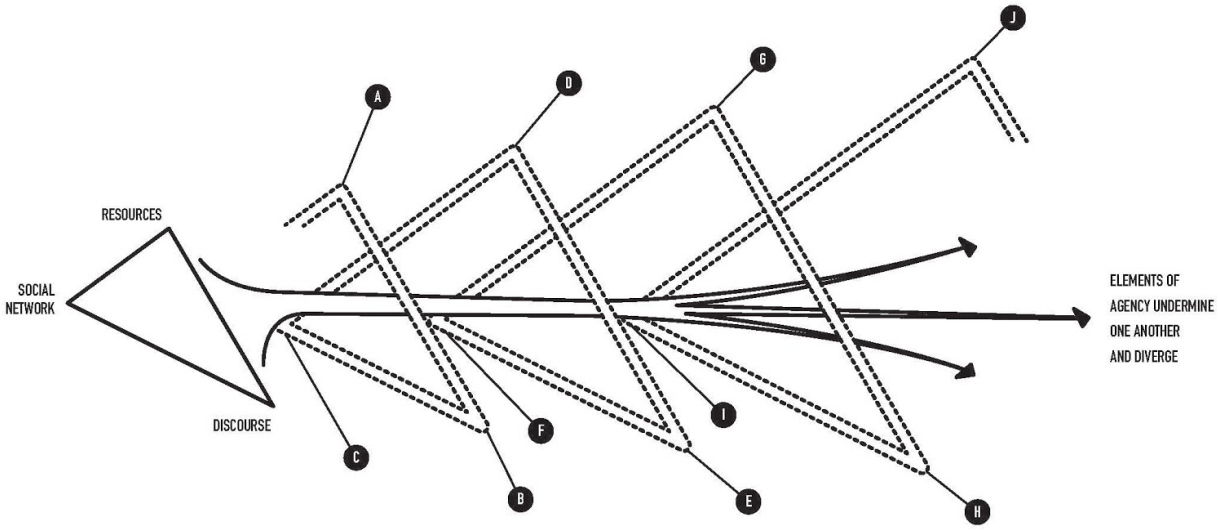

A	1914 - 2010	Established oil/gas industry but no geothermal industry
B	2012	Emergent academic knowledge of low-enthalpy geothermal potential but minimal public awareness
	2015	Renewable Energy Program launched but did not include low-carbon heat
C	2015	Geothermal heat undermined by cheap natural gas and deregulated market
D	2016	Town of Hinton's FEED study found unexpected technical complexities and costs
E	2017	Living Energy Project: low-enthalpy geothermal development tied to oil narrative
	2017 - 2018	Renewable energy received public opposition
F	2018	Targeted Viginia Hills wells were distant from social hubs; district heating pipelines needed
	2019	Governing party changed and Renewable Energy Program cancelled
G	2019	Low oil prices resulted in over 84,100 inactive oil and gas wells scattered across Alberta, but only a handful were considered as geothermal candidates
H	2018 - 2019	Academics and some proponents advocated for repurposing inactive oil and gas wells for geothermal heat
	2019	Industry proponents reluctant to develop geothermal heat projects due to lack of provincial geothermal regulation
I	2020	Provincial government announced inactive well cleanup program but made no mention of geothermal opportunity
J	2020	No low-enthalpy geothermal projects targeting inactive oil wells have come online yet

Figure 46: Key activities of institutional entrepreneurship demonstrated by actors in Alberta's oil-to-geothermal transitioning system between 2010 and 2019, shown in the form of a triangular helix representing the three elements of agency. Over time, the elements of agency undermine one another and diverge.

As Alberta's registry of abandoned oil and gas wells grows, many could be repurposed for geothermal production; however, the endeavour of subterranean borewell retrofitting introduces technical risks and reservoir maintenance due to new subsurface geochemical processes and therefore requires far more capital

investment and technical knowledge than currently present in the oil and gas sector. Beyond oil and gas knowledge transfer into this emerging geothermal sector, projects attempted in Alberta did not significantly benefit from knowledge transfer among the three proponents themselves, all of whom acted independently of one another. Finally, with regards to the mobilization of discourses, the increasing motivation for low-enthalpy geothermal heat in Alberta emerged largely because of a rapid increase in Alberta's list of inactive oil and gas wells, as opposed to any prominent motivation to reduce waste, minimize the ecological footprint of oil and gas companies, or improve agricultural or social resilience. Alberta's transition has been motivated by depressed oil prices, indicating that proponents were trying to innovate their way out of stranded asset risk as the crisis unfolded as opposed to pre-emptively. Overall, there exists a heroism of entrepreneurship in Alberta signified by the lonesome institutional work done by innovators motivated to solve crises without public or intersectoral support, further stymied by the targeting of difficult-to-extract resources. This lack of strategic mobilization of resources, networks, and discourses over the 10-year period of study has significantly stifled the innovation of geothermal within Alberta's oil and gas regime.

10.4 Hydrocarbon to geothermal transition in France

The French oil industry has existed since the 1740s, with more than 100 Mt of oil discovered via government programs since 1945 (Heritier, 1994). There is also a long history of low-temperature geothermal development in France, with development in the Paris Basin starting in 1962 at Carrieres-sur-Seine (Lopez et al., 2010). Currently, there are more than 30 geothermal power plants exploiting the Dogger aquifer (BRGM, 2014).

In the French oil-to-geothermal transition, three projects were developed sequentially by the same oil company starting in 2005, Vermilion Energy, whose engineers aspired to repurpose waste heat from active oil wells to reduce their carbon footprint. Vermillion's vision was to use a settling tank to separate the warm water from a hydrocarbon emulsion, and then pump the water through a surface-level heat exchanger to extract and distribute heat. Amid early efforts, the French government introduced a new subsidy for renewable heating applications in 2009. Vermilion, however, could not benefit from this scheme because it applied only to purely geothermal exploration costs, whereas Vermilion was co-producing geothermal energy from active oil wells. Nonetheless, after lobbying some regional chambers of commerce, Vermilion received mayoral and agribusiness support and the municipal permits for its first project. In 2012, the Parentis well in rural Bordeaux became the first oil well retrofitted by Vermilion. It uses 60 °C heat to power France's largest co-operative owned greenhouse, Tom d'Aqui. This project earned the French

government's Circular Economy Award in 2013. As we showed in early parts of this study, 60 ˚C heat is widespread in the subsurface of the Western Canadian Sedimentary Basin.

Leveraging its national recognition, Vermilion was selected to help AVENIA (a new French government initiative) identify other waste heat opportunities across France in 2016. Later the same year, Vermilion partnered with ENGIE, a national utility, to build pipeline infrastructure for district heating projects. Soon, another oil well in the same reservoir was retrofitted to provide space heating for a new social housing project, Les Arbousiers. At this point, Vermilion still lacked a geothermal license and was unable to profit from its geothermal resources. The company soon applied for a license so it could sustain its geothermal activities. In 2017, the French government passed a moratorium law on license applications or renewals for oil and gas exploration after 2040. This law garnered further interest in geothermal and alternate revenue generation activities from oil and gas companies. In 2018, an agreement involving Vermilion for an eco-conscious neighbourhood, Les Portes du Pyla, was reached. It would use 70°C waste heat from three wellheads from the Aquitaine Basin. This larger project, producing enough geothermal energy to heat 550 apartments and facilities, was developed in partnership with the municipality of Itteville, a French land developer, and a local energy distribution utility.

Vermilion was inaugurated in an EU Horizon 2020 consortium of organizations who will receive funding and share expertise to develop low-temperature geothermal energy. Through HORIZON 2020, Vermilion partnered with start-up ENOGIA to use their modular Organic Rankine Cycle heat exchanger at a proof-of-concept project at one of its oil wells in Chanoy. The prototype expects initial results in 2021.

Within 15 years, the three elements of agency exercised by Vermilion converged, resulting in significant momentum in its innovation in transitioning oil to geothermal producing, shown in Figure 49. Networks mobilized included local politicians, tangential industrial sectors like agribusiness cooperatives, infrastructure-providing intermediaries and sector-leading research and development consortiums who supported Vermilion's early innovations. These institutional actors helped create a stable niche that could fit Vermilion's innovation neatly within the existing energy, food and housing systems. In terms of the mobilization of resources, Vermilion's co-production of geothermal and oil from its wellheads made its resource mobilization strategy technologically feasible using simple above-the-surface heat exchangers which collect heat from hot brine. Seeing as these mature wells produce little oil to begin with and have a

high water cut, the eventual conversion to only water poses low geochemical risk to the well. Broadly similar conditions exist throughout the Western Canadian Sedimentary Basin.

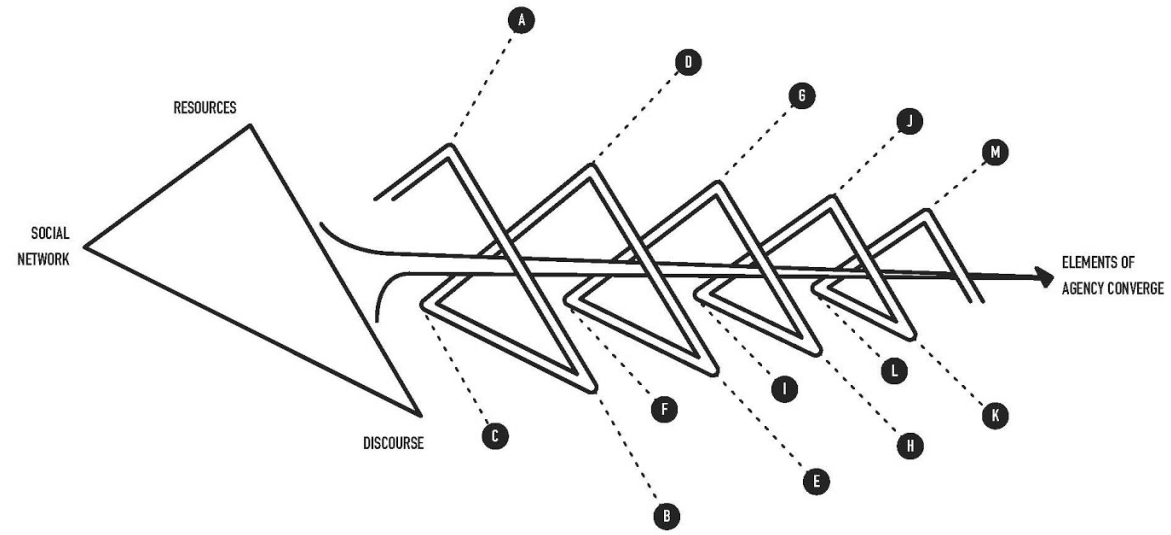

A	1740s - 2005 1969 - 2005	Established oil/gas industry Established geothermal industry
B	2005	Vermilion aimed to make use of waste heat in brine
C	2006	Vermilion lobbied Chamber of Commerce and won mayoral and argibusiness support/permits
D	2012	Vermilion connected heat exchanger for 10-hectare Tom d'Aqui greenhouse online
E	2013	Vermilion's Tom d'Aqui project awarded French government's Circular Economy Award
F	2016	Vermilion supported AVENIA to identify sources of waste heat from oil wells across France
	2016	ENGIE partnership established to build district heating pipelines
G	2016	Vermilion launched Les Arbousiers social housing project
H	2018	Vermilion started considering geothermal licence to be compensated for future district heating projects
I	2018	Oil/Gas Exploration Ban elucidated stranded asset risks in oil companies
	2018	Itteville initiated eco-neighbourhood destrict heating
J	2009 - 2018	ENOGIA developed modular Organic Rankine Cycle heat exchanger
K	2018	Vermilion and other oil companies conceptualized low-enthalpy geothermal electricity projects
L	2018	Vermilion and ENOGIA invited to MEET Consortium for R&D geothermal heat/electricity from oil wells
M	2019	Vermilion launched first ENOGIA ORC demonstration site at Chaunoy

Figure 47: Key activities of institutional entrepreneurship demonstrated by actors in France's oil-to-geothermal transitioning system between 2005 and 2019, shown in the form of a triangular helix representing the three elements of agency. Over time, the elements of agency recursively strengthen each other and converge.

As for knowledge transfer, engineers iterated designs between three projects, leading to gradual improvements. The French innovation also benefited from the sharing of resources between interested stakeholders – Horizon 2020 provided vital research funding, ENOGIA provided its prototype Organic

Rankine Cycle technology, whereas Vermilion hosted a demonstration project at its Chaunoy site. Finally, with regards to mobilizing discourses, Vermilion's initiative was motivated by its engineers wanting to make socially responsible use of the waste heat to benefit the local community. The vision was framed non-financially at first; in fact, none of the three early projects were profitable. Instead, they earned Vermilion public approval, highlighted by the CEO's statement in response to the Circular Economy Award:
"As a good corporate citizen, we continually focus on safety, health and the environment and this project demonstrates Vermilion's commitment to the communities in which we live and work, including local job creation and our respect for minimizing the environmental footprint of our operations." - Lorenzo Donodeo (Vermilion Energy, 2013)

Eventually, Vermilion expressed financial motivations when it applied for a geothermal licence. This decision was framed in terms of deferring the cost of well reclamation and reducing stranded asset risks, but this vision emerged as secondary to the project proponent's original social responsibility narrative. Vermilion's innovation practices consistently mobilized networks, resources, and discourses to strategically strengthen its agency, thus allowing it to become a major player in France's oil-to-geothermal transition.

10.5 Recommendations for successful transitioning in Alberta

Through this comparative case study, the relative presences, absences, and combinations of each of these elements through time have been illustrated, so that specific policy prescriptions can be made. First, in these two jurisdictions there is a clear interest demonstrated by a network of actors, deployment of resources to achieve a vision, and various forms of discourse by both the proponents and associated communities. Yet, the jurisdictions' varied attempts to coordinate elements of agency to achieve a geothermal transition have resulted in convergence in France but divergence in Alberta. The resulting analysis on the durational interaction of networks, resources and discourses suggests a handful of recommendations for how to enable geothermal innovation within the existing oil and gas sector through the interactive use of the three elements of agency. Next, the policy prescriptions for resourcing, discourse, and networks are discussed.

Leitch et al. (2019) examined the unexploited overlaps in resourcing. Third-party resources including financing, critical infrastructure, and knowledge-sharing can each counteract various barriers to entry for geothermal innovators. Albertan developers hoping to convert oil wells into geothermal wells face a significant barrier to entry due to the volatile nature of the Western Canadian Select oil market. France's

Vermilion Energy was able to develop its geothermal projects at low cost from productive oil wells since they did not suffer as much as Alberta from idling/abandonment during the 2008 or 2015 oil price collapses. Furthermore, Vermilion received in-kind support from a publicly owned utility to develop an above-ground heat exchange and pipeline network for distributing its resource, whereas Alberta's lack of utility support combined with the critical need for transporting heat from well sites to distant end-use locations further stymied development. To help Alberta's oil and gas industry enter the geothermal sector, various levels of government and utility companies can dedicate their own resources to support them by including low-enthalpy geothermal proponents within existing and future climate change incentive programs such as the Renewable Electricity Program (REP) and the Technology, Innovation and Emission Reduction (TIER) program. The Liability Management Framework managed by the Orphan Well Association could provide incentives for covering the costs of retrofitting suspended or abandoned wells for geothermal production. Dedicated grants for Alberta's privately owned utilities could promote the integration of geothermal or low-enthalpy heat into their resource mix. Beyond financing and critical infrastructure, policy can be used to diffuse knowledge by convening geothermal innovators. In France, the collaborative EU MEET Consortium played a crucial role in enabling knowledge collaboration between utilities, start-ups, and Vermilion. While Alberta's geothermal innovators have so far acted in silos, the province has a unique history in leading mission-oriented innovation through the Alberta Oil Sands Technology and Research Authority (AOSTRA), and many lessons can be adopted into its geothermal sector. Through AOSTRA, the government invested over CAD$1.4 billion (2019 dollars) to provide disruptive yet collaborative support between 1976 and 1996; assumed direct responsibility for creating the necessary extractive technologies; and created clear goals and robust mechanisms for knowledge diffusion across the emergent in situ oil sands mining industry (Hastings-Simon, 2019). Similar approaches involving public-private partnerships and competitive innovation grants/prizes could radically accelerate a jurisdiction's innovation and adoption of geothermal energy.

France's case study demonstrates that inter-sectoral policies can be designed to integrate the discourse on geothermal energy not only between oil producers and geothermal developers, but even other uses of geothermal energy beyond the energy sector. By appealing to transcendental ideals of protecting what is sacred, discourses can create social solidarity across these different institutional systems. France's agricultural sector played a pivotal role in unlocking low-enthalpy geothermal heat for greenhouse applications. Agriculture is a powerful partner because locally produced foods (wine, cheese, bread) are an integral part of French identity and regionality. Contrastingly, this study's analysis showed that agricultural

actors were absent from energy resource planning discourses in Alberta. In similar manner to France, given the transcendental value of agriculture and especially cattle in Alberta, using narratives to connect geothermal energy to this sector (e.g., geothermally heated greenhouses, geothermal co-generation with bio-energy, heating of drinking water for cattle, grain drying, etc.) can play a pivotal role in enhancing network-wide geothermal support. Beyond agriculture, other sacred sectors of Alberta's economy that can be engaged in geothermal co-creation include water, fishing, and eco-tourism. To strengthen this agriculture-geothermal cross-sectoral discourse, the resourcing can also be linked through policy incentives for using low-carbon or geothermal heat technologies like heat pumps and retrofitted oil wells at the small- and medium business level. And the discourses of such collaboration could be amplified through the retelling of stories involving successful partnerships (Pregger et al., 2020).

Beyond sector-based collaboration, Alberta's government can also enable partnerships between First Nations, Indigenous communities, and geothermal developers to build community-led development that enhances local economic development, independence from expensive diesel generation, and Indigenous-Canadian reconciliation. Māori prescribe bathing in designated hot springs to cure various ailments (Stokes, 2000). Similarly, Indigenous peoples in Canada use hot springs and sweat lodges for ceremony and healing. Such practices are private and sacred to the communities. Respecting these practices while also developing economic projects will catalyze community support, again, by appealing to transcendental values of water as sacred (Hikuroa et al, 2010).

To shape compelling narratives around geothermal energy, policy and legislation must recognize geothermal resources as distinct from power, heat, oil, gas, or other subsurface resources to create a niche for development (Schot & Geels, 2008; Leitch et al., 2019). In 2019, France adjusted its federal mining code to make the permitting process easier for geothermal exploration to enable future geothermal development. In Alberta, Government agencies have been dedicated to developing a geothermal resource policy in Alberta since 2013. In 2020, the provincial government finally received royal ascent for Bill 36: The Geothermal Resource Development Act (GRDA), which will be critical in shaping future discourse in the province. However, there exist criticisms around Bill 36. First, while Bill 36 aims for clarity for how geothermal resources are regulated while still underground, it excludes details on how geothermal projects fit within the current electricity regulatory regime in Alberta, regulated by the Alberta Utilities Commission (AUC), who still lacks guidance on how to review and approve geothermal power plants and grid connections. Second, there is no mention of regulations for using geothermal energy as a direct heat source

or as a co-generated product alongside oil and gas production. Third, there is ambiguity around the treatment of carbon credits/offsets related to geothermal projects, for instance whether an oil well co-producing geothermal energy is eligible for carbon credits under the "low carbon" definition of the government regulation (Government of Alberta, 2020). Fourth, Bill 36 makes it extremely easy for an oil and gas company to transfer liability associated with well cleanup and reclamation over to emerging geothermal developers, who see this as a high financial risk. Future geothermal policies in Alberta, such as one that makes it easier to lease an inactive well for the purposes of geothermal production, can be used to de-risk the transfer of oil and gas wells into the hands of emerging geothermal developers.

11 Conclusion

11.1 Summary of Major Results

- 480 oil and gas field throughout the Western Canadian Sedimentary Basin with the potential for geothermal retrofits were identified. Field temperatures ranged from 25 ˚C to over 130 ˚C at depths ranging from 1500 m to over 4500 m. Twenty fields showed strong potential for electricity production, and over 300 fields showed potential for conventional direct use applications. There is practically unlimited potential for innovative low-enthalpy (< 20 ˚C) uses such as snow melting.
- A robust Monte Carlo simulator was developed that can calculate an oil and gas field's geothermal potential on a reservoir volume and per-wellhead basis. These methods were applied to oil fields in Alberta's Swan Hill's region. On average, oil fields with temperatures ranging from 100 ˚C to 110 ˚C can produce ~25 MW_t of gross geothermal power per cubic kilometer (km^3) of reservoir volume. This equates to ~1.2 MW_e (gross) per km^3 of reservoir volume. The flow rates required to achieve these power outputs are ~5.25 kg/s per MW_t and ~57 kg/s per MW_e, respectively.
- After undergoing a careful data culling process, nearly 2000 fluid samples from four deep reservoirs were analyzed for potential geochemical risks during brine circulation in an active geothermal power production operation. Based on equilibrium thermodynamic modeling, geochemical risks, including mineral scale precipitation and associated infrastructure and formation damage, were generally considered low compared to other basin-hosted geothermal jurisdictions around the world. The most prevalent scaling risk is calcite, which is a known problem in the geothermal industry and therefore has many well-established methods for managing.
- To accompany the geochemical risk assessment, a state-of-the-art fluid/rock interaction laboratory was established at the University of Alberta. This laboratory can determine mineral precipitation rates at conditions (temperature, pressure, and brine composition) specific to potential development sites throughout the Western Canadian Sedimentary Basin. Results from such experiments can be used by developers to manage site-specific geochemical risks.
- To access the practically unlimited low-enthalpy geothermal resources available through hundreds of thousands of wells in the Western Canadian Sedimentary Basin, a deep borehole heat exchanger design was developed. Both the technical performance and costs associated with retrofitting wells as deep borehole heat exchangers were modeled. Models showed single well deep borehole exchangers producing temperatures as high as 20 ˚C for over 25 years at costs an order of magnitude lower than drilling new wells. Project specific optimization between producing higher

temperatures versus greater thermal power can be obtained by regulating the flow rate of the fluid circulating in the deep borehole heat exchanger.

- Cost and technical performance models for the deep borehole heat exchangers were applied as a case study to novel concept of warming cattle feed water at the Tomahawk Ranch in central Alberta. Here, the cost of retrofitting on-site wells as deep borehole exchangers ranged from as low at $200,000 for a suspended well to nearly $350,000 for an abandoned well. Retrofitted wells produced enough heat to warm cattle feed water from 4˚ C to 15 ˚C for an unlimited period of time, but the economic upside of provide the cattle herd warmer water in the winter remained unclear.
- A beta-version of the Geothermal Atlas of the Western Canadian Sedimentary Basin was developed and handed over to the Alberta Geological Survey for further development. This interactive, online resource provides developers and regulatory agencies with access to a variety of evaluation tools for determining the viability of geothermal energy development in localized areas throughout the Western Canadian Sedimentary Basin. Full functionality of the Atlas was developed for the Swan Hills region of Alberta.
- A comparative jurisdiction review was performed between the relative success story of the oil-to-geothermal transition in France to the relatively sluggish transition in Alberta. The review looked at three frameworks for energy transitions: evolutionary, relational, and duration. The primary elements of agency involved in a successful oil-to-geothermal transition were identified as access to resources, public discourse, and social networking. To date, in Alberta these elements have often undermined and diverged from each other, which has led to a lack of substantial growth in the geothermal sector, despite a robust and well-documented resource base

11.2 Recommendations for future work

- This study confirmed in great quantitative detail what was already known by many: the Western Canadian Sedimentary Basin contains vast geothermal resources. The primary obstacle to developing these resources is socio-political, not technical. For the geothermal energy industry to flourish in Alberta, the agencies of resource access, public discourse, and social networks must converge to a common set of values among stakeholders, rather than diverge into the special interests of individual parties. This will require greater cooperation and compromise between the oil and gas industry, potential geothermal power developers, energy regulators, and the general populace. Although the current Alberta government has made significant strides to establish a geothermal development regulatory framework, we recommend an evolution of this framework

that recognizes geothermal resources as their own entity, rather than an offshoot of oil and gas resources.

- To accelerate further development of the Geothermal Atlas of the Western Canadian Sedimentary Basin, accurate temperature data, fluid flow, and brine chemistry data from hundreds of thousands of wells throughout the Western Canadian Sedimentary Basin must be obtained, culled, and organized. We recommend the establishment of a discrete unit within the Alberta Geological Society to manage the ongoing development and administration of this essential tool for the geothermal industry's growth in Alberta.
- This project was primarily focused on lower-level technology readiness level (TRL) activities at the University of Alberta. Two significant outcomes of this study were the development of robust geotechnical modeling and fluid/rock experimentation capabilities at the university. Models and experimental results arising from this study need to be validated with real world data from the field, i.e. pilot projects. Geothermal developers can also leverage the considerable expertise and facilities at the University of Alberta to reduce the early stage technical and financial risk in new projects. Therefore, we recommend that developers continue to partner with university research groups and that these partnerships continue to receive robust financial support from provincial and federal funding agencies.
- To increase the electricity production potential of the Western Canadian Sedimentary Basin's geothermal resources, we recommend a research program focused on coupling conventional geothermal production with concentrated solar power systems. This coupling could boost the overall temperatures of produced geothermal fluids, thereby reducing the minimum temperature required to produced electricity. It would also smooth out the seasonal solar peaks provided by long, dry days in Alberta's summers while taking advantage of the enhanced surface temperature differentials created by Alberta's frigid winters. Coupling geothermal and concentrated solar production could turn two otherwise marginal resources into a genuine powerhouse for Western Canada.
- Novel and economically viable uses for low-enthalpy geothermal resources must be found. This study investigated using low-enthalpy resources to heat cattle feed water in the winter, but the economic upside of reducing the herd's caloric intake, as well as reducing premature death and miscarriages, was unclear. An obvious application of low-enthalpy heat in Alberta is snow melting. Removing snow from Alberta's roads and repairing roads damaged from freeze/thaw cracking costs

Alberta's taxpayers tens of millions of dollars per year. There are also significant environmental costs to salting the roads and operating and maintaining the heavy equipment required to plow and remove snow. There is ample heat under every one of Alberta's population centers to keep road beds dry and clear of snow throughout the Winter. This seemingly innocuous use of geothermal power could provide significant advantages to Alberta's economy and the quality of life for Albertans. Other such novel uses of low-enthalpy heat should also be explored.

- While this study was not focused on surface and near-surface mining of oil sands in the Athabasca regions of Alberta, significant heat has been injected into the subsurface in this region during steam-assisted gravity drainage operations (SAGD). A study should be commissioned to explore to what extent this heat can be recovered with geothermal technology. Recovering this heat, either for direct use or electricity production, could significantly reduce Alberta's overall carbon footprint.

References (Alphabetical)

Alberta Agriculture and Forestry (nd), Alberta Climate Information Service, Interpolated Weather Since 1961 for Alberta Townships [website] [Accessed Mar 5, 2020]. Available from: https://agriculture.alberta.ca/acis/township-data-viewer.jsp

Alberta Energy Regulator (Mar 31, 2015). Directive 011: Licensee Liability Rating (LLR) Program: Updated Industry Parameters and Liability Costs. [Internet]. [Cited 2019 Mar 1]. Available from: https://www.aer.ca/documents/directives/Directive011_March2015.pdf

Anfort, S.J., 1998. Regional-scale hydrogeology of Lower Cretaceous to Middle Devonian aquifers in southeastern Alberta. Geol. Geophys. U of Calgary, Calgary.

Anfort, S.J., Bachu, S., Bentley, L.R., 2001. Regional-Scale Hydrogeology of the Upper Devonian-Lower Cretaceous Sedimentary Succession, South-Central Alberta Basin, Canada. Am. Assoc. Pet. Geol. Bull. 85, 637–660.

Bachu, S. (1993). Basement heat flow in the Western Canada Sedimentary Basin. *Tectonophysics, 222*, 119-133.

Bachu, S., 1995. Synthesis and model of formation-water flow, Alberta Basin, Canada. Am. Assoc. Pet. Geol. Bull. 79, 1159–1178.

Bachu, S., 1997. Flow of formation waters, aquifer characteristics, and their relation to hydrocarbon accumulations, northern Alberta Basin. Am. Assoc. Pet. Geol. Bull. 81, 712–733.

Bachu, S., Hitchon, B., 1996. Regional-Scale Flow of Formation Waters in the Williston Basin1. Am. Assoc. Pet. Geol. Bull. 80, 248–264. https://doi.org/10.1306/64ED87A0-1724-11D7-8645000102C1865D

Banks, J. & Harris, N. (2018). Geothermal Potential of Foreland Basins: A Case Study from the Western Candadian Sedimentary Basin, *Geothermics, 76*.

Banks, J., Willems, C.J.L., Cowper, A., Nadkarni, K., Poulette, S., van Allen, C. (2020). Geothermal Power Potential of the Virginia Hills Oil Field, Part of the Swan Hills Carbonate Complex; Alberta, Canada. *Proceedings of the World Geothermal Congress 2020*. Reykjavik, Iceland, April 26 – May 2, 2020.

Bartel, C. A., & Garud, R. (2009). The role of narratives in sustaining organizational innovation. *Organizational science, 20*(1), 107-117.

Billings, G.K., Hitchon, B., Shaw, D.R., 1969. Geochemistry and origin of formation waters in the western Canada sedimentary basin, 2. Alkali metals. Chem. Geol. 4, 211–223. https://doi.org/https://doi.org/10.1016/0009-2541(69)90046-1

Bu, X., Ma, W., Li, H., Geothermal energy production utilizing abandoned oil and gas wells, Renewable energy 41 (2012) 80-85.

Callon, M. (1999). Actor-network theory—the market test. *The Sociological Review, 47*(1_suppl), 181-195.

Caulk, R., Tomac, I (2017). Reuse of Abandoned Oil and Gas Wells for Geothermal Energy Production. Renewable Energy 112 (2017) 388-397

Chatterjee, S., Sarkar, A., Deodhar, A.S., Biswal, B.P., Jaryal, A., Mohokar, H. V, Sinha, U.K., Dash, A., 2017. Geochemical and isotope hydrological characterisation of geothermal resources at Godavari valley, India. Environ. Earth Sci. 76, 97.

Chatterjee, S., Sinha, U.K., Biswal, B.P., Jaryal, A., Jain, P.K., Patbhaje, S., Dash, A., 2019. An integrated isotope-geochemical approach to characterize a medium enthalpy geothermal system in India. Aquat. Geochemistry 25, 63–89.

Connolly, Cathy A, Walter, L.M., Baadsgaard, H., Longstaffe, F.J., 1990. Origin and evolution of formation waters, Alberta basin, western Canada sedimentary basin. I. Chemistry. Appl. Geochemistry 5, 375–395.

Corrigan, J., (2003). Correcting Bottom Hole Temperature Data. ZetaWare, Utilities. http://www.zetaware.com/utilities/bht/default.html

Dachis, B., Shaffer, B., & Thivierge, V. (2017). All's well that ends well: Addressing end-of-life liabilities for oil and gas wells. C.D. Howe Institute Commentary, (492), COV. Retrieved from https://search.proquest.com/docview/1948408336

Duygan, M., Stauffacher, M., & Meylan, G. (2019). A heuristic for conceptualizing and uncovering the determinants of agency in socio-technical transitions. *Environmental Innovation and Societal Transitions, 33*, 13-29.

Environment and Climate Change Canada. (2018). Report national inventory 1990–2016: Greenhouse gas sources and sinks in Canada. Retrieved from https://unfccc.int/documents/65715

Environment and Climate Change Canada. (2020). National inventory report 1990-2018: Greenhouse gas sources and sinks in Canada. Retrieved from http://www.publications.gc.ca/site/eng/9.506002/publication.html

Environment Canada. (2019). Canadian Climate Normals 1981-2010 Station Data – Edmonton City Centre. Retrieved from https://climate.weather.gc.ca/climate_normals/results_1981_2010_e.html?searchType=stnProv&lstProvince=AB&txtCentralLatMin=0&txtCentralLatSec=0&txtCentralLongMin=0&txtCentralLongSec=0&stnID=1867&dispBack=0

Eppelbaum, L., Kutasov, I., Pilchin, A., Thermal Properties of Rocks and Density of Fluids, (2014) 99-149

ERA Ecosystem Services. (2014). Alberta SGER. Retrieved from http://www.eraecosystems.com/markets/alberta/

Fox, D. G. and Tylutki, T. P. (1998) 'Accounting for the effects of environment on the nutrient requirements of dairy cattle : Putting nutrition research into application of the arm', *Casein Micelle Structure: Modern Approaches to an Age Old Problem. Symposium*, 81(11), pp. 3085–3095

Francesco, T., Annamaria, P., Martina, B., Dario, T., Dušan, R., Simona, P., & Attilio, R. (2016). How to boost shallow geothermal energy exploitation in the adriatic area: the LEGEND project experience. *Energy Policy, 92*, 190-204.

Garland, G.D. & Lennox, D.H. (1962). Heat Flow in Western Canada. *Geophysical Journal International, 6*(2), 245-262.

Garud, R., & Gehman, J. (2012). Metatheoretical perspectives on sustainability journeys: Evolutionary, relational and durational. *Research Policy, 41*(6), 980-995.

Garud, R., Kumaraswamy, A., & Karnøe, P. (2010). Path dependence or path creation? *Journal of Management Studies, 47*(4), 760-774.

Garven, G., 1985. The role of regional fluid flow in the genesis of the Pine Point Deposit, Western Canada sedimentary basin. Econ. Geol. 80, 307–324. https://doi.org/10.2113/gsecongeo.80.2.307

Geels, F.W., Schot, J. (2007) Typology of sociotechnical transition pathways. Research Policy, 36.3, pp. 399-417

Gehman, J., Lefsrud, L. M., & Fast, S. (2017). Social license to operate: Legitimacy by another name? *Canadian Public Administration, 60*(2), 293=317

Government of Alberta. (2020, April). Specified Gas Reporting Standard. Edmonton, Alberta, Canada.

Grasby, S.E., Allen, D.M., Bell, S., Chen, Z., Ferguson, G., Jessop, A., Kelman, M., Ko, M., Majorowicz, J., Moore, M., Raymond, J., & Therrien, R. (2012). Geothermal energy resource potential of Canada. Natural Resources Canada. https://doi.org/10.4095/291488

Hagoort, J., Ramey's wellbore heat transmission revisited, SPE journal 9(04) (2004) 465-474.

Hähnlein, S., Bayer, P., Ferguson, G., & Blum, P. (2013). Sustainability and policy for the thermal use of shallow geothermal energy. *Energy Policy, 59*, 914-925.

Harrestrup, M., & Svendsen, S. (2014). Heat planning for fossil-fuel-free district heating areas with extensive end-use heat savings: A case study of the Copenhagen district heating area in Denmark. *Energy Policy, 68*, 294-305.

Hastings-Simon, S. (2019). Industrial Policy in Alberta: Lessons from AOSTRA and the Oil Sands. *The School of Public Policy Publications*.

Hitchon, B., Billings, G.K., Klovan, J.E., 1971. Geochemistry and origin of formation waters in the western Canada sedimentary basin—III. Factors controlling chemical composition. Geochim. Cosmochim. Acta 35, 567–598.

Hitchon, B., Billings, G.K., Klovan, J.E., 1971. Geochemistry and origin of formation waters in the western Canada sedimentary basin—III. Factors controlling chemical composition. Geochim. Cosmochim. Acta 35, 567–598. https://doi.org/https://doi.org/10.1016/0016-7037(71)90088-3

Hitchon, B., Brulotte, M., 1994. Culling criteria for "standard" formation water analyses. Appl. Geochemistry 9, 637–645. https://doi.org/https://doi.org/10.1016/0883-2927(94)90024-8

Houldsworth, M., & McDevitt, P. K. (1982). Geothermal energy: Non-electric potential in the USA. *Energy Policy, 10*(3), 203-211.

Jones, F.W. & Majorowicz, J.A. (1987). Some aspects of the thermal regime and hydrodynamics of the western Canadian sedimentary basin. *Geological Society, London, Special Publications*, *34*(1), 79-85.

Kohl, T., Salton, M., Rybach, L., Data analysis of the deep borehole heat exchanger plant Weissbad (Switzerland), Proceedings of the World Geothermal Congress, Tohoku, Japan, 2000.

Kubota, H., Hondo, H., Hienuki, S., & Kaieda, H. (2013). Determining barriers to developing geothermal power generation in Japan: Societal acceptance by stakeholders involved in hot springs. *Energy Policy, 61*, 1079-1087.

Kujawa, T., Nowak, W., Stachel, A.A., Utilization of existing deep geological wells for acquisitions of geothermal energy, Energy 31(5) (2006) 650-664.

Lam, H.L. & Jones, F.W. (1984). Geothermal gradients of Alberta in western Canada. *Geothermics*, *13*(3), 181-192

Lam, H.L., Jones, F.W., & Lambert, C. (1982). Geothermal Gradients in the Hinton Area of West-Central Alberta. *Canadian Journal of Earth Sciences, 19,* 755-766.

Lam, H.L., Jones, F.W., & Majorowicz, J.A. (1985). A Statistical Analysis of Bottom-Hole Temperature Data in Southern Alberta. *Geophysics, 50*(4), 677-684.

Laplaige, P., Jaudin, F., Desplan, A., & Demange, J. (2000). The French Geothermal Experience and Review and Perspectives. *Proceedings World Geothermal Congress, Kyushu – Tohoku, Japan.*

Lavigne, C. R. (2018). *Resource Assessment of Geothermal Reservoir in Western Alberta and Evaluation of Utilization Options Using Non-Renewable Energy Displacement.* Edmonton: University of Alberta.

Lawrence, T. B., & Phillips, N. (2004). From Moby Dick to Free Willy: Macro-Cultural Discourse and Institutional Entrepreneurship in Emerging Institutional Fields. *Organization, 11(5)*, 689-711

Leitch, A., Haley, B., & Hastings-Simon, S. (2019). Can the oil and gas sector enable geothermal technologies? Socio-technical opportunities and complementarity failures in Alberta, Canada. *Energy Policy, 125*, 384-395.

Líndal, B. (1973). Industrial and Other Applications of Geothermal Energy: (except power production and district heating). *Geothermal Energy: Review of Research and Development, Paris, UNESCO, 72*, 135-148.

Lindsey, C.R., Neupane, G., Spycher, N., Fairley, J.P., Dobson, P., Wood, T., McLing, T., Conrad, M. (2018). Cluster analysis as a tool for evaluating the exploration potential of Known Geothermal Resource Areas. Geothermics 72, 358–370.

Majorowicz, J., Gosnold, W., Gray, A., Safanda, J., Klenner, R., & Unsworth, M. (2012a). Implications of Post-Glacial Warming for Northern Hemisphere Heat Flow. *GRC Transactions,* 36.

Majorowicz, J., Unsworth, M., Chacko, T., Gray, A., Heaman, L., Potter, D.K., Schmitt, D., & Babadagli, T. (2012b). Geothermal Energy as a Source of Heat for Oil Sands Processing in Northern Alberta, Canada. In F.J. Hein, D. Leckie, & J. Suter (Eds.) *Heavy-oil and oil sand petroleum systems in Alberta and Beyond: AAPG Studies in Geology 64,* (pp. 1-22).

Majorowicz, J.A. & Jessop, A.M. (1981). Regional Heat Flow Patterns in the Western Canadian Sedimentary Basin. *Tectonophysics, 75*(3-4), 209-238.

Majorowicz, J.A. & Moore, M. (2014). The Feasibility and Potential of Geothermal Heat in the Deep Alberta Foreland Basin - Canada for CO2 Savings. Renewable Energy, 66, 541-549. http://dx.doi.org/10.1016/j.renene.2013.12.044

Majorowicz, J.A., Garven, G., Jessop, A., & Jessop, C. (1999). Present Heat Flow Along a Profile Across the Western Canada Sedimentary Basin: The Extent of Hydrodynamic Influence. In *Geothermics in Basin Analysis* (pp. 61-79). Springer, Boston, MA.

Majorowicz, J.A., Jones, F.W., Lam, H.L., & Jessop, A.M. (1984). The Variability of Heat Flow Both Regional and With Depth in Southern, Alberta, Canada: Effect of Groundwater Flow? *Tectonophysics, 106,* 1-29.

Majorowicz, J.A., Jones, F.W., Lam, H.L., & Jessop, A.M. (1985). Terrestrial Heat Flow and Geothermal Gradients in Relation to Hydrodynamics in the Alberta Basin, Canada. *Journal of Geodynamics, 4,* 265-283.

Malafeh, S., & Sharp, B. (2015). Role of royalties in sustainable geothermal energy development. *Energy Policy, 85*, 235-242.

Merck and Co., Inc (2020). Nutritional Requirements of Beef Cattle - Management and Nutrition - Merck Veterinary Manual. [online]. Available from: https://www.merckvetmanual.com/management-and-nutrition/nutrition-beef-cattle/nutritional-requirements-of-beef-cattle

Michael, K., Machel, H.G., Bachu, S. (2003). New insights into the origin and migration of brines in deep Devonian aquifers, Alberta, Canada. J. Geochemical Explor. 80, 193–219.

Nalla, G., Shook, G.M., Mines, G.L., Bloomfield, K.K. (2005) Parametric sensitivity study of operating and design variables in wellbore heat exchangers, Geothermics 34(3) 330-346.

Niewenhuis, G., Lengyel, T., Majorowicz, J., Grobe, M., Rostron, B., Unsworth, M.J., & Weides, S. (2015). Regional-Scale Geothermal Exploration Using Heterogeneous Industrial Temperature Data; a Case Study from the Western Canadian Sedimentary Basin. *Proceedings of World Geothermal Congress 2015 – Melbourne, Australia* (pp. 19-25).

Oberg, A., Lefsrud, L., & Meyer, R. (forthcoming). Organizational (Issue) Field Perspective on Climate Change. *Economic Sociology: The European Electronic Newsletter*.

Osborne VR, Hacker RR, McBride BW (2002). Effects of heated drinking water on the production responses of lactating Holstein and Jersey cows. *Canadian Journal of Animal Science*, 2002, 82(3): 267-273

Pereira, V. de V. (n.d.). *CALCIUM CARBONATE SCALING CONTROL IN GEOTHERMAL WELL PV8 IN SAO MIGUEL, AZORES, COMBINING CHEMICAL INHIBITION AND MECHANICAL REAMING*. 24.

Pinch, T. J., & Bijker, W. E. (1984). The social construction of facts and artefacts: or how the sociology of science nad the sociology of technology might benefit each other. *Social Studies of Science, 14*, 399.

Purkus, A., & Barth, V. (2011). Geothermal power production in future electricity markets—a scenario analysis for Germany. *Energy Policy, 39*(1), 349-357.

Ramey Jr, H. (1962) Wellbore heat transmission, Journal of petroleum Technology 14(04) pp. 427-435.

Reagan, A. J., Mitchell, K. L., Danforth, C. M., & Dodds, P. S. (2016). The emotional arcs of stories are dominated by six basic shapes. *EPJ Data Science, 5*(1), 1-12.

Reber, T. J., Beckers, K. F., & Tester, J. W. (2014). The transformative potential of geothermal heating in the US energy market: A regional study of New York and Pennsylvania. *Energy Policy, 70*, 30-44.

Rostron, B.J., Tóth, J., Machel, H.G. (1997) Fluid flow, hydrochemistry and petroleum entrapment in Devonian reef complexes, south-central Alberta, Canada.

Satman, A., Tureyen, O.I., Geothermal wellbore heat transmission: Stabilization times for "static" and "transient" wellbore temperature profiles, Geothermics 64 (2016) 482-489.

Seyboth, K., & Beurskens, L. L. (2008). Recognising the potential for renewable energy heating and cooling. *36*(7), 2460-2463.

Shi, Z., Liao, F., Wang, G., Xu, Q., Mu, W., Sun, X., 2017. (2017) Hydrogeochemical characteristics and evolution of hot springs in eastern Tibetan Plateau geothermal belt, western China: Insight from multivariate statistical analysis. Geofluids.

Siega, F. L., Herras, E. B., & Buning, B. C. (n.d.). *Calcite Scale Inhibition: The Case of Mahanagdong Wells in Leyte Geothermal Production Field, Philippines*. 6.

Stokes, E. (2000). The legacy of Ngatoroirangi: Maori customary use of geothermal resources.

Straus, J.M., Schubert, G. (1977) Thermal convection of water in a porous medium: Effects of temperature- and pressure-dependent thermodynamic and transport properties, Journal of Geophysical Research 82(2). pp. 325-333

Strebel, P., Cossin, D., & Khan, M. (2020). How to Reconcile Your Shareholders With Other Stakeholders. *MIT Sloan Management Review, 61*(4), 1-8.

Sui, D., Wiktorski, E., Røksland, M., Basmoen, T.A. (2018) Review and investigations on geothermal energy extraction from abandoned petroleum wells, Journal of Petroleum Exploration and Production Technology 89(5) pp. 908-915.

Vermilion Energy. (2013, December 4). *Vermilion Energy Inc. Receives National Ecology Award in France*. Retrieved from U.S. Securities and Exchange Commission:

Viau, C. (1987). The Swan Hills Formation and the Beaverhill Lake Group at Swan Hills Field and Adjacent Areas, Central Alberta, Canada. In F.F. Kraus O.G. Borrowes (Eds.), *DevonianLithofacies and Reservoir Styles in Alberta, Second International Symposium on the Devonian System, Canadian Society of Petroleum Geologists* (pp. 201-239). Core Conference Manual.

Voronov, M., and Weber, K. (2017) Emotional competence institutional ethos, and the heart of institutions. Academy of Management Review. Vol. 42.3

Wang, K., Yuan, B., Ji, G., Wu, X., (2018) A comprehensive review of geothermal energy extraction and utilization in oilfields, J Petrol Sci Eng 168. pp. 465-477.

Wanner, C., Eichinger, F., Jahrfeld, T., & Diamond, L. W. (2017). Causes of abundant calcite scaling in geothermal wells in the Bavarian Molasse Basin, Southern Germany. *Geothermics*, *70*, 324–338.

Weides, S., Moeck, I., Majorowicz, J., Grobe, M. (2014a). The Cambrian Basal Sandstone Unit in Central Alberta — an Investigation of Temperature Distribution, Petrography, and Hydraulic and Geomechanical Properties of a Deep Saline Aquifer. Canadian Journal of Earth Sciences, 51, 783-796. http://dx.doi.org/10.1139/cjes-2014-0011

Weides, S., Moeck, I., Majorowicz, J., Palombi, D., & Grobe, M. (2013). Geothermal exploration of Paleozoic formations in Central Alberta. Canadian Journal of Earth Sciences, 50(5), 519–534. https://doi.org/10.1139/cjes-2012-0137

Weides, S.N., Moeck, I., Schmitt, D.R., & Majorowicz, J.A. (2014b). An integrative geothermal resource assessment study for the siliciclastic Granite Wash Unit, northwestern Alberta (Canada). *Environmental Earth Sciences, 72*(10), 4141-4154.

Weissenberger, J.A.W., Wong, P.K., & Gilhooly, M.G. (2016). Stratigraphic Architecture of the Frasnian South Jasper Basin, North-Central Alberta Front Ranges. *Society for Sedimentary Geology*, 16.

Wight, N.M., Bennett, N.S. (2015) Geothermal energy from abandoned oil and gas wells using water in combination with a closed wellbore, Appl Therm Eng 89. pp.908-915

Yanagisawa, N., Matsunaga, I., Sugita, H., Sato, M., & Okabe, T. (2008). Temperature-dependent scale precipitation in the Hijiori Hot Dry Rock system, Japan. *Geothermics*, *37*(1), 1–18.

Zhang, L., Li, X., Zhang, Y., Cui, G.D., Tan, C.Y., Ren, S.R. (2017) CO2 injection for geothermal development associated with EGR and geological storage in depleted high-temperature gas reservoirs, Energy 123 (139-148.

Zhao, M., Ghidaoui, M.S., (2006) Investigation of turbulence behavior in pipe transient using a k-ε model, Journal of hydraulic research 44(5) 682-692.

Zotzmann, J., Vetter, A., & Regenspurg, S. (2018). Evaluating efficiency and stability of calcite scaling inhibitors at high pressure and high temperature in laboratory scale. *Geothermal Energy*, *6*(1), 18.